A STUDY OF MANGANESE DIOXIDE-HYDROGEN INSERTION COMPOUNDS PRODUCED BY DIFFERENT CHEMICAL INSERTION METHODS

JAVIER ALDAY

A thesis submitted to Middlesex University in partial fulfilment of the requirements for the degree of : Master of Philosophy

March 1.999

The work was carried out at the Energy Technology Centre, Middlesex University, School of Mechanical Engineering, Bounds Green Road, London N11 2 NQ and was funded by Celaya, Emparanza y Galdos S.A. (Cegasa).

ABSTRACT

The reduction of an electrolytic manganese dioxide (EMD) by two different chemical insertion methods (propan-2-ol and hydrazine hydrate) has been studied by XRD (X-Ray Diffraction), FTIR (Fourier Transform infrared) and Electrode Potential Measurements.

The level of H insertion may be represented by $MnOOH_r$, where r goes from ≈ 0,1 in the starting material (due to non-stoichiometry) up to 1.0 in the most reduced material. H insertion into EMD led to approximate isotropic lattice expansion up to r values close to 0.7 - 0.8 for the propan-2-ol reduction method. This observation was consistent with a homogeneous solid state reduction with formation of a solid solution in which H^+ and e^- are mobile. In the region r = 0,7-0,8 to 1,0, new XRD non-moving lines emerged, while the original lines continued to move, indicating anisotropic lattice expansion. This is due to the appearance of microdomains of the end product within the solid solution, implying that H^+ and e^- were no longer mobile in the crystal structure but located in position, which has been supported by FTIR measurements looking carefully at wavenumber regions where O-H vibration occurred.

For the hydrazine hydrate reduced samples, the O-H bond formation takes place at a much earlier stage of reduction. Examination of the XRD patterns indicated

heterogeneous solid state reduction had occurred after r = 0,4. Heterogeneous reduction was presumed to have occurred by H location in the outside layers of the particles.

A study of the potential of the compounds obtained under both reduction methods has been carried out, together with the study of the stability of the H inserted compounds in KOH electrolyte. Potential measurements confirmed development of a heterogeneous potential coinciding to the appearance of new peaks on X-ray diffraction and the formation of O-H bonds as shown in FTIR. This behaviour appears at a much earlier level of reduction for the hydrazine hydrate reduced samples than for the propan-2-ol reduced samples. The results confirm previous findings that H inserted compounds are unstable at a level related to the formation of microdomains in KOH at concentrations similar to those used in alkaline manganese batteries, which limits the capacity of those batteries.

CONTENTS

1.- INTRODUCTION

Manganese dioxide is the positive active material used in Leclanché and alkaline manganese batteries [1] which together dominate the primary battery market. At the same time, it is also used in the recently developed electrochemical system coupled with lithium and an organic electrolyte.

Manganese dioxide has numerous crystallographic forms which result in wide variations in many of its properties. Much of the progress made in recent years in the performance of primary cells is attributed to the production and improvement in electrolytic manganese dioxide [2] (known throughout the industry as EMD) [3]. As early as 1918, Van Arsdale and Maier [4] had pointed out that the use of EMD as a dry cell depolarizer increased the cell discharge capacity and they also reported the preparation of the EMD by the method currently employed. EMD, in common with other battery active varieties, is not stoichiometric, containing apparently substantial amounts of protonic species, $MnOOH_{0.1}$ ($MnO_{1.95}$) being a typical formula. This was elucidated only in 1984 when Ruetschi [5] conjectured that " non-stoichiometry originates essentially from Mn^{4+} vacancies that are compensated in the lattice by 4 OH^- ". According to this explanation, the crystal structure, composed of closely packed O^{2-} ions which are octahedrally co-ordinated to Mn^{4+} ions, contains Mn vacancies. Each vacancy is electrostatically compensated by four protons, which are present in the form of OH^- ions that replace O^{2-} in the lattice, without noticeable change in lattice parameters.

EMD is used at present for high quality Leclanché cells, and mainly for the fast growing market for alkaline manganese cells. EMD is difficult to characterise. Its structure is known to incorporate defects. γ-MnO_2 has been described [6] as built up from pyrolusite elements interspersed in a ramsdellite matrix (called De Wolff defect). More recently, Chabre and Pannetier [7] have shown evidence of another kind of structural defect, identified as microtwinning. These structural defects, whose details are still largely unknown, as well as the poor quality of X-ray diffraction patterns, explain why EMD (and many manganese dioxides) are poorly characterised materials.

It is now widely accepted that manganese dioxide discharges by abstraction of H^+ from the electrolyte and reception of electrons from the external circuit via carbon black or graphite conductors [8]. Both proton and electron insert into the manganese dioxide structure and the reaction may be conveniently represented as follows :

$$\mathbf{MnOOH_r} + \Delta H^+ + \Delta e^- \quad \text{=====>} \quad \mathbf{MnOOH_{r+\Delta}} \qquad (1)$$

where r represents the level of H insertion which changes from about 0.1 in the starting material to 1.0 at the theoretical completion of the discharge.

In addition to direct X-ray diffraction analysis and transformations in which EMD can participate, further structural information is provided by H insertion in $MnOOH_{0.1}$ ($MnO_{1.95}$). Such studies have been undertaken in the past [9, 10, 11]. The properties of the $MnOOH_r$ compounds are crucial to the performance of batteries. Their instability may lead to reduced capacity yields in alkaline electrolyte [12]. Coleman [13] was probably

the first to attempt a comprehensive theoretical model for the observed potential changes during the electrochemical reduction of MnO_2. Normally, the insertion compounds of EMD form a series of solid solutions which exhibit decreasing electrode potentials with increasing H insertion level. The electrode potentials may be accurately modelled by assuming that the inserted H exists as two thermodynamically independent components, H^+ and e^- [14, 15, 16].

Whilst a chemical process for insertion of H [9, 12, 17, 18] into manganese dioxide has obvious advantages over an electrochemical procedure in terms of the absence of complicating phases such as the electronic conductor and zinc compounds, there is one inherent difficulty: it is inevitable that the particles with the higher surface to volume ratio will receive the greater amount of H insertion per unit weight. In other words all chemical processes must result in r in $MnOOH_r$ being higher initially for the smaller particles. Equalisation of r among particles of different sizes may occur as a consequence of subsequent processes [18].

Brenet [19] observed that when γ-MnO_2 was reduced, the oxide lattice initially dilated, and deduced that the reduction had occurred homogeneously. Potential measurements have confirmed that the reaction takes place in a homogeneous phase [20, 21, 22, 23]. In the same manner, it has been shown that both chemical and electrochemical reduction of EMD proceeds via a single phase over the complete range $MnOOH_{0.1}$ - $MnOOH_{1.0}$ [10, 11, 24, 25, 26, 27, 28, 29, 30].

According to Chabre and Pannetier [7], this statement can be largely attributed to the lack of accurate structural characterisation of the EMD and its reduced materials. Anyway, this concept of homogeneous phase reaction to describe the reduction up to one e^- per Mn has prevailed up to the present. However, Gabano et al [9,31] reported that the composition range over which the homogeneous phase exists might be dependent on the reduction procedure, the nature of the reducing agent, and the imposed reaction rate.

It is believed that the reduction up to one electron per Mn in concentrated alkaline electrolytes proceeds in the same way as in ammonium and zinc chloride solutions. Kozawa and Powers [32] noticed the influence of the duration of the measurements on the shape of the discharge curves and other authors have reported the appearance of Mn_3O_4 above half reduction [33, 34, 35, 36, 37, 38]. The use of hydrazine in 30 wt.% KOH for H insertion, for example, led to the consumption of the smallest particles and to the deposition of δ-MnO_2 on the surface of the larger particles [12]. Maskell et al [11], and Gabano et al [31] carried out their reductions very slowly in order to increase the likelihood that all parts of the manganese dioxide were reduced at similar rates. In a later work, Ohzuku et al [39] reported for a hydrazine hydrate reduction X-ray diffraction patterns which looked like those expected for a heterogeneous reduction although they claimed that the evidence showed that a single phase reaction had taken place.

In the most recent works [18, 40] using chemical insertion, careful XRD measurements have indicated that above a certain level of insertion (70-80%), some degree of irreversibility sets in as approximately 50% of the inserted H was no longer mobile. The appearance of restricted mobility coincides with the emergency of additional

XRD lines [18, 40] and the emergence of OH^- vibration bonds in FTIR spectroscopy [40]. The irreversibility which sets in at high levels of insertion opens up the possibility of using faster chemical reductions to generate non-uniform compounds (heterogeneity) by forming restricted mobility regions in the surface layers.

The aim of this work is to study the effect of different methods of chemically inserting hydrogen on the structure and properties of compounds arising from a commercial electrodeposited manganese dioxide. More specifically, the present work has been carried out in order to establish whether the hydrogen insertion into EMD occurs homogeneously or heterogeneously when using a hydrazine hydrate reduction method [41]. Such heterogeneity (non-uniform compounds) is of interest because of : (1) its relevance to battery behaviour at high discharge rates; (2) possible modifications to stability behaviour; and (3) changes in the relationship between electrode potential and H insertion. A comparison will be established with another method (Propan-2-ol) in which the hydrogen insertion is known to occur homogeneously [18].

XRD and FTIR spectroscopy will be used diagnostically to establish whether H insertion occurs homogeneously or heterogeneously and the effect of such differences on electrode potentials, stability and battery behaviour will be examined. XRD diffraction is the technique which has been most widely used to establish the structures of the various crystalline forms of manganese dioxide and its reduction products. Concise reviews of these structures and their interrelationship have been presented by Burns and Burns [42, 43]. Infrared spectra of manganese dioxides are readily obtained using modern instrumentation. Potter and Rossman [44] presented a study of tetravalent manganese

dioxides. More recently, Desai et al [45] have reviewed the properties of manganese dioxides including studies relating the absorption bands to Mn-O and O-H stretching and bending vibration. The FTIR spectrum provides a fingerprint of the material which allows much information to be obtained. Since chemical and structural differences between samples of MnO_2 are reflected in the infrared spectrum, FTIR spectrometry is a very valuable technique for studying and characterising manganese dioxides [46].

Many research projects over the past years have been carried out with the goal of improving the understanding of the redox processes that occur at the manganese dioxide electrode . However, there are not so many works about the stability of EMD at various stages of reduction. For example, Holton et al [12] have been the only ones to study this stability in concentrated alkaline electrolytes.

The starting material chosen for the following study was a commercial electrodeposited gamma manganese dioxide (EMD) manufactured by CEGASA with an initial composition of r in $MnOOH_r$ equal to 0.072 (x in MnO_x [x = 2 - r/2] equal to 1.964). CEGASA is the leading manufacturer of dry cells in Spain. When the need for the production of a high quality dry battery was seen, CEGASA constructed in 1954 a plant for the production of 500 tons per year of EMD. In 1962, the production was increased to 1500 tons per year, and, in 1972, the plant was renovated and the production was increased to 4000 tons per year. Surplus not used by CEGASA is sold to European battery manufacturers. The chemical and physical characteristics of the CEGASA EMD, are very similar to those of the existing EMD's in the market. The largest EMD producers are in Japan, USA, South Africa and Australia.

2.- PREPARATION AND CHEMICAL ANALYSIS OF H INSERTED SAMPLES

2.1.- CHEMICAL REDUCTIONS OF MANGANESE DIOXIDE

The purpose of chemically inserting H in a non aqueous environment was to produce a range of H insertion materials reflecting as far as possible a solid state reaction process without subsidiary complicating reactions [12, 39]. These arise due to the re-establishing of equal concentrations of H in each particle when smaller particles (with a higher surface to volume ratio) are unavoidably inserted to a greater degree whatever the chemical H insertion technique used. Establishment of equilibrium may involve soluble intermediates, particularly in an aqueous medium, with the consequent possible appearance of phases not fundamentally characteristic of the insertion process [18]. In this work, Propan-2-ol and Hydrazine Hydrate were chosen for the chemical reductions of the EMD.

2.1.1.- Propan 2-ol reduction.

This method was chosen as it was known to reduce EMD homogeneously [41], keeping the level of H insertion as uniform as possible throughout the particles of $MnOOH_x$. The samples obtained by this method will be compared with those produced by the hydrazine hydrate reduction method.

The method consists on suspending 11.7 g of EMD in 100 ml of Propan 2-ol. The reduction was carried out at reflux temperature (82.5 °C) and the reduction degree of the samples was controlled by varying the reflux time. The amount of Propan-2-ol was in about five times excess. After the chosen time had passed, the hot mixture was filtered on sintered glass, cooled and dried at ambient temperature for about 1 hour. The reaction may be represented as :

$$2\ MnO_2 + CH_3\text{-}CHOH\text{-}CH_3 \longrightarrow 2\ MnOOH + CH_3\text{-}CO\text{-}CH_3 \qquad (2)$$

A first set of twenty-six samples (labelled 1 - 26) was prepared with this method. However, with the above explained method it was very difficult to obtain samples with r in $MnOOH_r$ in the ranges (1) 0.072-0.4 (x between 1.96-1.80) and (2) 0.88-1.0 (1.56-1.5).

In the first range (1), it seemed that, as Propan-2-ol was in about 5 times excess, the reduction from $MnOOH_{0.072}$ to $MnOOH_{0.4}$ occurred almost instantaneously. This may indicate a high rate of diffusion of inserted H away from the surface : the high surface area of the oxide and the excess of Propan-2-ol probably contributed to the high rate of diffusion. In order to try and achieve the samples with low H insertion, a second set of samples (labelled 27-28) was prepared by reduction with Propan-2-ol at 45 °C. As the required samples were not obtained, a further attempt (third set of samples (29-31)) was carried out with reduction at room temperature. However, even at room temperature, the reduction in this range occurred very quickly.

After these unsuccessful attempts, the idea of modifying the ratio of EMD/Propan-2-ol was tried. In this way, the same amount of EMD as previously described (11.7 g) was put in contact with 5, 10, 20, 40 and 60 ml of Propan-2-ol (instead of 100 ml as before). The fourth set of samples (32-36) prepared in this way (at room temperature), gave the required samples in the range of 0.072-0.40.

Once the oxidation state of $MnOOH_{0.4}$ ($MnO_{1.80}$) had been achieved, the rate of H insertion became slower. A possible explanation of the two rates of H insertion is as follows. Initially, Propan-2-ol occupied the internal pores which formed the predominant part of the surface area (and in consequence rapid H insertion ensued). When the Propan-2-ol in the pores had been consumed, further insertion required its replenishment by diffusion through the pores to the oxide surface at the same time as the product (acetone, CH_3-CO-CH_3) was diffusing away from the insertion sites.

For range (2), H insertion was very difficult to achieve due to the restricted mobility inside the solid solution, caused, according to Tye and Tye [74], by the formation of microcrystalline domains of fully inserted material at high levels of insertion which inhibit H diffusion. For this reason a fifth set of samples (37-39) was prepared with replacement of the "spent" Propan-2-ol during the reduction with "new" Propan-2-ol, and using very long periods of boiling time.

A summary of the above mentioned behaviour of the reduction of the EMD with Propan-2-ol at boiling temperature is shown in Figure 2.1. It is clearly shown both the "very fast" reduction in the initial stage, and the "very slow" reduction at the final stage.

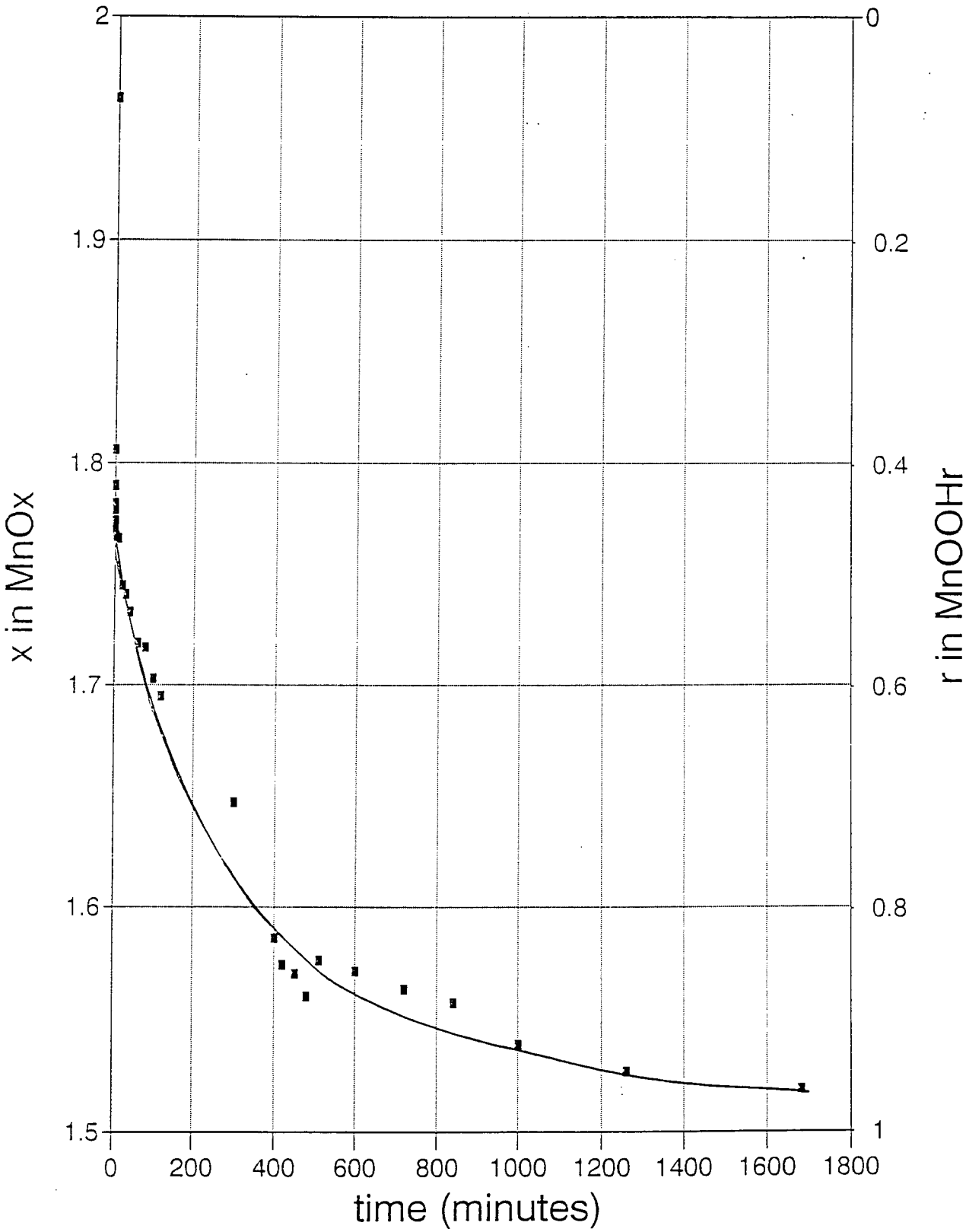

Figure 2.1.- Reduction degree with Propan-2-ol versus boiling reduction time

2.1.2.- Hydrazine hydrate reduction.

The same procedure as described by Larcin [47] was employed. Unlike propan-2-ol, this reduction was carried out at room temperature. About 20 g. of EMD were suspended in 35 - 40 ml of hexane in 50 ml conical flasks containing stirring bars. One ml portions of a solution of hydrazine hydrate in Propan 2-ol were added to the vigorously stirred suspensions every 50 - 60 minutes. An hour after the last hydrazine addition, the sample was filtered on sintered glass, dried at 50 °C for about 15 minutes and outgassed for about another 15 minutes. The reaction was :

$$4\ MnO_2 + N_2H_4.H_2O \longrightarrow 4\ MnOOH + N_2 + H_2O \qquad (3)$$

Three different sets of samples were prepared according with this method; two of them in order to produce a series of samples ranging in composition from $MnOOH_{0.072}$ (starting material) to $MnOOH_1$ and the other to establish the influence of the rate of reduction on the hydrogen insertion mechanism.

In the hereafter called "sixth set", a total of 20 samples (labelled 40 to 59) were prepared. The concentration was calculated to produce a reduction of x (in MnO_x) approximately equal to 0.025 (13.5 g $N_2H_4.H_2O$ in 100 ml of solution) with each addition. As the most reduced sample achieved in that set was $MnO_{1.562}$ ($MnOOH_{0.876}$), a new (seventh) set of 5 samples (60 - 64) was obtained after 12, 13, 14, 15 and 17 one ml additions respectively of a more concentrated hydrazine hydrate solution (21.26 g $N_2H_4.H_2O$ in 100 ml solution).

The eighth set of three samples (65 - 67) was prepared at a slow reduction rate (6.75 g $N_2H_4.H_2O$ in 100 ml solution) after 20, 30 and 40 one ml addition respectively.

2.2.- CHEMICAL ANALYSIS

Oxidation states were determined using the potentiometric titration procedure of Vetter and Jaeger [21]. The accuracy of this method has already been checked for similar samples to the ones obtained here [40, 48].

The $MnOOH_x$ samples were dissolved in an excess of $FeSO_4$ in acidic media, according to the reaction :

$$MnO_x + 2x\ H^+ + (2x\text{-}2)\ Fe^{2+} \text{ ======} > Mn^{2+} + (2x\text{-}2)\ Fe^{3+} + x\ H_2O \qquad (4)$$

The excess of ferrous sulphate was potentiometrically back-titrated by $KMnO_4$:

$$MnO_4^- + 8\ H^+ + 5\ Fe^{2+} \text{ ======} > Mn^{2+} + 5\ Fe^{3+} + 4\ H_2O \qquad (5)$$

The manganese content of the samples were measured by $KMnO_4$ titration in sodium pyrophosphate solution according to the reaction :

$$4\ Mn^{2+} + MnO_4^- + 8\ H^+ + 5\ H_2P_2O_7^{2-} \text{ ======} > 5\ Mn(H_2P_2O_7)_3^{3-} + 4\ H_2O \qquad (6)$$

The degree of oxidation was calculated from the amount of ferrous sulphate consumed by reaction (4) and from the manganese content of the sample given by reaction (6).

Using this procedure, about 0.16 g of $MnOOH_r$ were transferred into a 250 ml beaker and depending on the oxidation state of the sample, 25 to 40 ml of a ferrous sulphate solution (about 40 g of $FeSO_4(NH_4)_2SO_4.6H_2O$ + 20 ml concentrated H_2SO_4 in 1 litre of solution) were added. The solution was diluted to 50 ml with water and the dissolution carried out with a magnetic stirrer for about 30 minutes. A platinum electrode and a saturated calomel electrode were then placed into the solution and the excess ferrous sulphate potentiometrically titrated with $KMnO_4$ solution (about 3.3 g $KMnO_4$ in 1 litre of water). The $KMnO_4$ solution volume at the equivalence point was recorded as V_1. The pH of the solution was then adjusted to 6.5 to 7.5 by addition of sodium pyrophosphate (8 - 13 g depending in the amount of $FeSO_4$ added), and the second titration with $KMnO_4$ was carried out potentiometrically. The amount of $KMnO_4$ used was registered as V_2. The $KMnO_4$ concentration relative to the $FeSO_4$ concentration was measured by potentiometric titration. The permanganate solution volume at the end of this titration was recorded as V_0.

The amount of $FeSO_4$ consumed during the sample dissolution correspond to (V_0-V_1) ml of $KMnO_4$ (concentration equal to c_k moles/l). According to reaction (5), $5c_k(V_0$-$V_1)$ millimoles of $FeSO_4$ were consumed. During the second titration, the sum of manganese from the sample and from the first titration was measured. From the stoichiometry of reaction (6), the volume of $KMnO_4$ corresponding to the manganese

content of the sample was therefore $(V_2-V_1/4)$ ml or $4c_k(V_2-V_1/4)$ millimoles of Mn in the sample.

From equation (4), each mole of MnO_x dissolved by consuming (2x-2) moles of $FeSO_4$, produced 1 mole of Mn^{2+}, so :

$$2(x-1) = \frac{5c_k(V_0-V_1)}{4\ c_k(V_2-V_1/4)} \qquad (7)$$

and.

$$x = 1 + (5/8)\ \frac{(V_0-V_1)}{(V_2-V_1/4)} \qquad (8)$$

Three determinations of the oxidation state were always carried out with each sample. The values obtained were very similar, confirming the accuracy of the chosen method.

Tables 2.1 to 2.8 show the average values of the oxidation state obtained for the eight set of samples mentioned in section 2.1.

Table 2.1.- Chemical analysis of the propan-2-ol reduction 1st set of samples.

Sample no.	Reduction	x in MnO_x	r in $MnOOH_r$
0	Starting material	1.964	0.072
1	5 seconds (reflux temperature)	1.790	0.420
2	10 seconds (")	1.806	0.388
3	20 seconds (")	1.784	0.433
4	30 seconds (")	1.791	0.418
5	40 seconds (")	1.775	0.451
6	50 seconds (")	1.772	0.456
7	1 minute (")	1.780	0.440
8	2 minutes (")	1.769	0.462
9	5 minutes (")	1.768	0.464
10	10 minutes (")	1.767	0.466
11	20 minutes (")	1.745	0.510
12	30 minutes (")	1.741	0.518
13	40 minutes (")	1.733	0.534
14	60 minutes (")	1.720	0.560
15	80 minutes (")	1.718	0.564
16	100 minutes (")	1.704	0.592
17	120 minutes (")	1.696	0.608
18	300 minutes (")	1.648	0.704
19	400 minutes (")	1.587	0.826
20	420 minutes (")	1.575	0.850
21	450 minutes (")	1.571	0.858
22	480 minutes (")	1.561	0.878
23	510 minutes (")	1.576	0.848
24	600 minutes (")	1.572	0.856
25	720 minutes (")	1.564	0.872
26	840 minutes (")	1.558	0.884

Table 2.2.- **Chemical analysis of the propan-2-ol reduction 2nd set of samples.**

Sample no.	Reduction	x in MnO_x	r in $MnOOH_r$
27	5 minutes (45 °C)	1.787	0.426
28	30 minutes (")	1.770	0.460

Table 2.3.- **Chemical analysis of the propan-2-ol reduction 3rd set of samples.**

Sample no.	Reduction	x in MnO_x	r in $MnOOH_r$
29	1 minute (20 °C)	1.828	0.344
30	4.5 minutes (")	1.818	0.364
31	8 minutes (")	1.797	0.406

Table 2.4.- **Chemical analysis of the propan-2-ol reduction 4th set of samples.**

Sample no.	Reduction	x in MnO_x	r in $MnOOH_r$
32	5 ml propan-2-ol (1 minute)	1.949	0.102
33	10 ml propan-2-ol (")	1.924	0.152
34	20 ml propan-2-ol (")	1.886	0.228
35	40 ml propan-2-ol (")	1.867	0.266
36	60 ml propan-2-ol (")	1.841	0.318

Table 2.5.- **Chemical analysis of the propan-2-ol reduction 5th set of samples.**

Sample no.	Reduction	x in MnO_x	r in $MnOOH_r$
37	14 hours (replacement of propan-2-ol each 7 hours , reflux temperature)	1.539	0.922
38	21 hours (")	1.527	0.946
39	28 hours (")	1.519	0.962

Table 2.6.- **Chemical analysis of the hydrazine hydrate reduction 6th set of samples.**

Sample no.	Reduction	x in MnO_x	r in $MnOOH_r$
0	Starting material	1.964	0.072
40	1 ml (13.5 g. $N_2H_4.H_2O$ solution)	1.935	0.130
41	2 ml (")	1.915	0.170
42	3 ml (")	1.895	0.210
43	4 ml (")	1.867	0.266
44	5 ml (")	1.842	0.316
45	6 ml (")	1.810	0.380
46	7 ml (")	1.800	0.400
47	8 ml (")	1.768	0.464
48	9 ml (")	1.752	0.496
49	10 ml (")	1.741	0.518
50	11 ml (")	1.721	0.558
51	12 ml (")	1.689	0.622
52	13 ml (")	1.682	0.636
53	14 ml (")	1.676	0.648
54	15 ml (")	1.652	0.696
55	16 ml (")	1.634	0.732
56	17 ml (")	1.615	0.700
57	18 ml (")	1.598	0.804
58	19 ml (")	1.585	0.830
59	20 ml (")	1.562	0.876

Table 2.7.- **Chemical analysis of the hydrazine hydrate reduction 7th set of samples.**

Sample no.	Reduction	x in MnO_x	r in $MnOOH_r$
60	12 ml (21.26 g. $N_2H_4.H_2O$ solution)	1.569	0.862
61	13 ml (")	1.550	0.900
62	14 ml (")	1.527	0.946
63	15 ml (")	1.522	0.956
64	16 ml (")	1.506	0.988

Table 2.8.- **Chemical analysis of the hydrazine hydrate reduction 8th set of samples.**

Sample no.	Reduction	x in MnO_x	r in $MnOOH_r$
65	20 ml (6.75 g. $N_2H_4.H_2O$ solution)	1.729	0.542
66	30 ml (")	1.673	0.654
67	40 ml (")	1.599	0.802

3.- POWDER X-RAY DIFFRACTION

Powder XRD has proved to be of a great value to the battery industry and to be a powerful technique in the investigation of MnO_2-H insertion compounds [18, 49].

The information obtained with this technique is that of the intensity of diffraction (as counts per second) against 2θ, where θ is the angle (in degrees) between an atomic plane in a crystal and both the incident and diffracted beams. Peak positions are then related to the separation between parallel atomic planes by the Bragg equation :

$$\mathbf{n}\,\lambda = \mathbf{2}\,\mathbf{d}\,\mathbf{sin}\,(\theta) \qquad (9)$$

where λ is the wavelength of the X-rays and d is the interplanar spacing, both in the same units (commonly angstroms), and n is the order of diffraction (1, 2, ..., n) with no units.

X-ray diffraction (XRD) has been used to establish the structures of various crystalline forms of manganese dioxide. It involves the identification and location of manganese, oxygen and hydrogen in the unit cells. Studies and reviews concerning this technique have been widely presented [42, 50-...-56]. Fleischer and Richmond [57], Brenet and Héraud [58], and Cole et al [59] used XRD to characterise a large number of manganese dioxides obtained by various methods, and the crystal phases such as α, β, γ, δ, and ε were identified. Most of the ambiguities involved in the nomenclature have been

resolved by Tauber [60]. Nye et al [61] were the first to provide a basis for describing the crystal structure of the dioxides by tracing their genesis to MnO.OH compounds. The structures certainly involve near hexagonal close packing of oxygen and hydroxyl ions with half of the octahedral sites occupied by Mn^{4+} and some Mn^{3+} ions. Consequently, octahedra form in which the Mn^{4+} ion is surrounded by six O^{2-} ligands [50].

Synthetic γ-manganese dioxides exhibit a wide range of differing crystal structures characterised mainly by their x-ray diffraction patterns [62, 63]. These range from a peak rich variety with some peaks showing selective broadening and shifts from the positions of orthorhombic ramsdellite to that of a typical commercial Electrodeposited Manganese Dioxide (EMD) which normally displays only six broad peaks reflecting apparent hexagonal symmetry [64] (peaks labelled in this work A to F, following the nomenclature used by Fitzpatrick and Tye [18]). A typical EMD pattern is shown in Figure 3.1.

Both the anomalous broadening and the shift are satisfactorily explained on the basis of a structural model consisting of randomly alternating layers of ramsdellite and pyrolusite units (de Wolff model [6, 65]). In view of this random structural intergrowth, regular periodicity of a superlattice is not apparent [66]. Such lattice disorder causes synthetic γ-manganese dioxides phases to have extensive defects and vacancies as well as to be non-stoichiometric and impure [43]. These factors, together with the small crystallite sizes of natural and synthetic phases, give rise to a variety of X-ray powder diffraction lines, as well as the observed asymmetric and selective line broadening.

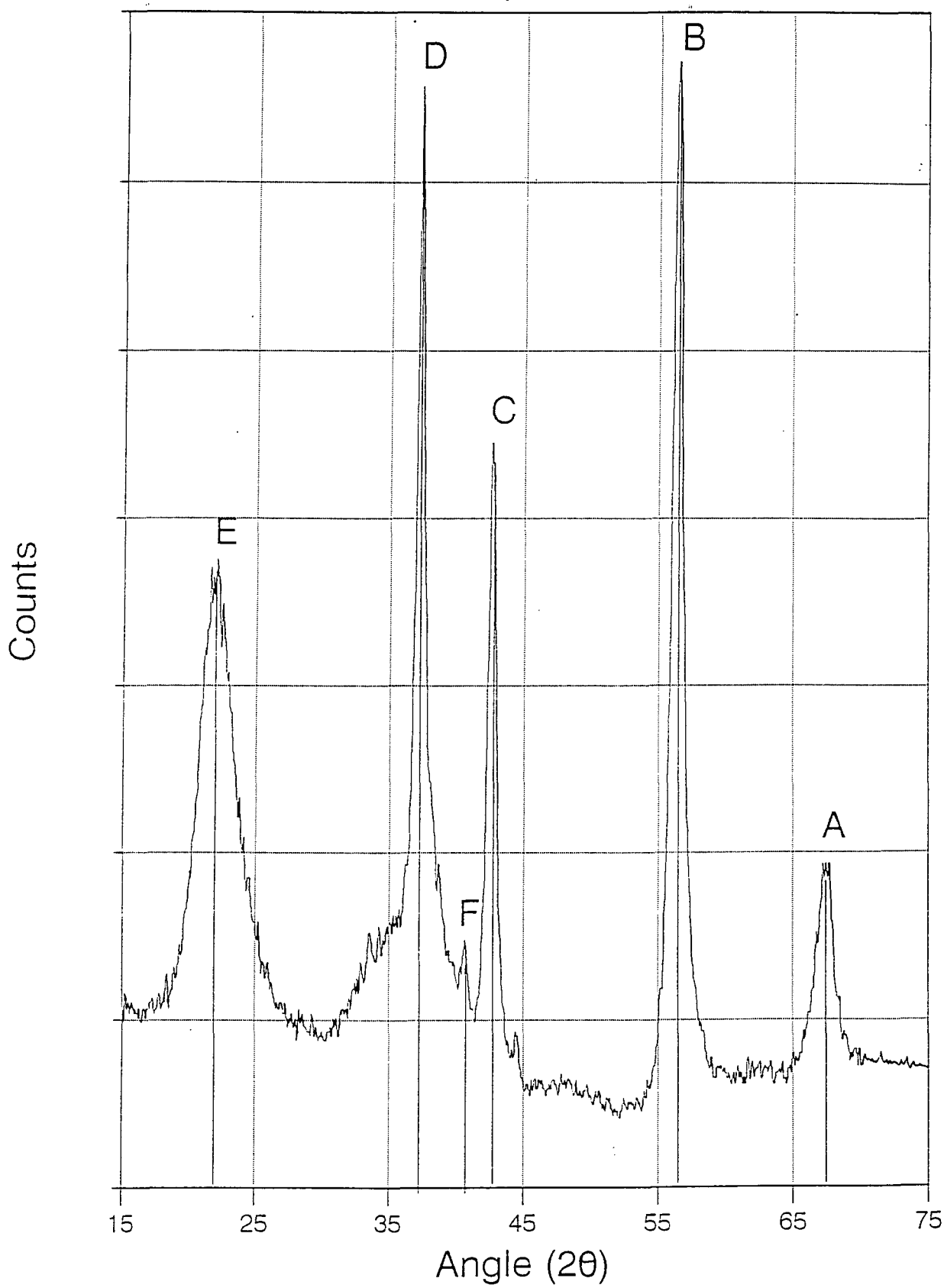

Figure 3.1.- Typical EMD X-ray diffraction pattern with the peak nomenclature here employed.

Pannetier and Chabre [64, 7] have succeeded in explaining the range of observed powder x-ray diffraction patterns with a new structural model which incorporates two types of crystal defects into an idealised ramsdellite host structure. The first type of defect is the above mentioned "de Wolff defect" which exploits the fact that ramsdellite and pyrolusite possess intimately related structures due to the similarity of their oxygen frameworks. The pyrolusite structure may be described as infinite single chains of edge sharing octahedra which are connected by corners to other single chains whereas the ramsdellite structure contains double chains (See Figure 3.2).

The second type of defect is that of random microtwinning of the ramsdellite structure on some specific planes. A full description of this type of fault may be found in [7] (Figure 3.3). Effectively microtwinning introduces a second type of random disorder.. The results of this new structural model explains why the X-ray pattern of EMD possesses apparent hexagonal symmetry. The reason being that certain peaks in the X-ray diffraction pattern coalesce into combined peaks as the microtwinning percentage approaches 100% [67]. Following this explanation, a new classification of γ-manganese dioxides has been recently proposed by Chabre and Pannetier [7], providing a model characterised by only two numbers : P_r for the amount of de Wolff disorder and T_w for microtwinning. They concluded from an analysis of several XRD patterns that most available γ-manganese dioxides fall into four main families :

a.- Natural ramsdellite which appears to contain very little structural defects.

b.- Chemical manganese dioxides (CMD) with microtwinning percentages in the range 20-40 % and de Wolff defect value close to 0.3.

c.- Electrolytic manganese dioxides (EMD) with microtwinning percentage close to 100 % and de Wolff defect value in the range 0.45 to 0.5.

d.- Heat-treated γ-manganese dioxides with low microtwinning percentage (less than 20 %) but de Wolff defect close to 0.7 or larger.

It is now well established that γ-manganese dioxides act as host structures for H insertion [9, 11, 17, 18, 68]. Although a new insight into the crystal structures of these host materials has emerged [7, 64, 69, 70, 71], the nature of the H inserted derivatives whether they are produced in a battery or by chemical insertion techniques has not been resolved.

By measuring d versus r in $MnOOH_r$ (or x in MnO_x) insight may be obtained into changes in structure which occur during dilation by H insertion into a manganese dioxide. In general, sharp changes in slope or discontinuities in the lattice parameters of a solid solution with composition may be connected with changes in symmetry of the crystal lattice [72]. Following this idea, powder X-ray diffraction of the reduced samples was used in order to establish whether the H insertion occurred homogeneously or heterogeneously in the two reduction methods studied.

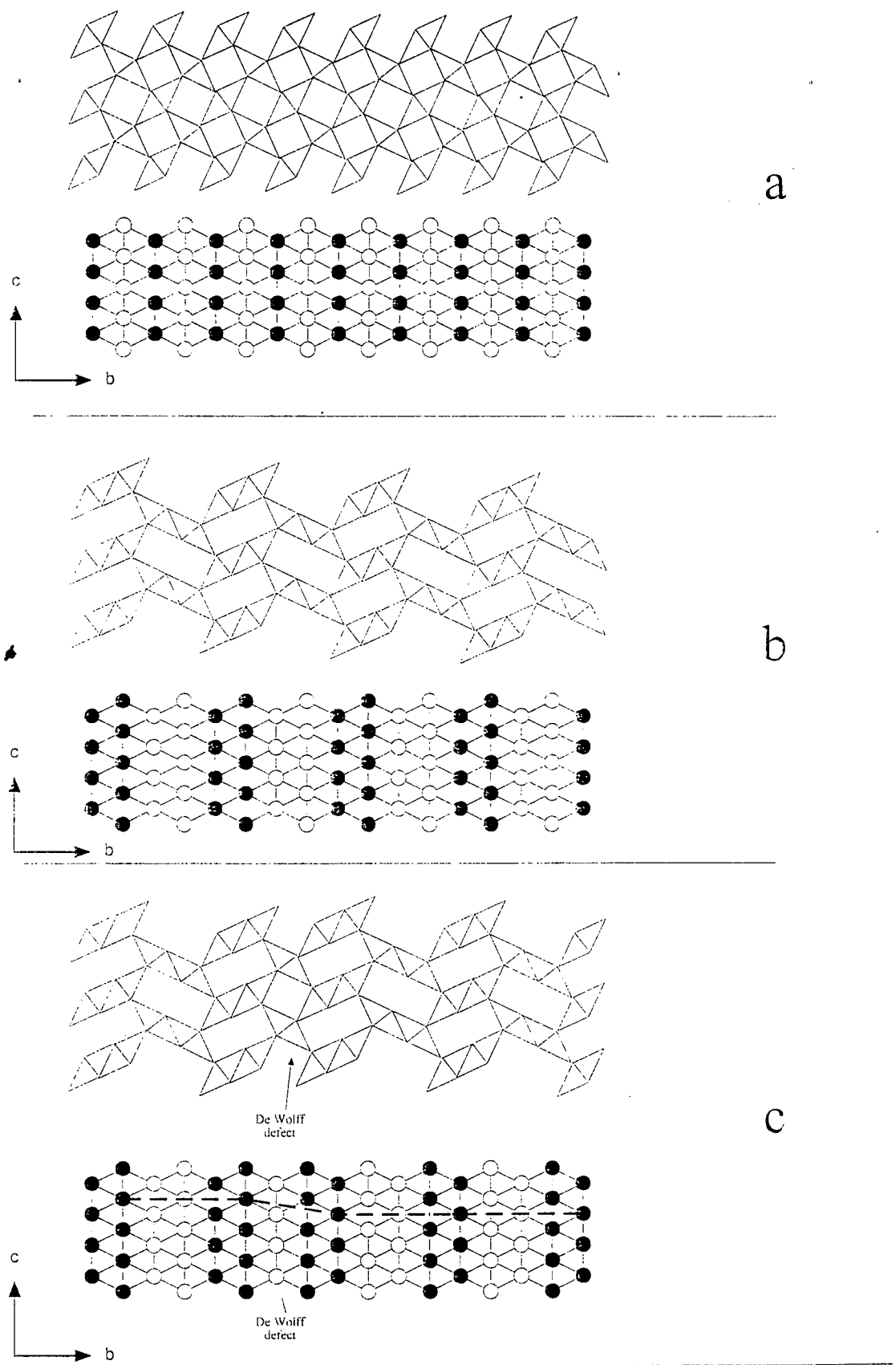

Figure 3.2.- From [7]. Schematic representation of a few MnO_2 polymorphs:
Usual polyhedral representation (up).
Lattice gas representation of the cationic lattice (bottom). Oxygen lattice omitted for clarity, full and empty circles refer to Mn atoms with different x coordinates, e.g., x=0 and 1/2.

a pyrolusite ß-MnO_2: "Single" chains.
b ramsdellite: "Double" chains.
c y-MnO_2: de Wolff deffect.

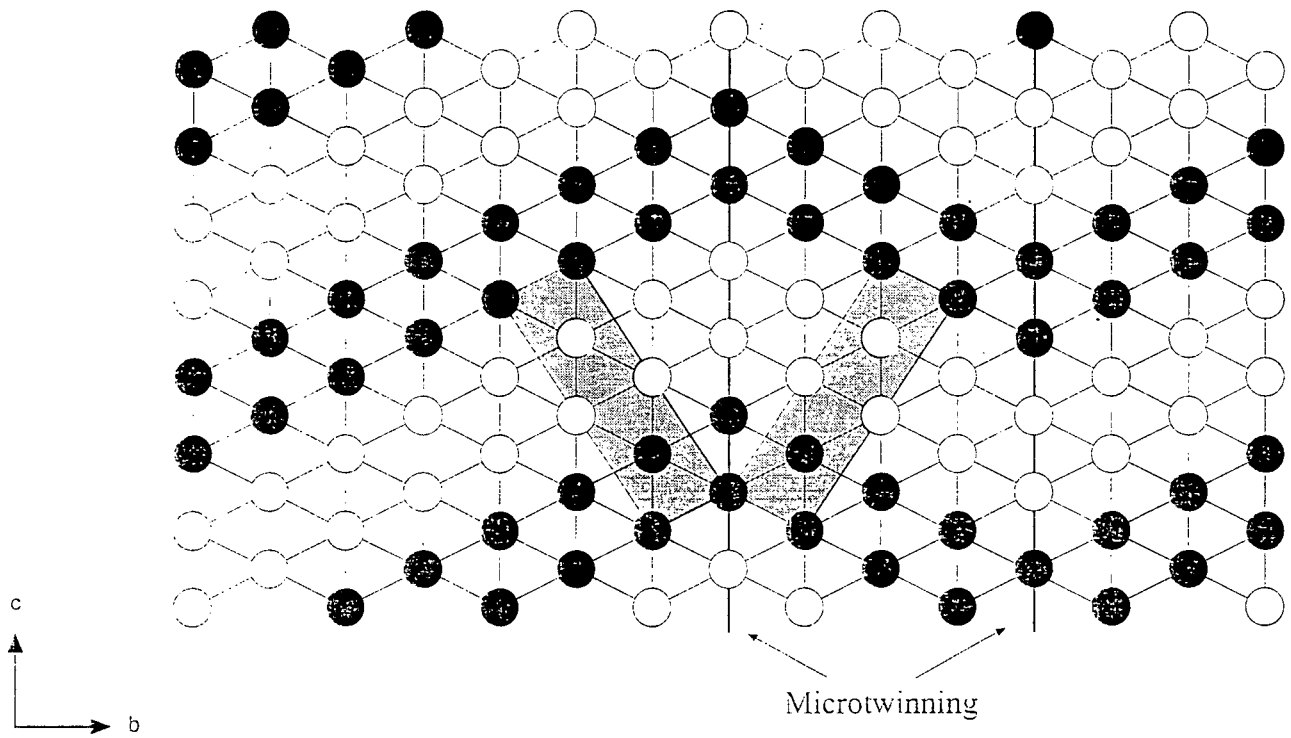

Figure 3.3.- From [7]. Schematic representation of microtwinning. Only Mn atoms are represented. Full circles: x=0; Open circles: x=1/2

3.1.- EXPERIMENTAL METHOD

The following equipment manufactured by Phillips and controlled by APD 1700 Software was employed:

- PW 1730/10 high performance 4 kW 60 kV constant potential generator.
- PW 2253/20 broad focus copper anode X-ray tube (Cu $\alpha_{1,2}$ wavelengths = 1.54060, 1.54439 angstroms).
- PW 1050/81 goniometer and step motor.
- PW 1710/00 diffractometer control.
- PW 1752/00 graphite monochromator.
- PW 1711/10 xenon proportional counter.
- PW 1170/00 sample changer.

The conditions used for all the patterns here reported were:

- Generator set at 45 kV and 55 mA.
- Goniometer scan speed of 0.01° of 2θ per second (0.01°/s).
- Diffractometer settings of 1° for the divergence and scatter slits and 0.1 mm for the receiving slit.
- Proportional counter pulse height selection between 35 and 70%.
- Scans were taken from 2θ = 10° to 2θ = 75°.
- Minimum peak significance : 0.80.
- Peak position criterion was top of smoothed data.

All samples were ground in an agate mortar for about 3 minutes. Grinding of the samples helped to increase the "randomness" of the crystallites "making them free" from large particles, without affecting the crystalline structure. Samples were them back-filled into aluminium sample holders and pressure applied against a glass plate to ensure a flat form surface.

Because the XRD source gradually decreases in intensity with use, all patterns were normalised to a fixed source intensity by adjusting them by a factor which gives a constant area for the 2θ=26.429 peak of Arkansas stone. Smoothing of the data was carried out in order to minimise the effect of noise produced during the measurement. The method involved calculation of the moving average for a series of adjacent 2θ steps; in this work three 0.01° steps spanning the designated 2θ value were used.

3.2.- PEAKS REPRODUCIBILITY/PRECISION STUDY.-

Provided a material has sharp X-ray lines, the error in the precision with which peak positions are determined can be reduced to almost negligible proportions. This is not the case with EMD. Two techniques for improving the precision of determination of peak positions are described below :

i.- Addition of a calibration substance. This correction is made by linear extrapolation between two peaks of the calibration substance of accurately known position situated on either sides of the measured EMD peaks. The ideal calibration substance should have maxima near, but not overlapping, those being measured and have sharp peaks which can be measured precisely. It also should have no chemical action neither form solid solutions with the substance to be measured.

ii.- Using CuKα radiation (α_1 wavelength = 1.54060 A, α_2 wavelength = 1.54439 A), above 40° 2θ, the Kα_1, α_2 doublet just begins to be resolved and at 58° 2θ is essentially completely resolved. Thus, an artificial shift in line position is produced by the automatic fitting program employed by the software (the program fits a parabola to nine points around the top of the peak). Precision could be improved by using appropriate software to eliminate the Kα_2 component.

In order to check the precision and provide a basis for comparison with improved techniques, eight different samples of CEGASA EMD were prepared in different sample holders. The average peak position and the standard deviation obtained are shown in Table 3.1.

As in this study of the propan-2-ol and hydrazine hydrate reduced samples, series of triplicate measurements were carried out, it means that 95% of the means of the triplicates will be within $\pm 1.96\sigma_{n-1}/\sqrt{3}$ of the true mean.

Table 3.1.- Estimates of peak position average and standard deviation from eight samples.

PEAK	E	D	F	C	B	A
2θ	21.8273	37.2262	40.6751	42.6624	56.4149	67.6052
σ_{n-1}	0.1342	0.0745	0.0735	0.0484	0.0764	0.0775
$1.96\sigma_{n-1}/\sqrt{3}$	0.1519	0.0843	0.0832	0.0548	0.0865	0.0877

Looking at Table 3.1, an acceptable precision was obtained with $1.96\sigma_{n-1}/\sqrt{3}$ values less than 0.1, except for peak E (the software peak detection presents problems with this type of broad peak). Anyway, this peak is the least useful for establishing if the H insertion occurs homogeneously or heterogeneously.

3.2.1.- Improvement technique (i).

A substance commonly used as external source of reference is KCl (JCPDS card 4-0587). 0.3 g of KCl plus 1.2 g of EMD were mixed, and three samples prepared and mounted as previously described. The peak positions obtained with CEGASA EMD with and without systematic error correction with KCl peaks are shown in Table 3.2.

Table 3.2.- Systematic error correction with KCl as external source of reference (Values of 2θ) and F values obtained from ANOVA.

PEAK	E	D	F	C	B	A
Without correction	21.9253	37.2834	-----	42.6752	56.6449	67.6392
σ_{n-1}	0.1778	0.0144		0.0256	0.0999	0.0662
With Correction	21.9371	37.2725	-----	42.6575	56.5725	67.6217
σ_{n-1}	0.1690	0.0050		0.0222	0.0649	0.0482
F-ratio	0.001	1.533	-----	0.816	1.110	0.131

As reflected in this table (σ_{n-1}), although an improvement was achieved with the use of this external source of reference in some of the peaks, it was not as high as expected.

The tabulated F value for this case with a confidence level of 95% ($F_{95\%}(1,4)$) is equal to 7.71. As the F values obtained for all the peaks were lower than this value, this indicates that there was no significantly difference between the peak values obtained with and without this correction. Moreover, two of the EMD peaks were "contaminated" by the proximity of KCl peaks.

3.2.2.- Improvement technique (ii).

With respect to the filtering of the $K\alpha_2$ component, a very small improvement was achieved (only used together with an external source of reference), but with considerable loss in intensity, which made the procedure inadvisable for the present study.

Because of the acceptable precision/reproducibility obtained, and the problems found with the different attempts to improve the data, it was decided to use the sample procedure without refinements for the X-ray pattern of the reduced samples. Three different holders were prepared with each reduced sample and the peak positions were determined as the average of the three X-ray patterns. In this way, the error limits were those mentioned in Table 3.1. for a 95% probability as $1.96\sigma_{n-1}/\sqrt{3}$..

3.3.- PROPAN-2-OL REDUCED SAMPLES.

Peak positions (2θ) and the interplanar spacings obtained from Bragg's law for the complete range of reduction from the first, second, third and fourth sets of samples obtained with the propan-2-ol reduction method reported in section 2.1.1. are shown in Table 3.3. (as an average value of at least three diffractograms for every r or x value).

In the same way, the pattern evolution with the reduction degree of the samples is shown in Figure 3.4, where the nomenclature for the new peaks which appear is presented. The only difference in the nomenclature employed in this work from the one proposed by Fitzpatrick and Tye [18] is the peak labelled H by Fitzpatrick, which it is assumed in this research to be peak F'. The peak that occasionally appeared at 44.6° , was due to the aluminium sample holder and has nothing to do with the $MnOOH_r$ patterns.

When looking at Figure 3.4. it is possible to note that the insertion of H up to r values close to 0.7 proceeded without any change in the main features of the diffraction patterns, except the movement of peak positions due to lattice dilation and some changes in intensity, as is well known in the literature [9, 11, 17, 18, 19, 25, 26, 73]. So, up to this r value, the evolution did not show the emergence of additional diffraction peaks.

At higher insertion values (greater than r=0.8), the main peaks decreases substantially in intensity, and new peaks emerged (I, J, manganite and G), as also noted by Fitzpatrick and Tye [18].

The former peaks continue to shift with insertion level. Tye and Tye [74] explained that this indicates the coexistence of solid solution and final product at the higher levels of insertion. Moreover, in this region, H mobility appears to be partially restricted due to the presence of stable microdomains of the end-product. Maclean and Tye [75] have pointed out that some shearing at microtwinning planes occurs in this region of high reduction level.

It is worth noting that these differences in behaviour of the XRD patterns correspond to the region where, as previously explained in 2.1.1., the insertion in the solid solution of $MnOOH_x$ was very difficult to achieve.

Table 3.3.-Peak position(2θ) and interplanar spacings(Å) of the samples reduced with propan-2-ol.

ANGLE (2θ)

x	r	E	Mangan	J	D'	D	I	F'	F	C'	C	B'	B	G	A'	A
1.964	0.072	21.830				37.230			40.680		42.660		56.420			67.610
1.949	0.102	21.740				37.231			40.615		42.598		56.351			67.442
1.924	0.152	21.837				37.234			40.555		42.650		56.315			67.393
1.886	0.228	21.925				37.132			40.262		42.523		56.141			67.186
1.867	0.266	21.705				37.120			40.132		42.500		56.124			67.161
1.841	0.318	21.784				36.987			39.999		42.248		55.996			66.806
1.806	0.388	21.595				36.880			39.955		42.185		55.610			66.680
1.784	0.433	21.700				36.750			39.863		42.035		55.333			66.313
1.775	0.451	21.625				36.595			39.755		41.850		55.130			65.985
1.769	0.462	21.704				36.720			39.856		42.008		55.340			66.200
1.745	0.510	21.630				36.625			39.780		41.870		55.215			65.950
1.720	0.560	21.833				36.660			39.803		41.933		55.255			66.093
1.696	0.608	21.943				36.507			39.723		41.777		55.140			65.740
1.648	0.704	21.825				36.235			39.770		41.530		54.885			65.170
1.609	0.782	21.320		34.370		36.055			39.825		41.405		54.685	62.040		65.040
1.587	0.826	21.125		34.120		35.885			39.780		41.250		54.725			64.995
1.558	0.884	21.306	26.140	33.997		35.768	37.584		39.765		41.131		54.635	62.070		64.896
1.539	0.922	21.087	26.260	33.516		35.229	37.424		39.580		40.653		54.236	61.601		64.676
1.527	0.946	21.267	26.195	33.596		35.210	37.167		39.360		40.623		54.179	61.602		64.635
1.519	0.962	20.909	26.211	33.461		35.153	36.898		39.354		40.435		54.022	61.625		64.622

Interplanar spacings (Angstroms)

x	r	E	Mangan	J	D'	D	I	F'	F	C'	C	B'	B	G	A'	A
1.964	0.072	4.073				2.416			2.219		2.120		1.632			1.386
1.949	0.102	4.090				2.416			2.222		2.123		1.633			1.389
1.924	0.152	4.072				2.416			2.225		2.121		1.634			1.390
1.886	0.228	4.056				2.422			2.241		2.127		1.639			1.394
1.867	0.266	4.096				2.423			2.248		2.128		1.639			1.394
1.841	0.318	4.082				2.431			2.255		2.140		1.643			1.401
1.806	0.388	4.117				2.438			2.257		2.143		1.653			1.403
1.784	0.433	4.097				2.447			2.262		2.150		1.661			1.410
1.775	0.451	4.111				2.457			2.268		2.159		1.667			1.416
1.769	0.462	4.096				2.449			2.263		2.152		1.661			1.412
1.745	0.510	4.110				2.455			2.267		2.158		1.664			1.417
1.720	0.560	4.073				2.452			2.266		2.155		1.663			1.414
1.696	0.608	4.052				2.462			2.270		2.163		1.666			1.421
1.648	0.704	4.074				2.480			2.267		2.175		1.674			1.432
1.609	0.782	4.169		2.610		2.492			2.264		2.182		1.679	1.497		1.435
1.587	0.826	4.207		2.629		2.504			2.267		2.189		1.678			1.436
1.558	0.884	4.172	3.410	2.638		2.511	2.394		2.268		2.196		1.681	1.496		1.437
1.539	0.922	4.215	3.395	2.675		2.549	2.404		2.278		2.220		1.692	1.506		1.442
1.527	0.946	4.180	3.403	2.669		2.550	2.420		2.290		2.222		1.694	1.506		1.443
1.519	0.962	4.250	3.401	2.679		2.554	2.437		2.290		2.232		1.698	1.506		1.443

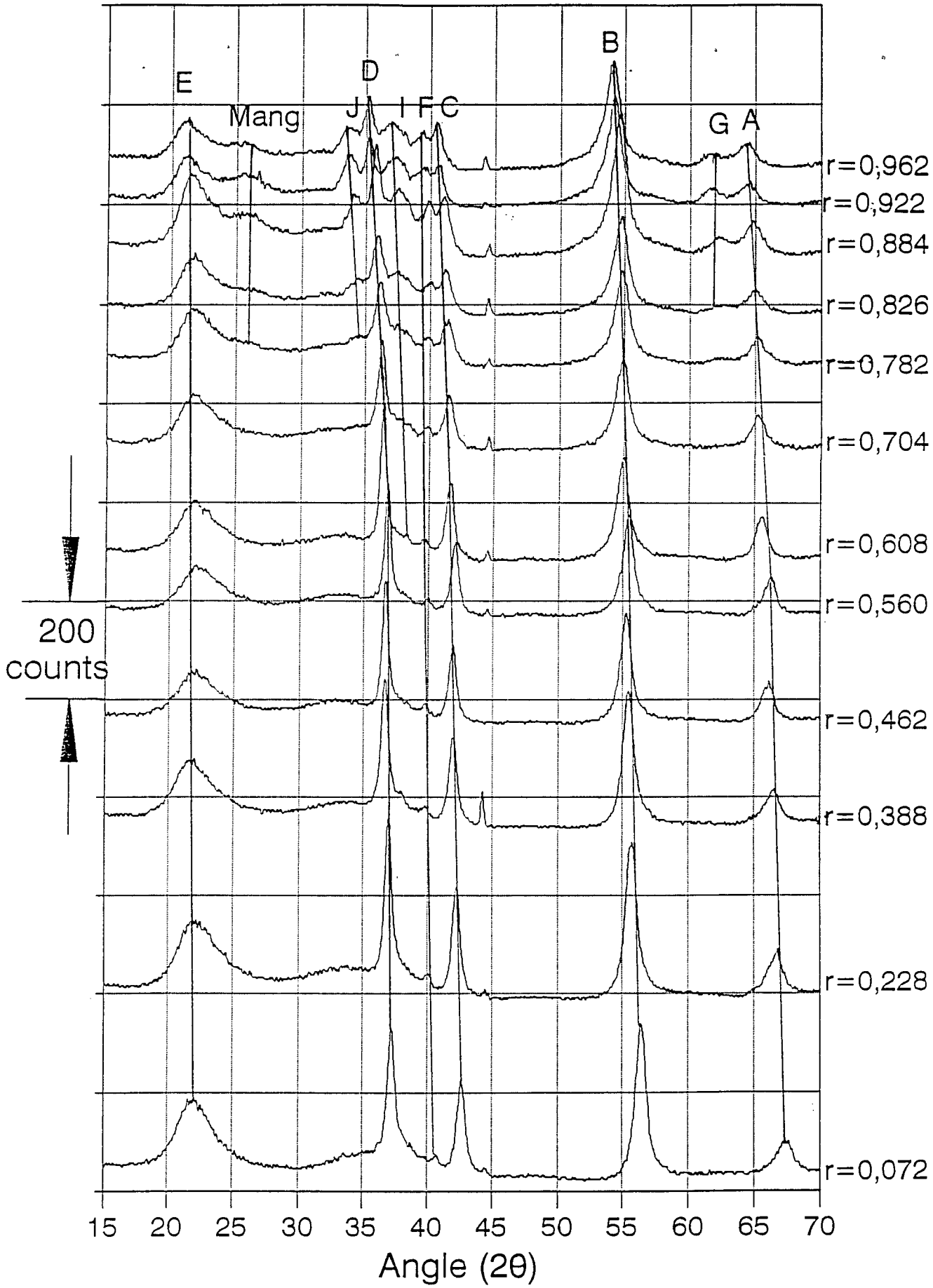

Figure 3.4.- X-ray diffraction evolution for propanol-2-ol reduction method

3.4.- HYDRAZINE HYDRATE REDUCED SAMPLES.

The complete peak positions (2θ), and the interplanar spacings obtained from Bragg's law for the fifth and sixth sets of samples obtained with the hydrazine hydrate reduction reported in section 2.1.2. are expressed in Table 3.4 (as an average value of at least three diffractograms carried out with each sample).

In a similar way as was done with the Propan-2-ol reduced samples, the pattern evolution with the reduction degree of the samples is presented in Figure 3.5. On this occasion, an heterogeneous behaviour of the reduction is clearly observed when r increases above 0.380. The heterogeneous behaviour is shown by the appearance of new peaks which grow at the expense of the original ones. This is shown with more detail in Figures 3.6, 3.7, and 3.8. The new "manganite peaks" which also appear at the end of the reduction are shown in Figure 3.9.

Therefore, clear differences exist between this evolution and the one already discussed for the Propan-2-ol reduced samples in section 3.3., where the new peaks that appear in these hydrazine samples are not present at such low H insertion levels. With the Propan-2-ol method, the new lines only appear at r values of 0.8 and above. Towards the end of the reduction, the patterns begin to look very similar in both methods, being almost identical for the final reduction products (r value very close to 1).

The appearance of the new peaks in the diffraction patterns at such a low degree of reduction has not been reported to the author's knowledge, and must be a clear consequence of the reduction method employed. It should be noted that the large number of samples produced was essential to confirm that the new peaks were growing at expenses of the old ones, as this enabled changes in the X-ray patterns to be followed over very small ranges of r (0.04-0.06) (x: 0.02-0.03).

Table 3.4.-Peak position(2θ) and interplanar spacings(Å) of the samples reduced with hydrazine.

ANGLE (2θ)

x	r	E	Mangan	J	D'	D	I	F'	F	C'	C	B'	B	G	A'	A
1.964	0.072	21.827				37.226			40.675		42.662		56.415			67.605
1.935	0.130	21.844				37.227			40.609		42.667		56.343			67.412
1.915	0.170	21.830				37.241			40.492		42.613		56.285			67.374
1.895	0.210	22.047				37.149			40.399		42.535		56.169			67.234
1.867	0.266	21.802				37.114			40.143		42.512		56.114			67.141
1.842	0.316	21.654				37.037			40.046		42.410		56.020			67.161
1.810	0.380	21.623		34.083	35.765	36.986		39.806			42.317	54.584	55.828		65.049	66.895
1.800	0.400	21.073		33.904	35.617	36.849		39.746			42.195	54.579	55.730		65.006	66.717
1.768	0.464	21.532		33.910	35.674	36.948		39.841			42.247	54.571	55.727	61.881	65.002	66.694
1.752	0.496	21.425	26.132	33.984	35.659	36.869		39.831		41.071	42.139	54.601	55.610	61.965	64.978	66.535
1.741	0.518	21.360	26.121	33.919	35.547	36.807		39.718		41.011	42.053	54.553	55.561	61.712	64.945	66.500
1.721	0.558	21.322	26.165	33.904	35.625	36.833		39.757		41.059	42.125	54.551	55.604	61.769	65.015	66.544
1.689	0.622	21.526	26.139	33.923	35.661	36.751		39.782		41.030	42.029	54.613	55.350	61.750	65.131	66.270
1.682	0.636	21.382	26.216	33.965	35.609	36.726	37.992	39.746		40.974	42.042	54.568		61.675	64.996	66.097
1.676	0.648	21.345	26.017	33.897	35.587	36.679		39.697		40.927	41.967	54.572		61.828	64.975	66.206
1.652	0.696	21.368	25.980	33.930	35.631	36.768	37.828	39.741		41.013	41.969	54.587		61.631	65.010	
1.634	0.732	21.348	26.306	33.986	35.677	36.739	38.002	39.816		41.048		54.596		61.791	65.007	
1.615	0.770	21.193	26.084	33.847	35.553		37.462	39.690		40.944		54.515		61.718	64.901	
1.598	0.804	21.251	26.174	33.948	35.565		37.671	39.732		40.970		54.535		61.705	64.906	
1.585	0.830	21.458	25.914	33.886	35.603		37.577	39.661		41.028		54.548		61.882	65.003	
1.569	0.862	21.262	26.118	33.900	35.624		37.404	39.655		41.007		54.587		61.690	65.043	
1.562	0.876	21.297	26.034	33.862	35.564		37.399	39.755		40.946		54.504		61.825	64.933	
1.550	0.900	21.283	26.174	33.927	35.638		37.420	39.748		41.053		54.614		61.825	65.013	
1.527	0.946	21.175	26.178	33.858	35.579		37.308	39.693		40.951		54.495		61.676	64.990	
1.522	0.956	21.358	26.209	33.980	35.656		37.441	39.832		41.075		54.653		61.871	65.083	
1.506	0.988	21.094	26.143	33.815	35.511		37.367	39.604		40.949		54.463		61.633	64.935	

Interplanar spacings (Angstroms)

x	r	E	Mangan	J	D'	D	I	F'	F	C'	C	B'	B	G	A'	A
1.964	0.072	4.072				2.415			2.218		2.119		1.631			1.386
1.935	0.130	4.069				2.415			2.222		2.119		1.633			1.389
1.915	0.170	4.071				2.414			2.228		2.122		1.634			1.390
1.895	0.210	4.032				2.420			2.233		2.125		1.638			1.392
1.867	0.266	4.076				2.422			2.246		2.126		1.639			1.394
1.842	0.316	4.104				2.427			2.251		2.131		1.642			1.394
1.810	0.380	4.110		2.631	2.511	2.430		2.264			2.136	1.681	1.647		1.434	1.399
1.800	0.400	4.216		2.644	2.521	2.439		2.268			2.142	1.681	1.649		1.435	1.402
1.768	0.464	4.127		2.643	2.517	2.433		2.263			2.139	1.682	1.649	1.499	1.435	1.402
1.752	0.496	4.147	3.410	2.638	2.518	2.438		2.263		2.198	2.144	1.681	1.653	1.498	1.435	1.405
1.741	0.518	4.160	3.411	2.643	2.525	2.442		2.269		2.201	2.149	1.682	1.654	1.503	1.436	1.406
1.721	0.558	4.167	3.406	2.644	2.520	2.440		2.267		2.198	2.145	1.682	1.653	1.502	1.434	1.405
1.689	0.622	4.128	3.409	2.643	2.518	2.445		2.266		2.200	2.150	1.680	1.660	1.502	1.432	
1.682	0.636	4.156	3.399	2.639	2.521	2.447	2.368	2.268		2.203	2.149	1.682		1.504	1.435	
1.676	0.648	4.163	3.425	2.645	2.523	2.450		2.270		2.205	2.153	1.682		1.501	1.435	
1.652	0.696	4.158	3.430	2.642	2.520	2.444	2.378	2.268		2.201	2.153	1.681		1.505	1.435	
1.634	0.732	4.162	3.388	2.638	2.517	2.446	2.368	2.264		2.199		1.681		1.501	1.435	
1.615	0.770	4.192	3.416	2.648	2.525		2.401	2.271		2.204		1.683		1.503	1.437	
1.598	0.804	4.181	3.405	2.641	2.524		2.388	2.269		2.203		1.683		1.503	1.437	
1.585	0.830	4.141	3.438	2.645	2.522		2.394	2.272		2.200		1.682		1.499	1.435	
1.569	0.862	4.179	3.412	2.644	2.520		2.404	2.273		2.201		1.681		1.504	1.434	
1.562	0.876	4.172	3.423	2.647	2.524		2.404	2.267		2.204		1.684		1.501	1.436	
1.550	0.900	4.175	3.405	2.642	2.519		2.403	2.268		2.199		1.680		1.501	1.435	
1.527	0.946	4.196	3.404	2.647	2.523		2.410	2.271		2.204		1.684		1.504	1.435	
1.522	0.956	4.160	3.400	2.638	2.518		2.402	2.263		2.197		1.679		1.500	1.433	
1.506	0.988	4.212	3.408	2.651	2.528		2.407	2.276		2.204		1.685		1.505	1.436	

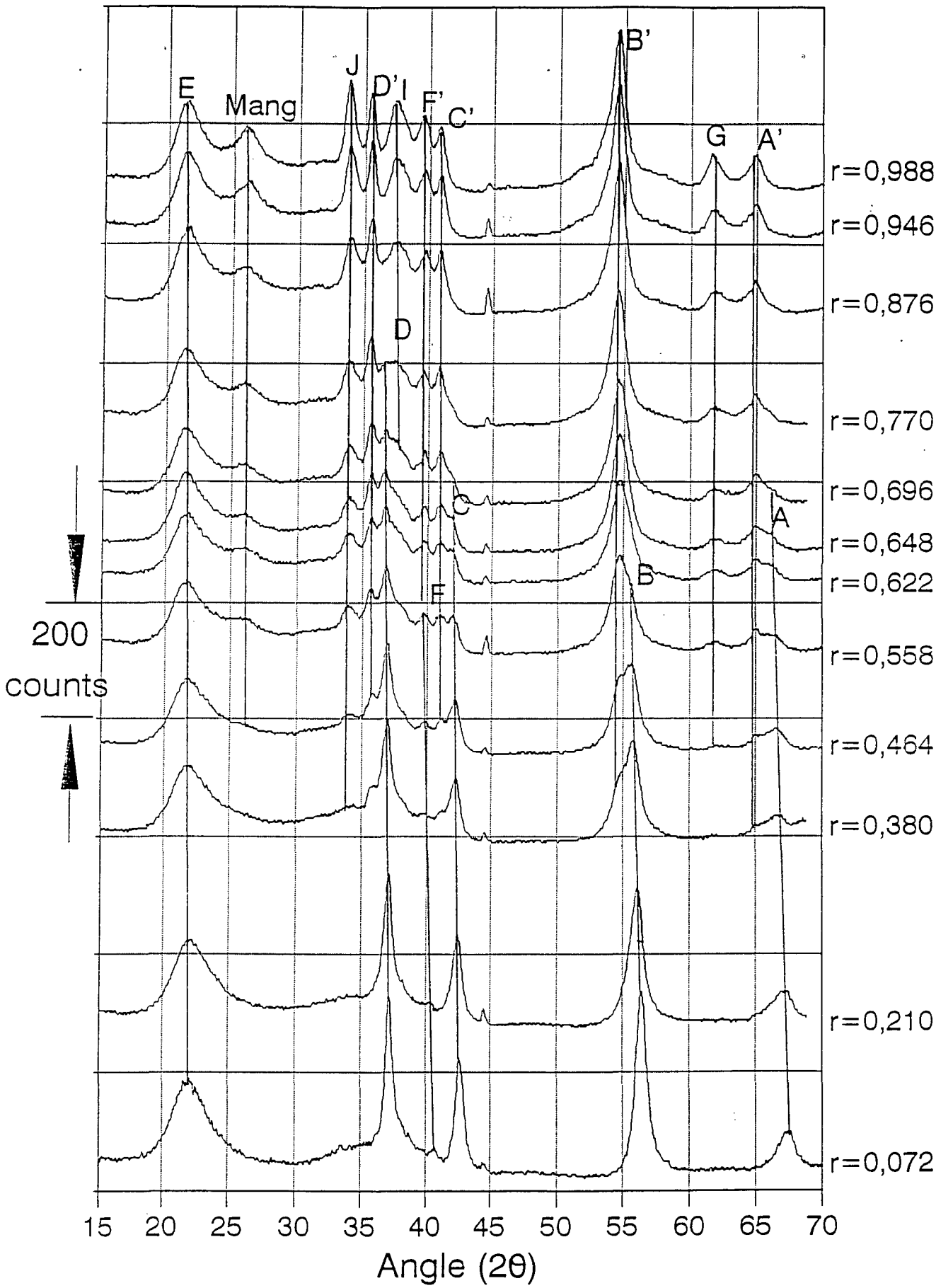

Figure 3.5.- X-ray diffraction evolution for hydrazine reduction method

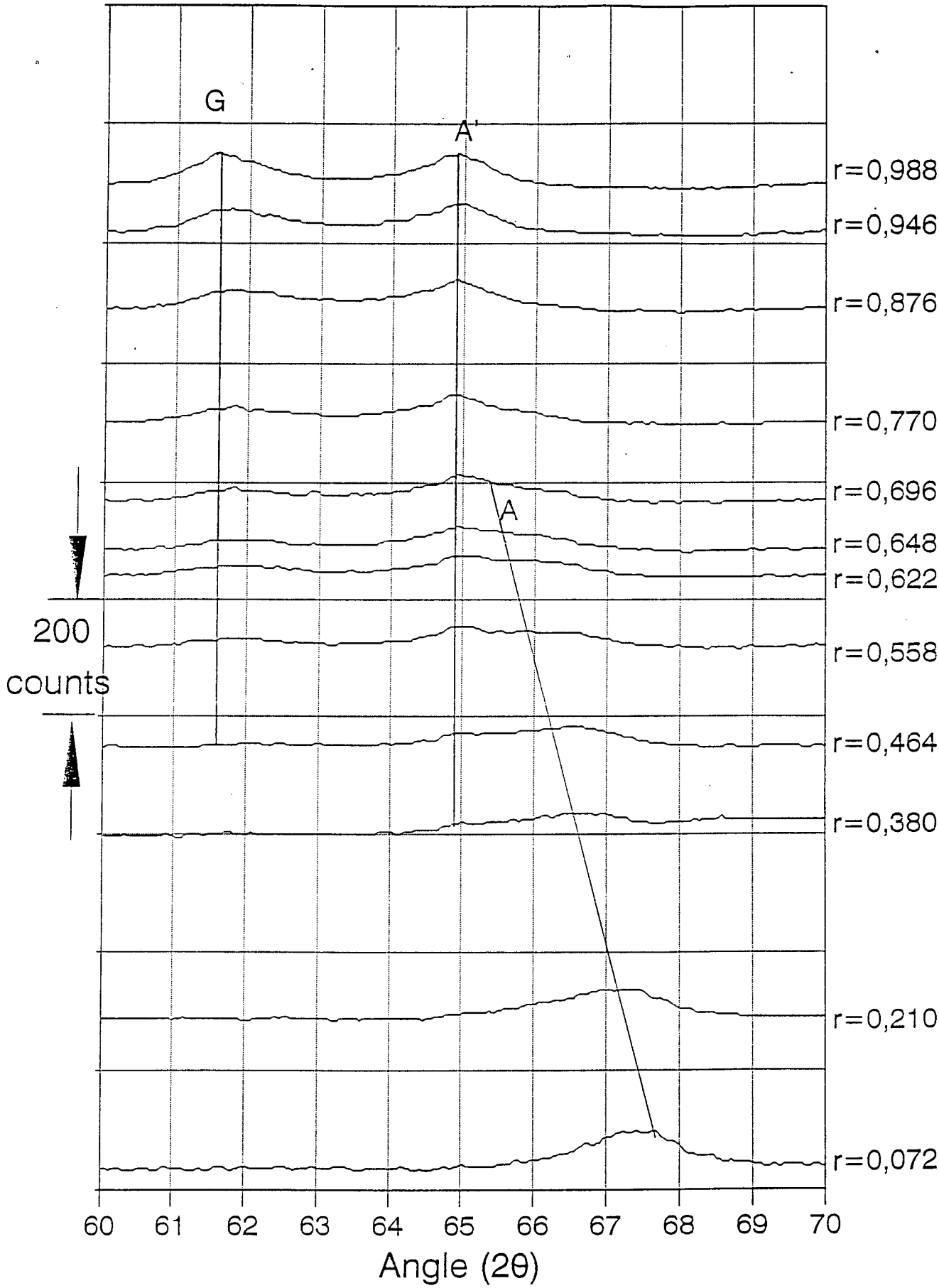

Figure 3.6.- Peaks A, A' and G evolution hydrazine reduction method

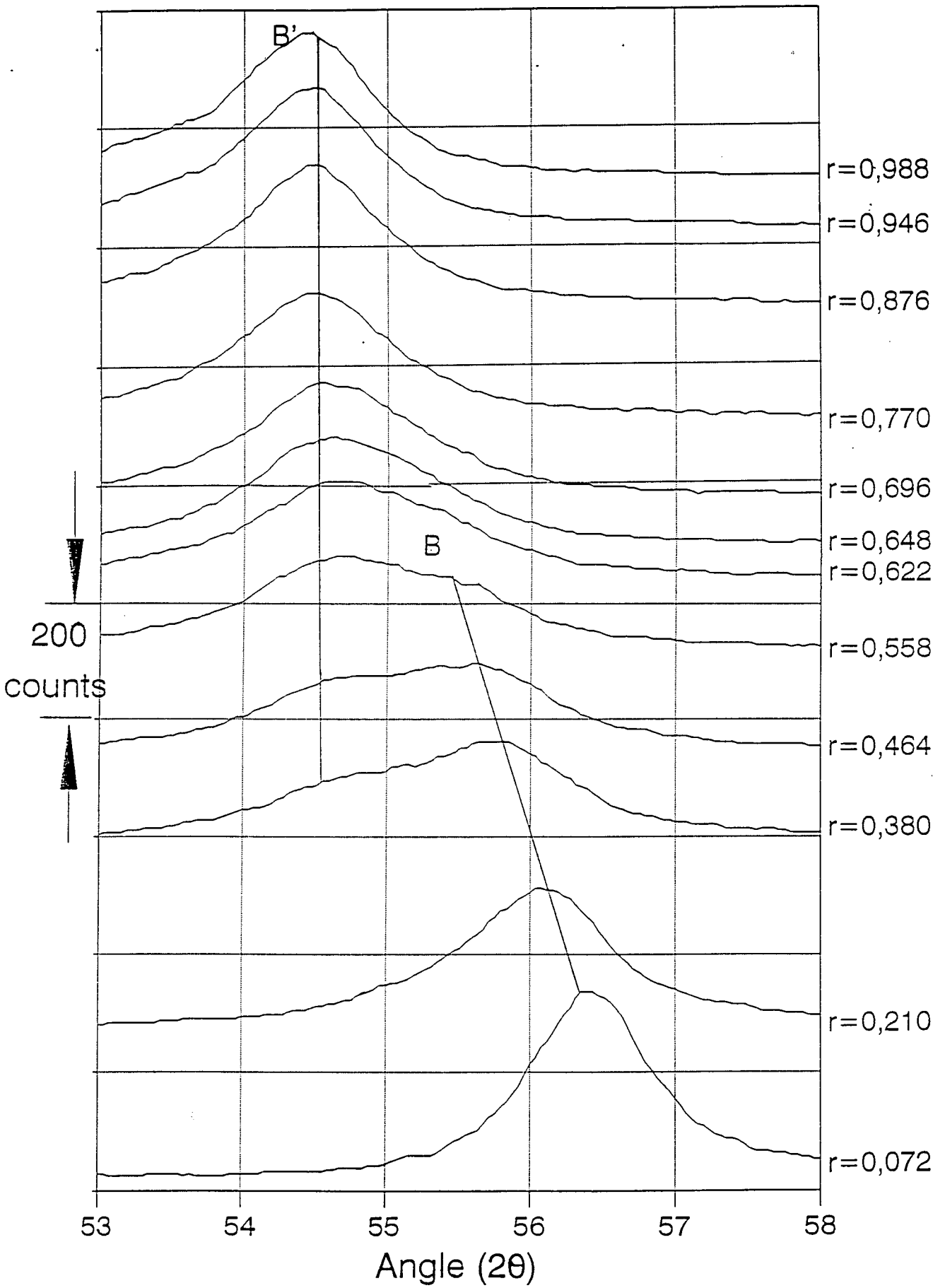

Figure 3.7.- Peaks B and B' evolution hydrazine reduction method

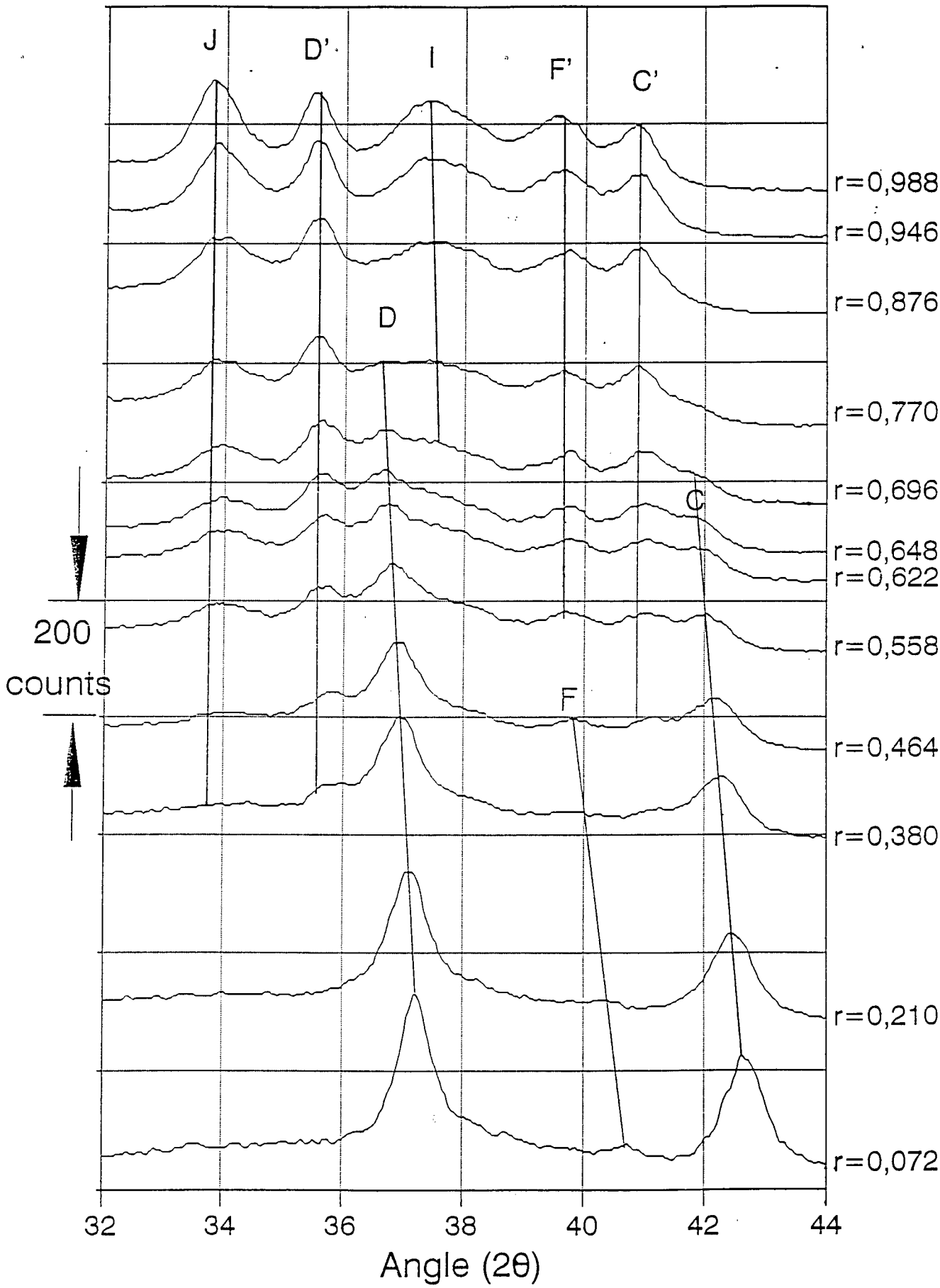

Figure 3.8.- Peaks C, C', F, F', I, D, D' and J evolution hydrazine reduction method

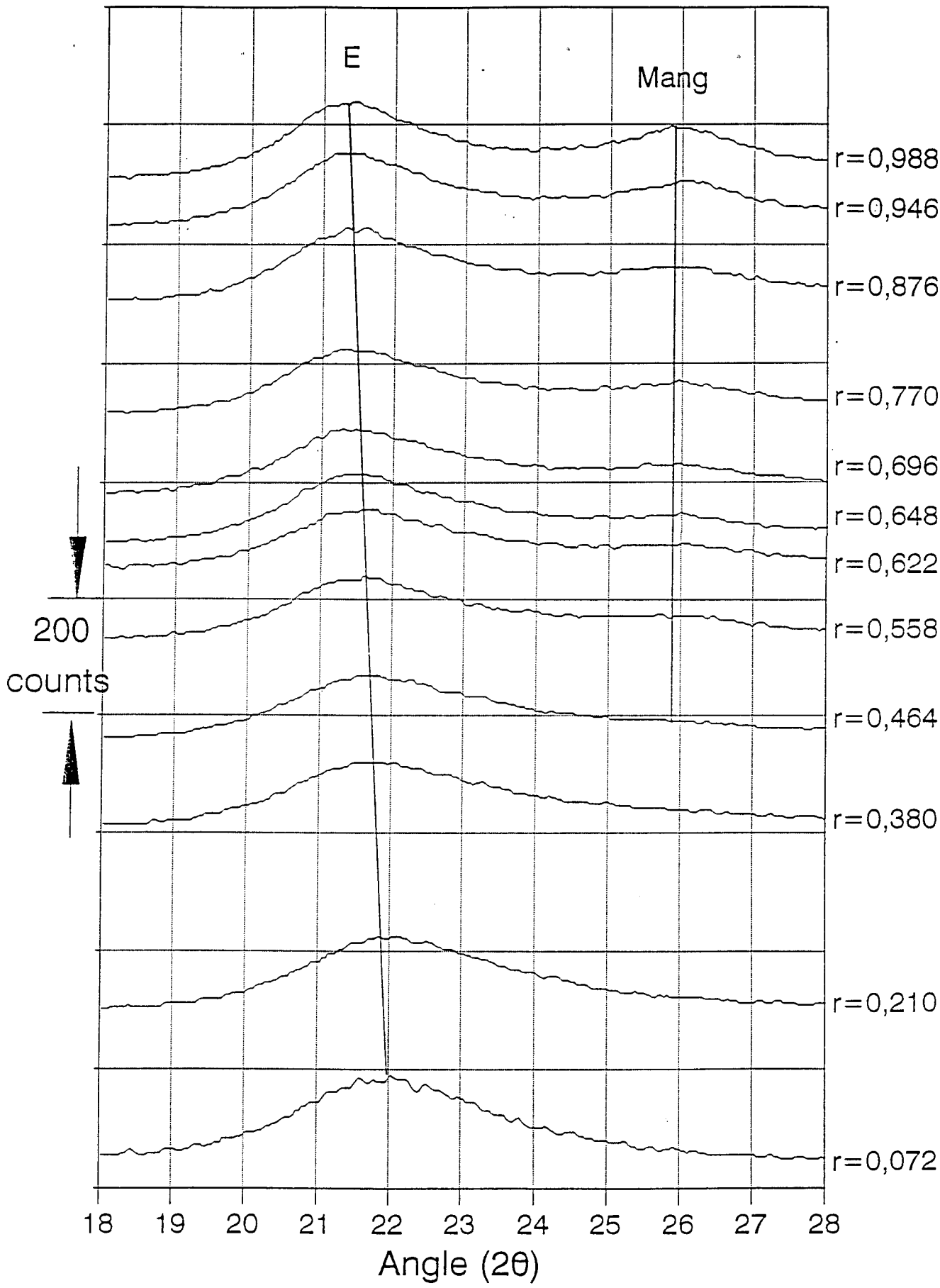

Figure 3.9.- Peaks E and Manganite evolution hydrazine reduction method

3.4.1.- Heterogeneous behaviour verification

Two different methods were chosen in order to verify the heterogeneous behaviour proposed in the previous section. The first was based on the proposition that, in case of heterogeneous reduction, due to the existence of two different phases, it should be possible to predict the X-ray pattern of the samples by weighted addition of the patterns of the products at the edges of the heterogeneous reduction zone.

The onset of a heterogeneous region arises from an imbalance between the H insertion rate at the surface and the diffusion of H away from the surface: this controls the value of r (or x) at the surface. When this value exceeds a certain value, heterogeneity sets in. On this basis one would expect heterogeneity to set in earlier at the sites more accessible to the reductant than at those which are less accessible. There is thus a lack of clarity as to which starting point to take to simulate XRD patterns in the heterogeneous region. However an r value of 0.316 (x= 1.842) was chosen as the boundary for the simulation. For the other end-member, various H inserted members were tried : $MnOOH_{0.988}$, $MnOOH_{0.900}$ and $MnOOH_{0.804}$. These comparisons between actual and calculated XRD patterns are shown for the compositions $MnOOH_{0.696}$ and $MnOOH_{0.518}$ in Figures 3.10 and 3.11.

From these figures, it is observed that the best match was obtained with $MnOOH_{0.804}$, so it was used as end-member for further calculations.

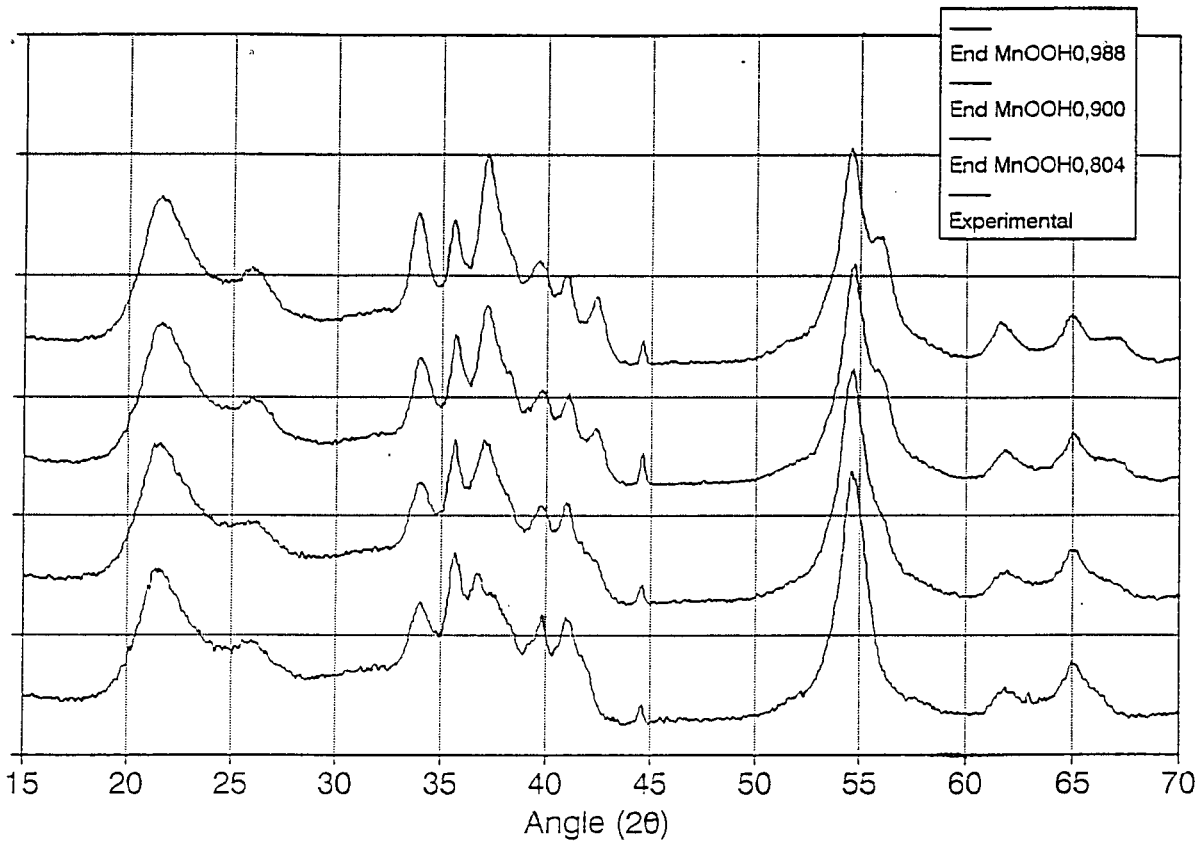

Fig 3.10.- Comparison of mathematical mixture (using different end members) and experimental diffraction patterns for MnOOH0,696.

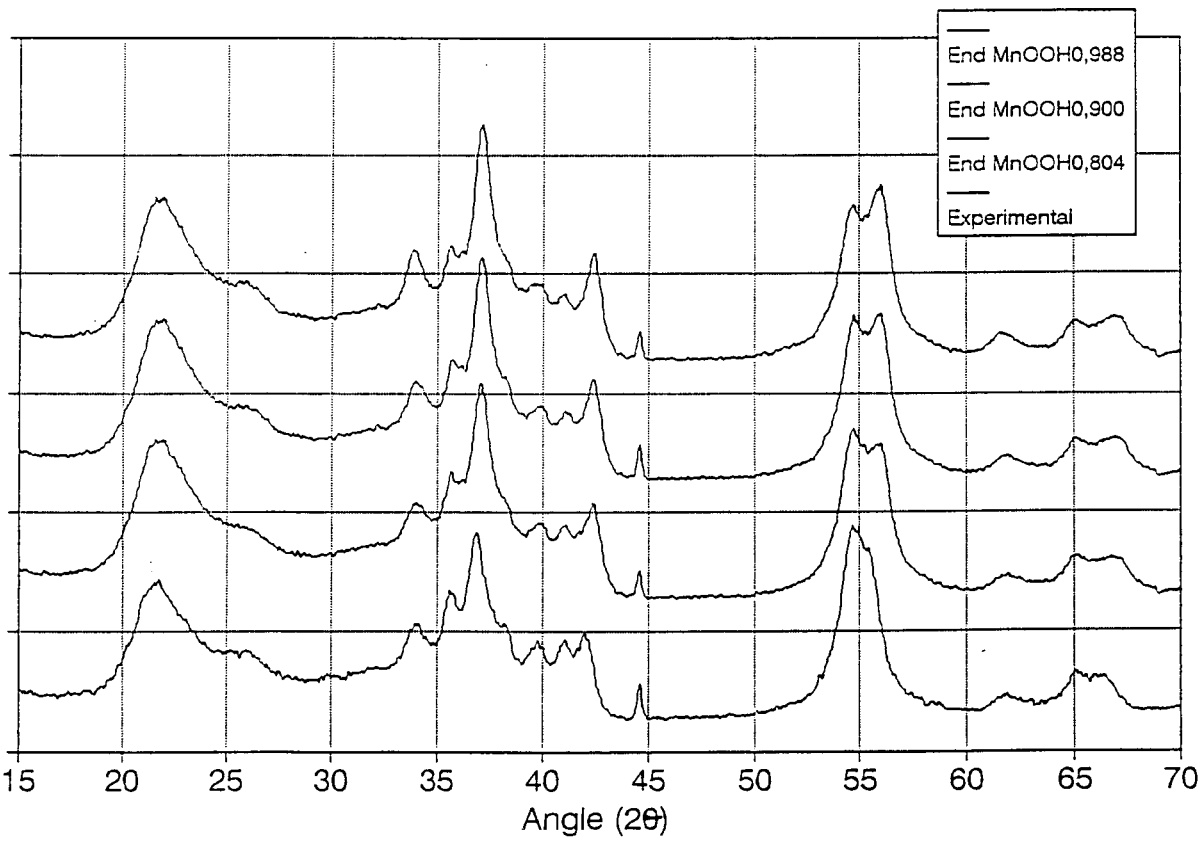

Fig 3.11.- Comparison of mathematical mixture (using different end members) and experimental X-ray diffraction patterns for MnOOH0,518.

$MnOOH_{0.804}$ is approximately the composition at which restricted mobility starts and OH formation commences [18, 74]. It seems reasonable that the product over heterogeneous reduction should be to a phase which is not the ultimate product but one with a structure and composition at which low internal H mobility commences. With more insertion the tendency is to increase the amount of the low mobility structure rather than to increase its H content. So, microdomains are not crystallised islands of end product but low mobility regions which do not yet have their final total H insertion content.

The mathematical mixing for other experimental conditions using as end-members $MnOOH_{0.804}$ and $MnOOH_{0.316}$ is shown in Figures 3.12 to 3.20. As it is noted, an almost exact prediction was achieved (small differences observed can be attributable to experimental errors). The biggest differences are in the region of $2\theta=55°$ for r values of 0.52, 0.56, 0.62 and 0.66. In this region, the shoulder on the high angle side is less significant or does not appear in the experimental patterns. This is presumably because the heterogeneous region starts not at r=0.316, but between 0.316 and 0.380; in which case, peak B for the end-member would be a slightly lower 2θ and this change would result in a less prominent shoulder on the high angle side of the calculated patterns in better agreement with the experimental patterns.

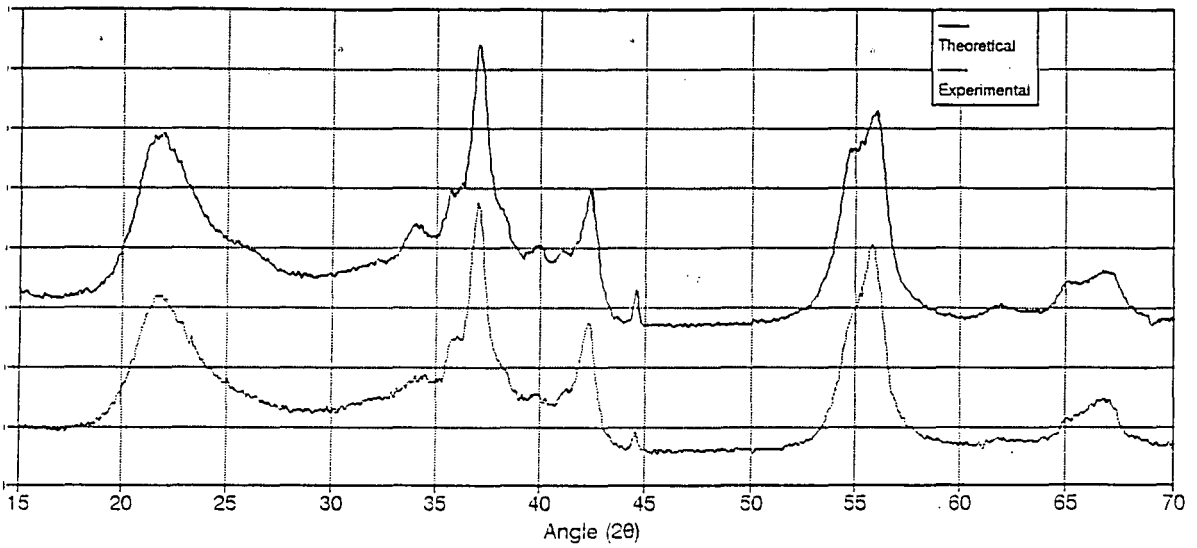

Fig 3.12.-Comparison of math. mixture (86,9% MnOOH0,316 / 33,1% MnOOH0,804= MnOOH0,380) and experimental (MnOOH0,380) X-ray diffraction patterns.

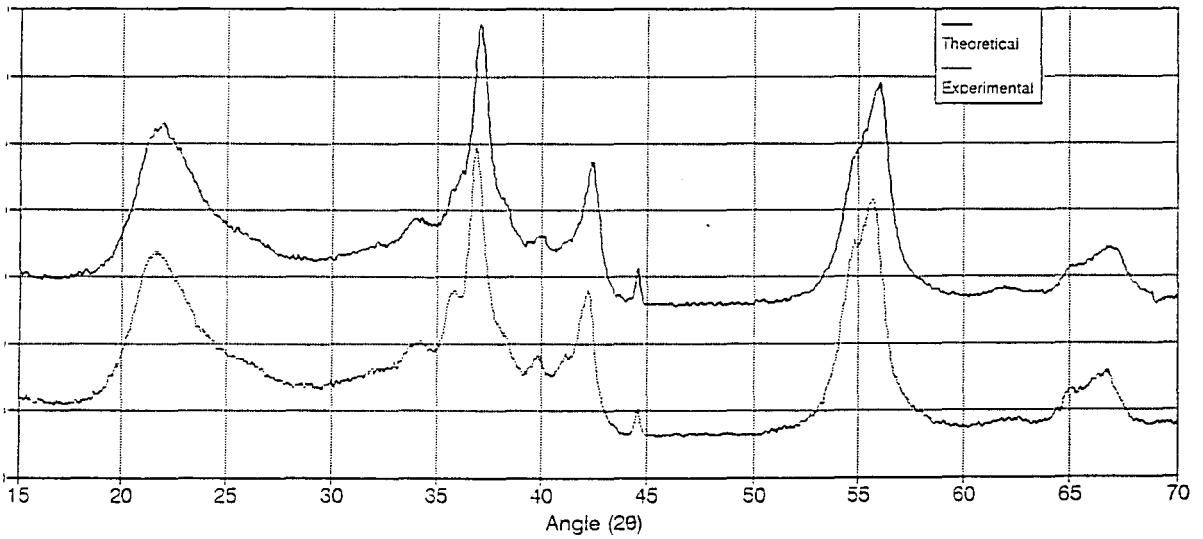

Fig 3.13.- Comparison of math. mixture (82,8% MnOOH0,316 / 17,2% MnOOH0,804= MnOOH0,400) and experimental (MnOOH0,400) X-ray diffraction patterns.

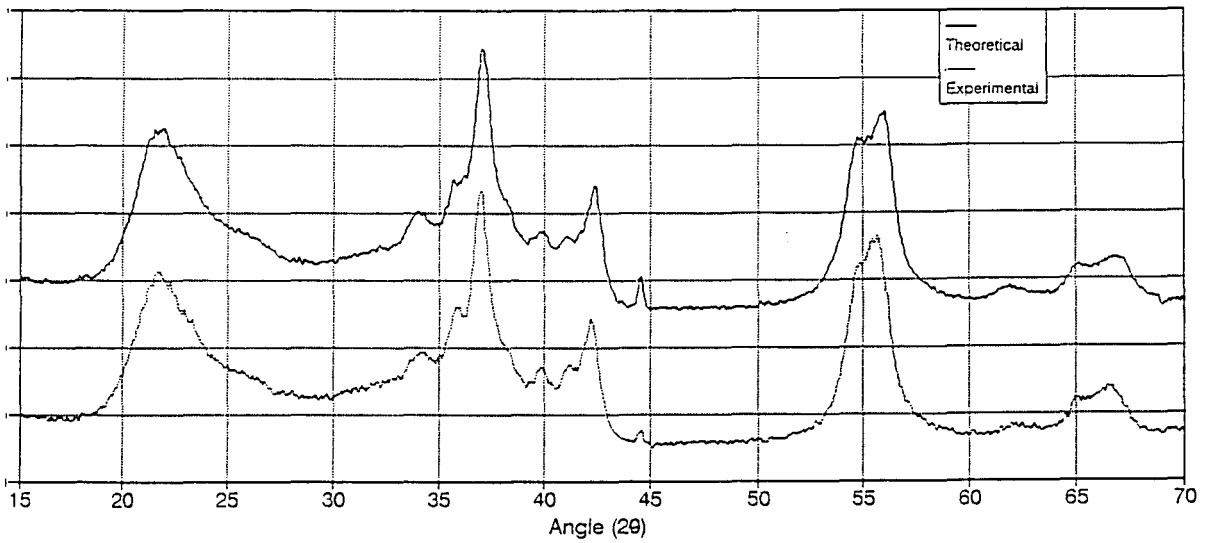

Fig 3.14.- Comparison of math. mixture (69,7% MnOOH0,316 / 30,3% MnOOH0,804= MnOOH0,464) and experimental (MnOOH0,464) X-ray diffraction patterns.

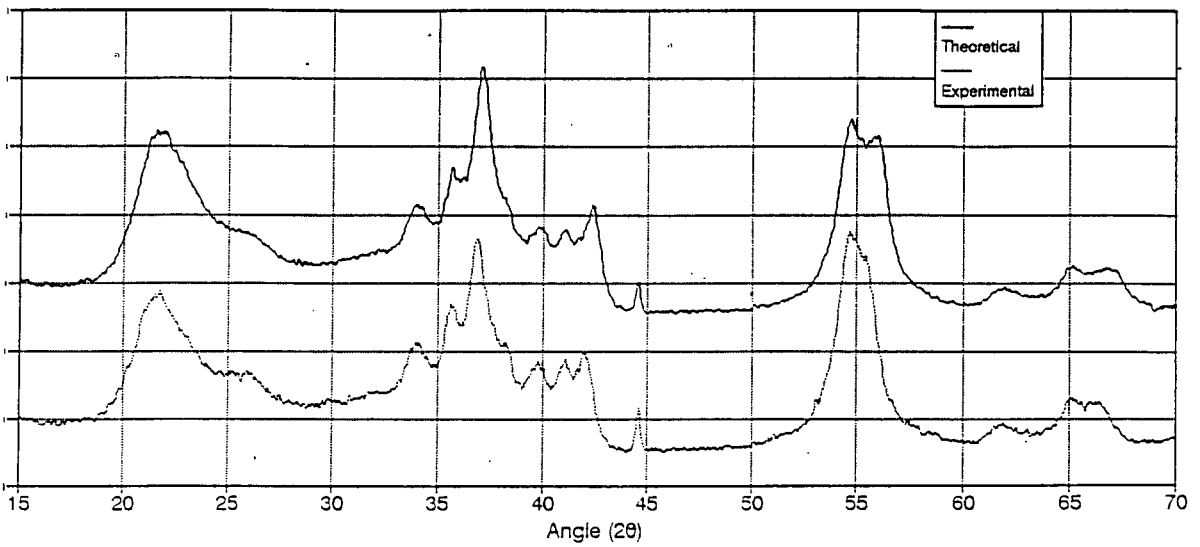

Fig 3.15.- Comparison of math. mixture (58,6% MnOOH0,316 / 41,4%MnOOH0,804= MnOOH0,518) and experimental (MnOOH0,518) X-ray diffraction patterns.

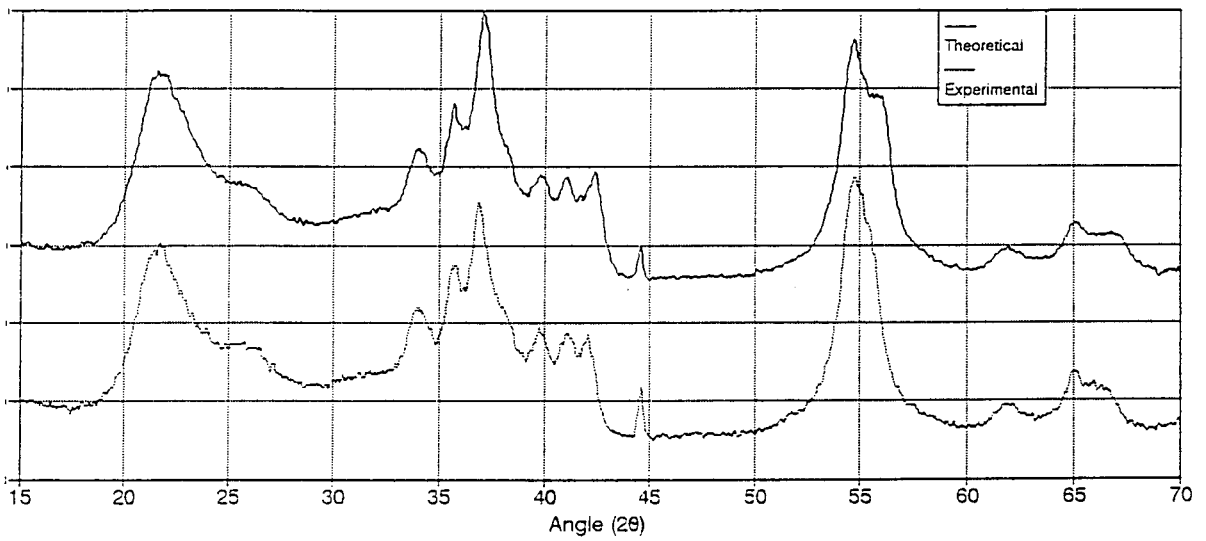

Fig 3.16.- Comparison of math. mixture (50,4% MnOOH0,316 / 49,6% MnOOH0,804= MnOOH0,558) and experimental (MnOOH0,558) X-ray diffraction patterns.

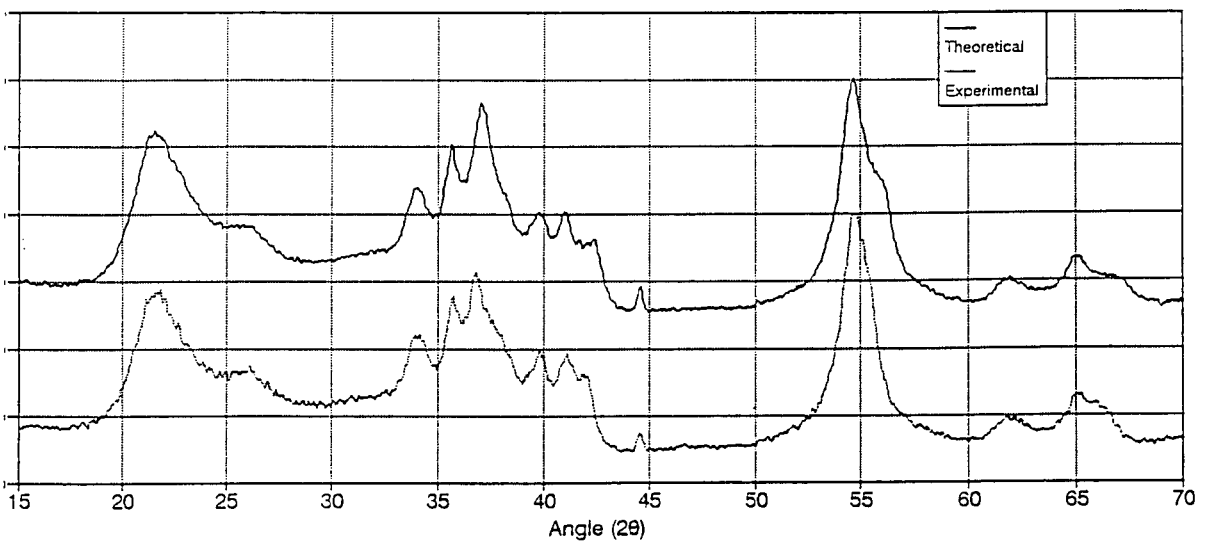

Fig 3.17.- Comparison of math. mixture (37,3% MnOOH0,316 / 62,7% MnOOH0,804= MnOOH0,622) and experimental (MnOOH0,622) X-ray diffraction patterns.

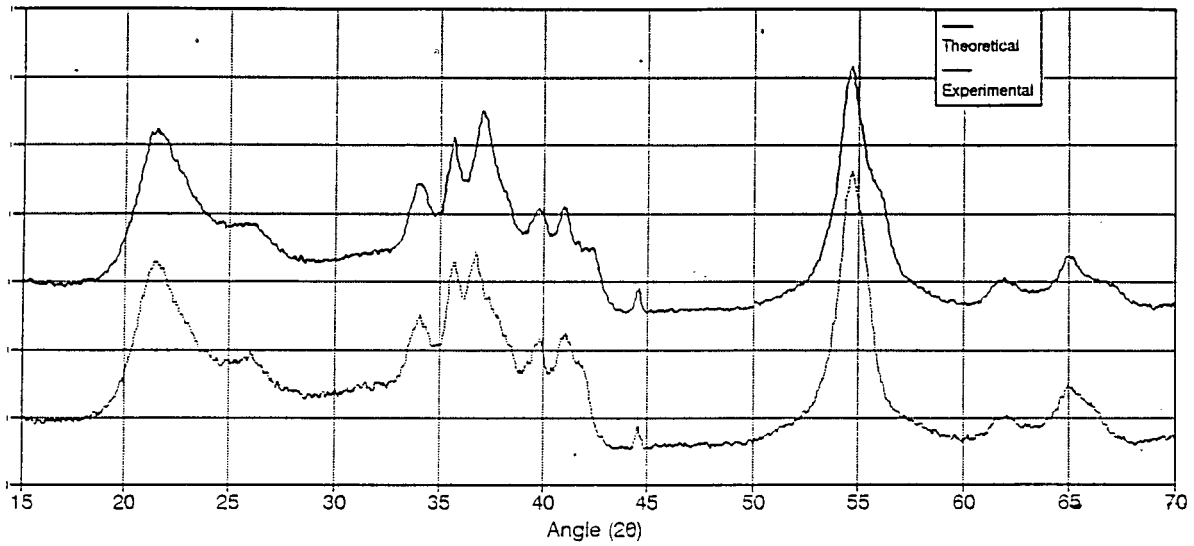

Fig 3.18.- Comparison of math. mixture (32,0% MnOOH0,316 / 68,0% MnOOH0,804 = MnOOH0.648) and experimental (MnOOH0,648) X-ray diffraction patterns.

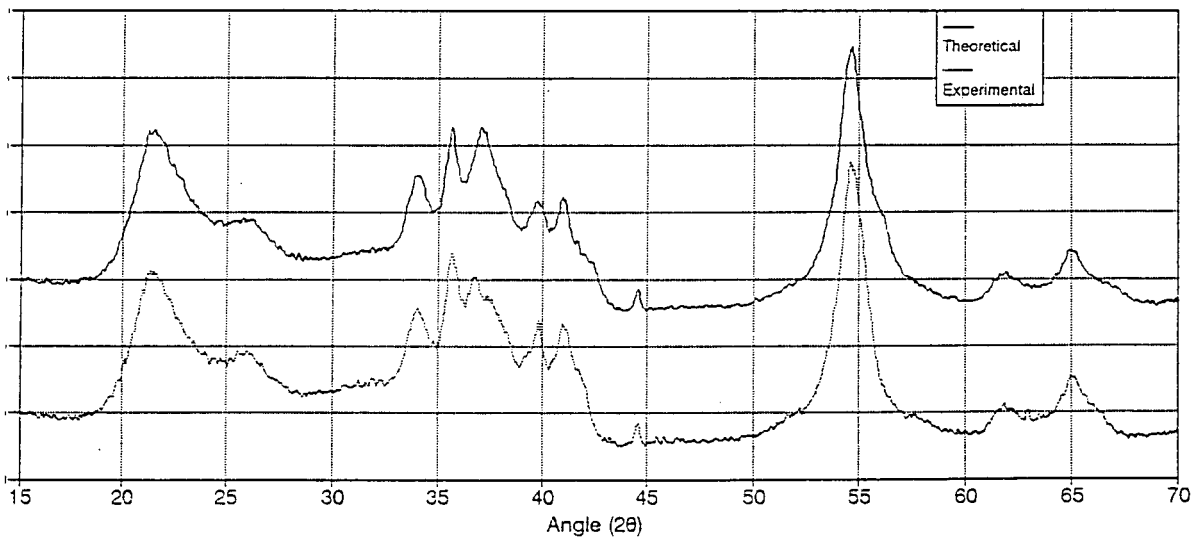

Fig 3.19.- Comparison of math. mixture (22,1% MnOOH0,316 / 77,9% MnOOH0,804 = MnOOH0,696) and experimental (MnOOH0,696) X-ray diffraction patterns.

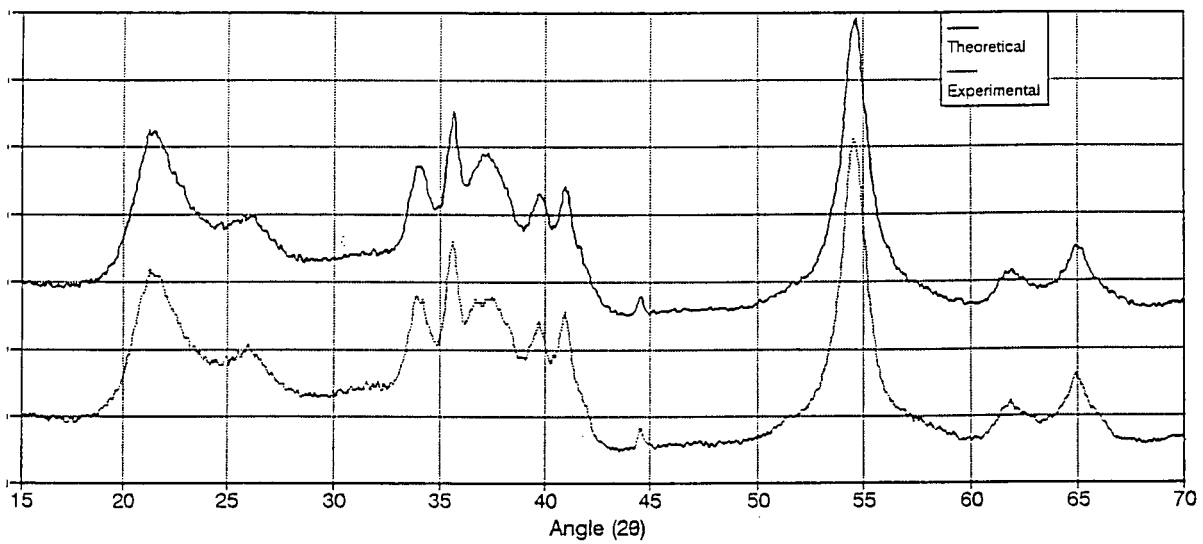

Fig 3.20.- Comparison of math. mixture (7,0% MnOOH0,316 / 93,0% MnOOH0,804 = MnOOH0,770) and experimental (MnOOH0,770) X-ray diffraction patterns.

The second method of verifying heterogeneous behaviour is based on an observation of Fitzpatrick and Tye [18] whereby a dry mixture of two homogeneous H inserted compounds of different H insertion level showed pairs of XRD peaks which coalesced with time thereby demonstrating interparticulate mobility and a diffusion gradient between the two mixed compounds. This behaviour is not possible if the reduction takes place in an heterogeneous way.

Two different dry mixtures were prepared: one with the samples $MnOOH_{0.316}$ and $MnOOH_{0.988}$ (50 % / 50 %), and the other with the samples $MnOOH_{0.072}$ and $MnOOH_{0.988}$ (50 % / 50 %). The differences between the original X-ray diffraction pattern and that after 38 or 41 days, respectively, of being mixed are shown in Figures 3.21 and 3.22, together with the difference curves between "after time" and initial patterns. It is obvious that the mixture prepared with $MnOOH_{0.316}$ and $MnOOH_{0.988}$ had not changed significantly after the time in storage, which confirms again the heterogeneous behaviour of the reduction at r values higher than 0.316 (x values lower than 1.842). However in the other mixture it is possible to see partial coalescence of some of the peaks, due to the presence of homogeneous behaviour for r values between 0.072 and 0.316 (x between 1.964 and 1.842).

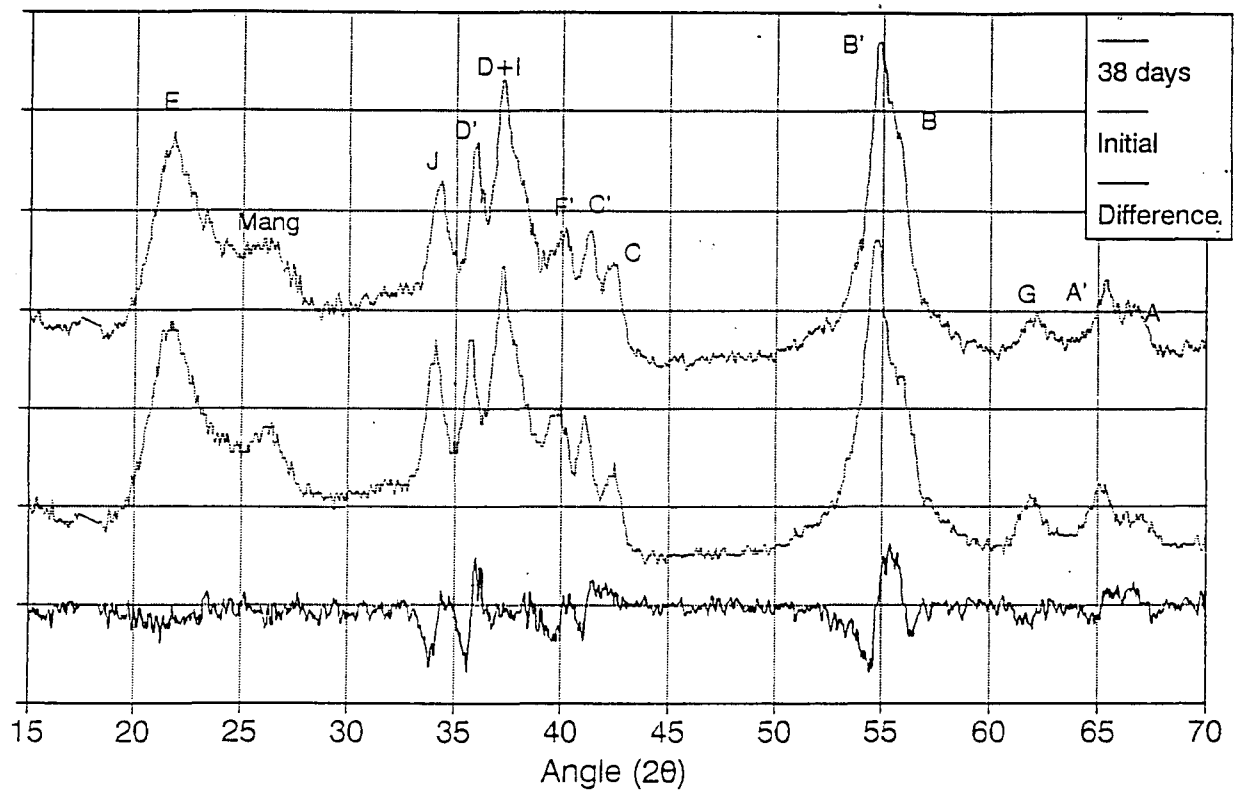

Figure 3.21.- Physical mixture between MnOOH0,316 and MnOOH0,988. Initial and after 38 days X-ray diffraction patterns.

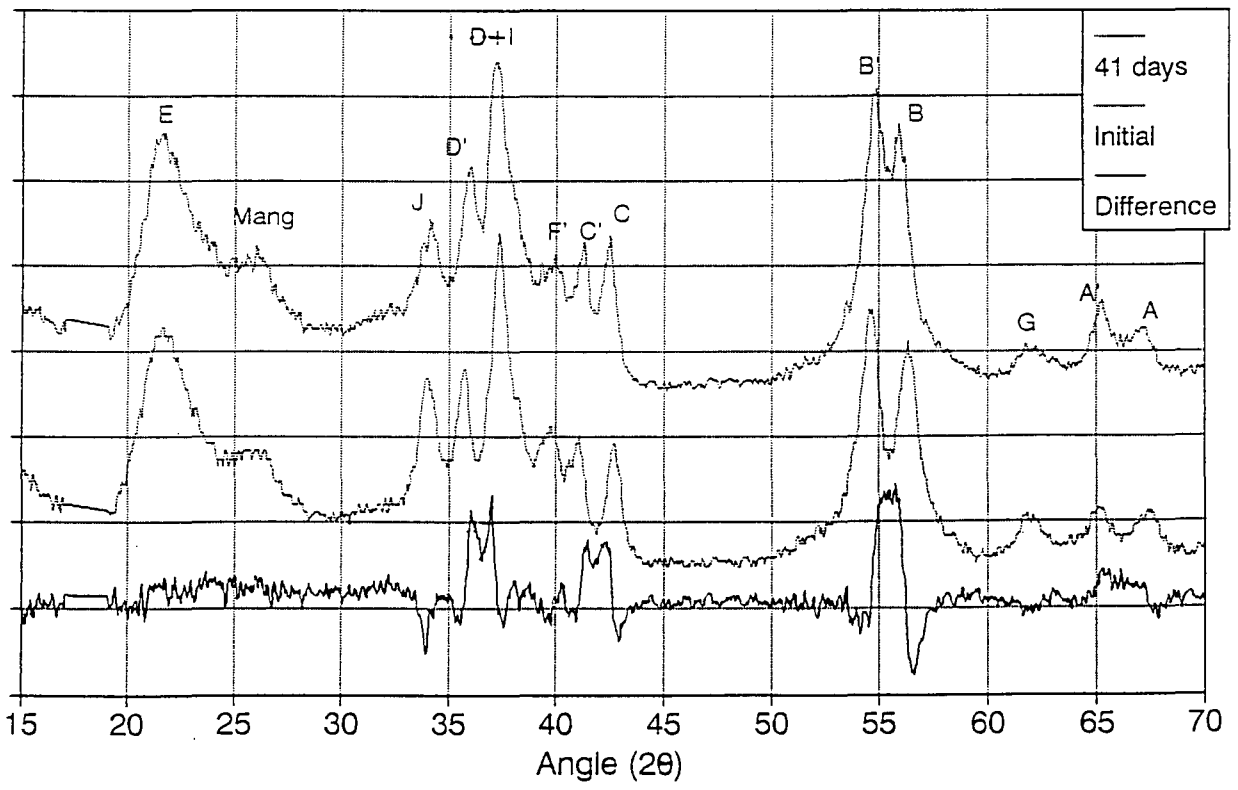

Figure 3.22.- Physical mixture between MnOOH0,072 and MnOOH0,988. Initial and after 41 days X-ray diffraction patterns.

3.4.2.- "Slow" hydrazine hydrate reduced samples.

X-ray diffractions of the eighth set of samples mentioned in section 2.1.2. ("slow" hydrazine hydrate reduction) were performed, and compared with the equivalent (in H insertion level) X-ray patterns of the sixth and seventh sets of samples in Figures 3.23, 3.24 and 3.25. These comparisons reveal, as expected, the influence of the reduction rate on the mechanism of H insertion, and agree with the findings of Gabano et al [31] mentioned earlier.

It is possible to check, for an intermediate reduction level (Figure 3.23) that the emergent peaks that appear in the "quick reduced sample" (2θ values of 26.2° [Manganite] ; 33.9° [J] ; 35.6° [D'] ; 39.8° [F'] ; 41.1° [C'] ; 54.6° [B'] ; 61.8° [G] ; and 65.0° [A']) are less evident for the "slow reduced sample". In the same way it is very clear that some peaks from the starting material that have disappeared in the "quick reduced sample" remain in the "slow reduced sample" (2θ values of 55.6° [B] ; and 66.5° [A]). For higher reduction levels (Figures 3.24 and 3.25), the differences are not so clear, being the most remarkable difference the more pronounced appearance of Manganite, J and G peaks.

These observations were expected as the range of H insertion over which the behaviour is homogeneous should be smaller for the samples produced by the "quick" method, commencing at a lower r value. When the reactant introduces the inserted H at

the surface of the manganese dioxide slowly, diffusion of the inserted species away from the surface ensures that the insertion level is almost uniform everywhere. In this situation, the insertion level at which heterogeneity commences is not reached prematurely and in consequence the range of r for which the insertion is homogeneous is close to the maximum possible, i.e. that which would pertain if the insertion took place infinitely slowly. In case of quick reductions, the inserted H are not given sufficient time to diffuse to the interior of the $MnOOH_r$ material, so heterogeneity and emergent peaks in XRD pattern appear at a lower insertion level.

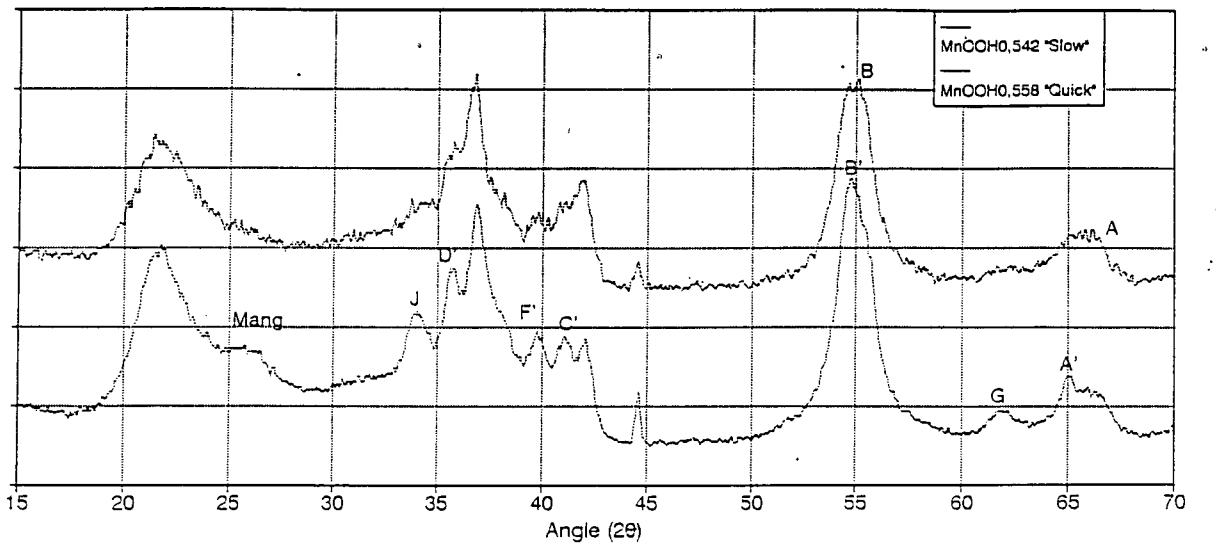

Fig 3.23.- Comparison of different reduction methods :
"Slow" (MnOOH0,542) and "Quick" (MnOOH0,558) hydrazine reduction methods.

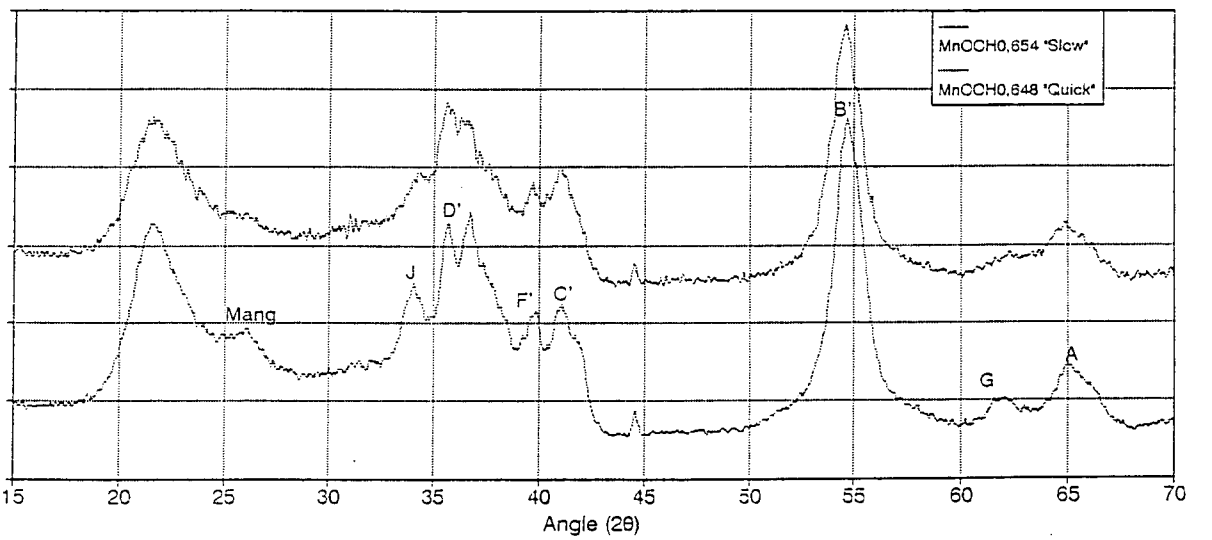

Fig 3.24.- Comparison of different reduction methods :
"Slow" (MnOOH0,654) and "Quick" (MnOOH0,648) hydrazine reduction methods.

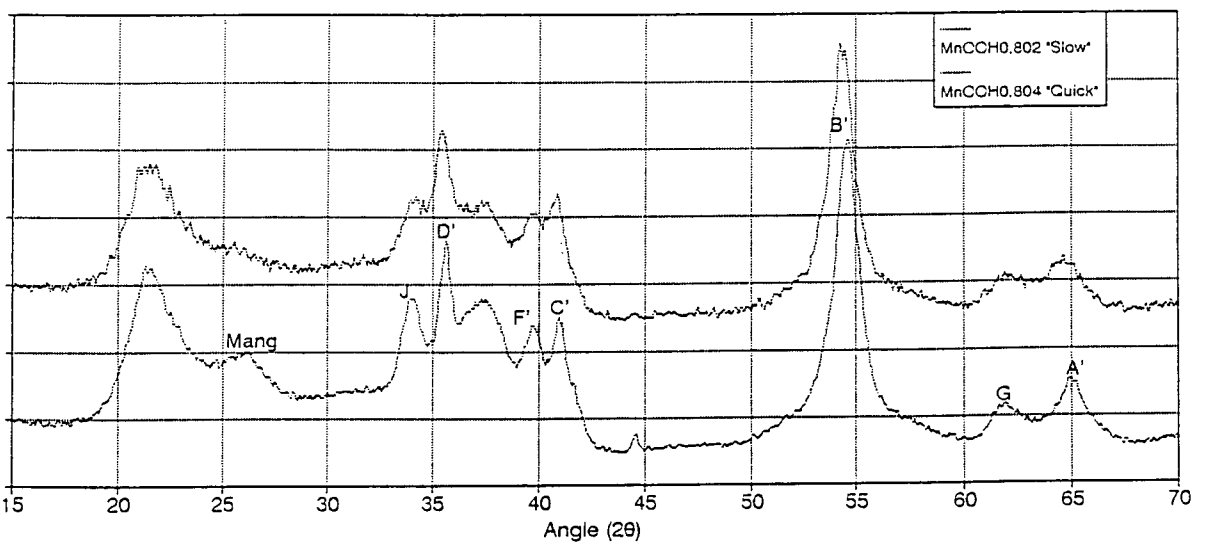

Fig 3.25.- Comparison of different reduction methods :
"Slow" (MnOOH0,802) and "Quick" (MnOOH0,804) hydrazine reduction methods.

The results presented here fully agree with the behaviour observed in batteries containing a manganese dioxide cathode, where the total coulombic capacity present is not available under all discharge conditions. The capacity given by a battery is dependent on the discharge regime [1]. When a battery is discharged at low load resistances (which could be similar as "quick" hydrazine hydrate reduction method), recuperation processes are restricted and capacity yields are low. With increasing load resistance ("slow" reduction method), the yields increase due to improved recuperation and the greater possibility of homogenisation within the material.

This concordance in behaviour indicates the importance of the generation and study of non-uniform compounds with H insertion in a higher proportion in the surface layers. Such non-uniformity is promoted by a high rate reduction with hydrazine hydrate. Special care is then clearly needed when choosing conditions for chemical insertion as the choice affects the character of the $MnOOH_x$ compounds.

However, this fact has not been taken into account in the past. For example, Miyake [76] stated that "the reduction method of MnO_2 with hydrazine is similar to the electrochemical reduction of MnO_2 in dry cells", without mentioning the conditions of such hydrazine reductions. In the same way, Ohzuku and Hirai [39], using a "step-wise reduction by the hydrazine method", similar to the one used in this investigation, concluded that (1) the H insertion into MnO_2 proceeded (under their conditions) in a single phase and (2) the hydrazine method could be used as a characterisation technique for MnO_2.

3.5.- DIFFERENCES BETWEEN PROPAN-2-OL AND HYDRAZINE HYDRATE REDUCED SAMPLES.

3.5.1.- Interplanar spacings vs H insertion level.

The differences in pattern evolution with degree of reduction arising from the two reduction methods are more clearly observed by plotting the interplanar spacings of the different peaks against the degree of reduction. These are presented comparatively for both hydrazine hydrate and propan-2-ol methods in the figures 3.26 to 3.39.

For the Propan-2-ol samples, an increase is observed of the interplanar spacings of all the peaks (A to F) relative to those of the starting with reduction. This is due to the lattice expansion with H insertion. It is worth to noting that peak F follows a strange behaviour in comparison with the others, with a horizontal region for r values between 0.45 and 0.80. Although it is not evident from the present work, as previously mentioned [18], this could be due to the appearance of a new peak (labelled H in that work) that is interfering the measurement of peak F values.

In the same way as was noted before by Fitzpatrick and Tye [18], there appear to exist also for Propan-2-ol samples some changes in the H insertion which appear in these graphs as slope changes at r values of 0.25, 0.45, and 0.80. At r = 0.25, the change is thought to be due to the generation of enlarged regions of disorder between crystallites.

The change at r = 0.45 (mid-reduction) has been attributed [16, 77] to changes in the type of site occupied by the inserted species and a change in configurational entropy of the inserted species. At insertion levels higher than r = 0.8 the unit cell changes shape, with a change in character of the X-ray diffraction pattern, and a clear decrease in intensity of the original peaks together with evolution of new peaks. Peaks A, B, C, D and F continued to shift even for r > 0.8. This is compatible with the conclusion of Fitzpatrick and Tye [18] that the solid solution extended over the complete range of r (0-1).

The manganite peaks in the propan-2-ol samples only appear at the end of the reduction for r values higher than 0.8-0.9, and to a lesser extent than in a previous study carried out with propan-1-ol [41]. This may be due to the lower reflux temperature employed in the reduction with propan-2-ol in this research, 82.5° (2-ol) vs 97.8° (1-ol) [78].

However, for the hydrazine samples the anisotropy as previously explained starts earlier. The structure begins to dilate (in a similar way as for the propan-2-ol samples) until the appearance of new peaks which grow at the expense of the original ones that disappear at an r value close to 0.4 (x equal to 1.8), typical behaviour of a heterogeneous reduction. There is also a region of overlap between the old and the new peaks. Once the heterogeneity has set it, the interplanar spacing of all new peaks A', B', C', D', F', I, J and G remains constant.

Another interesting feature of these figures is that the d spacings for peaks A', B', C', D' and F' obtained with the Hydrazine reduction method, do not correspond with the

values found at full H insertion using Propan-2-ol, but to values obtained between r = 0.8-0.9. Since the d spacings of peaks A', B', C', D' and F' (Hydrazine reduction) are essentially independent of r, this means that the final products of the two reduction methods, although very similar are not quite the same, as previously indicated in Section 3.4.

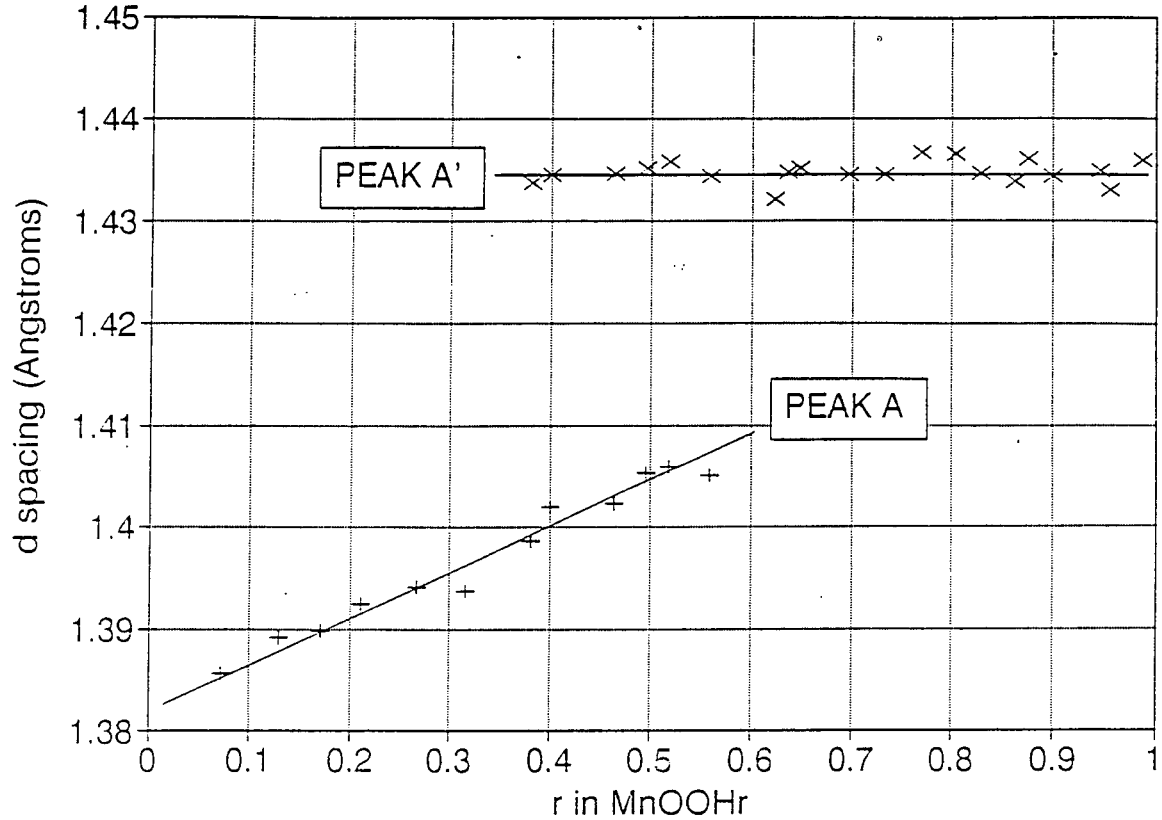

Figure 3.26.- Interplanar spacings of peak A vs H insertion. hydrazine hydrate reduction method.

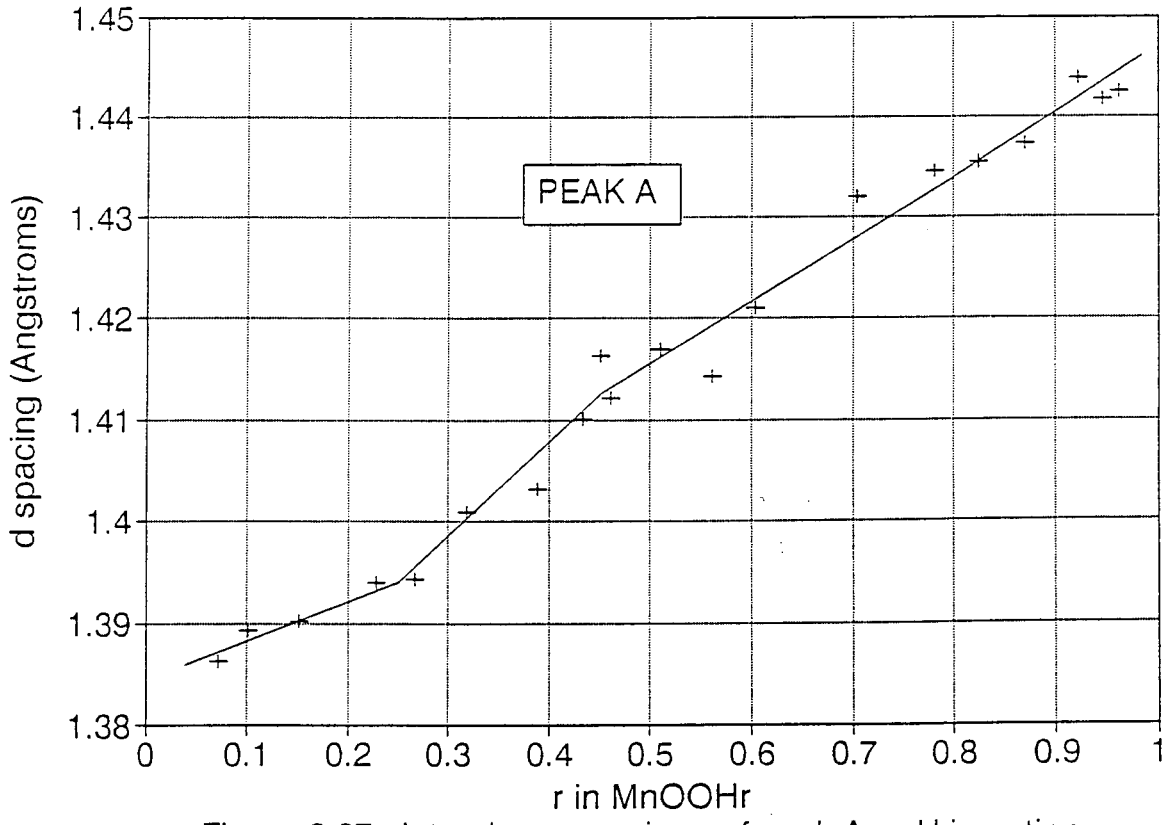

Figure 3.27.- Interplanar spacings of peak A vs H insertion. propan-2-ol reduction method.

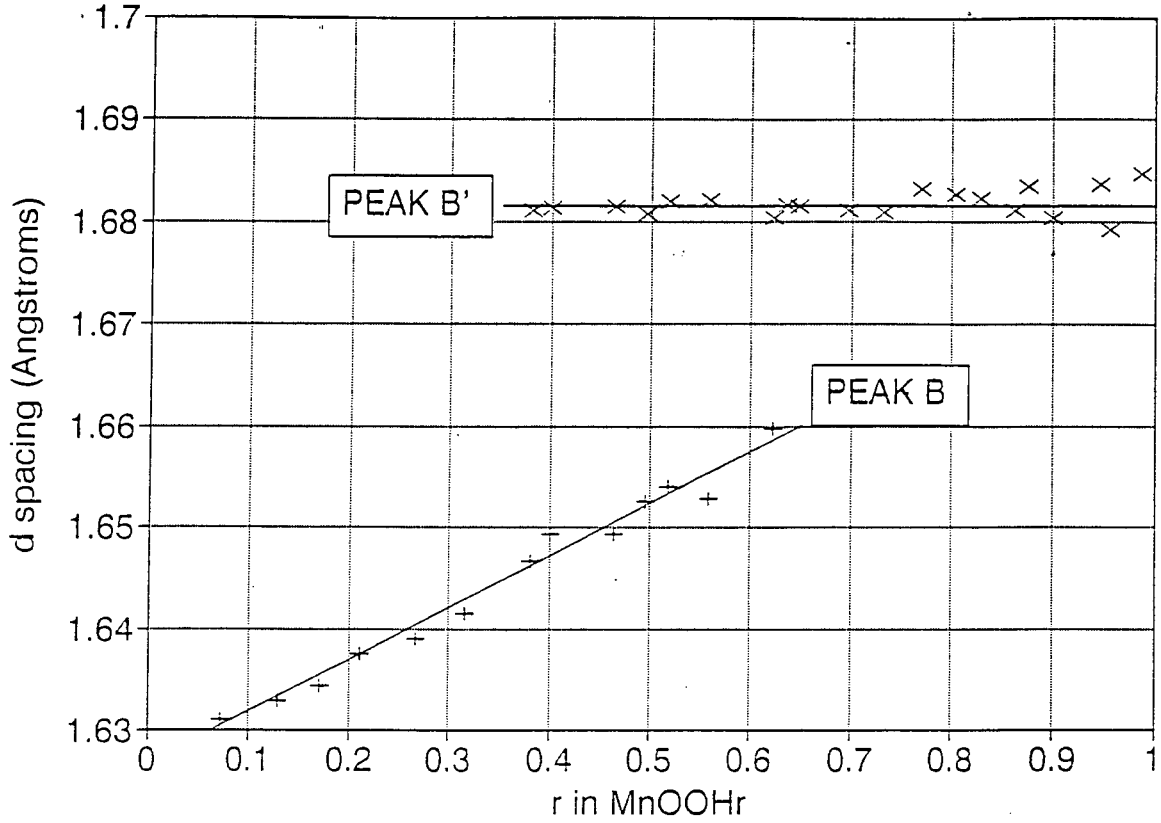

Figure 3.28.- Interplanar spacings of peak B vs H insertion.
hydrazine hydrate reduction method.

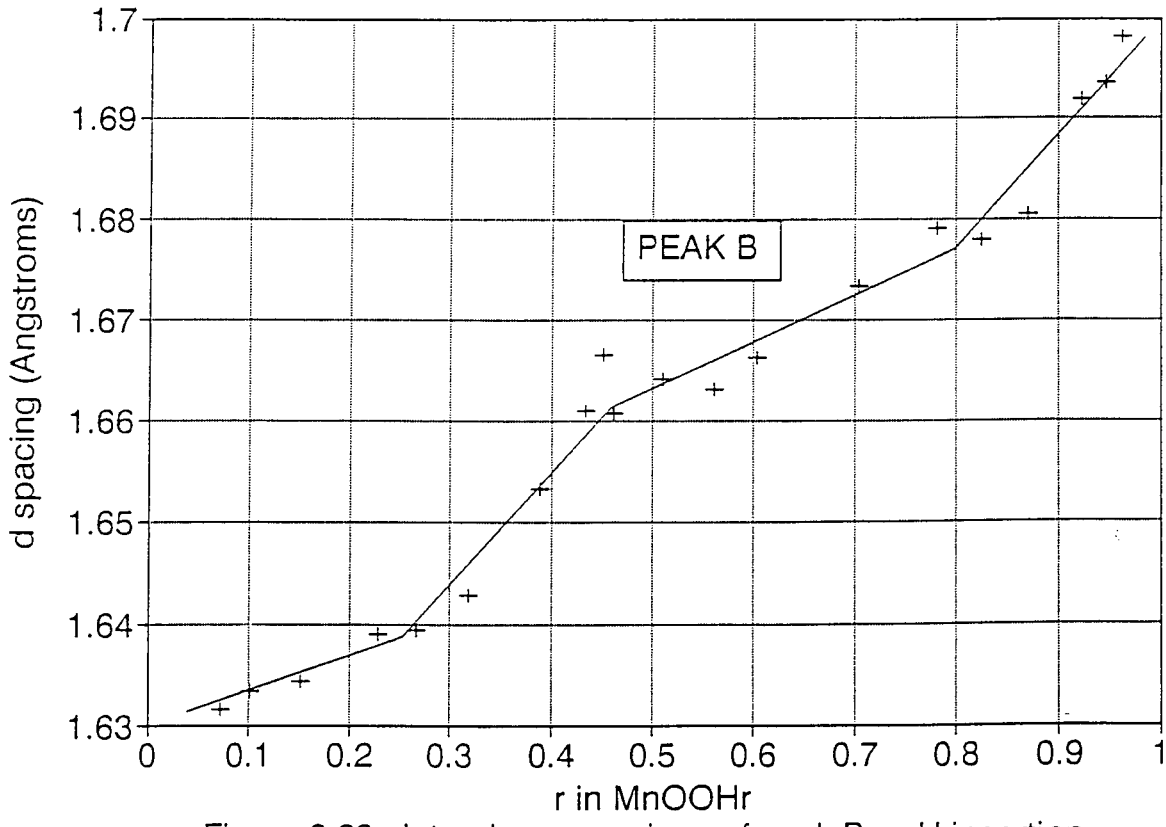

Figure 3.29.- Interplanar spacings of peak B vs H insertion.
propan-2-ol reduction method.

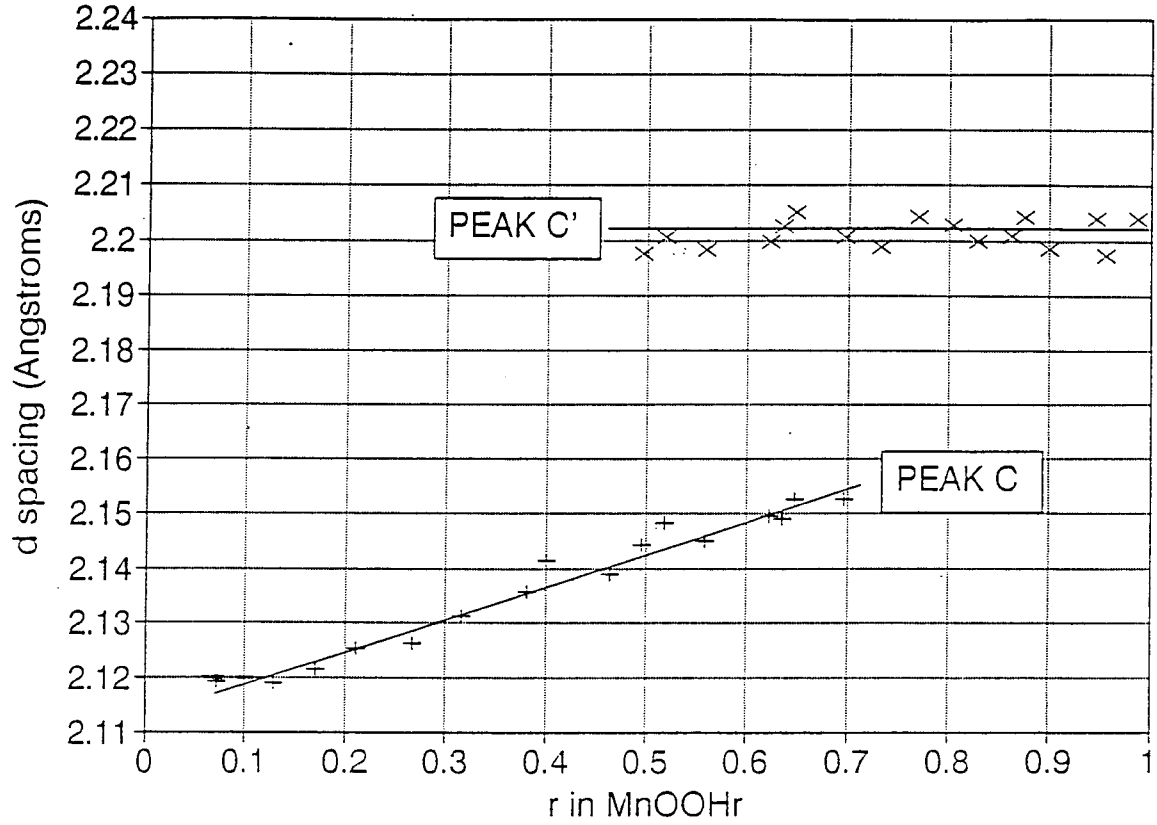

Figure 3.30.- Interplanar spacings of peak C vs H insertion. hydrazine hydrate reduction method.

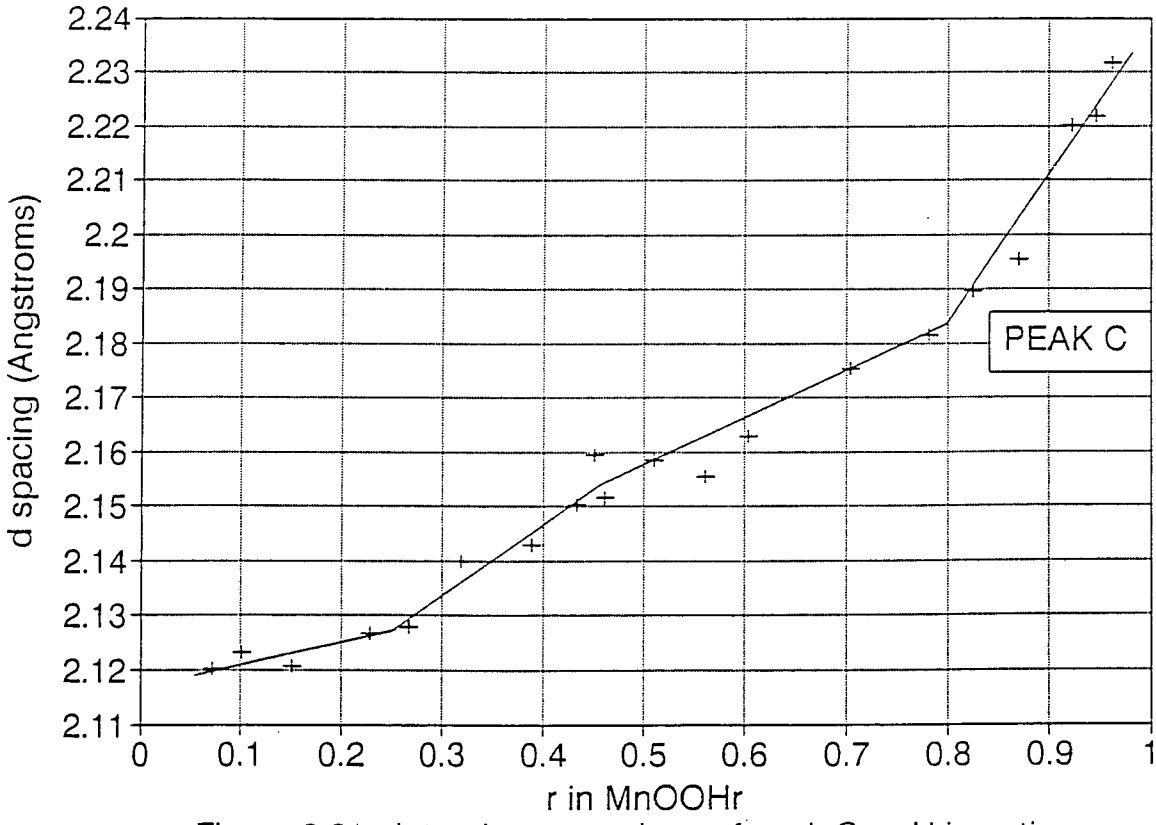

Figure 3.31.- Interplanar spacings of peak C vs H insertion. propan-2-ol reduction method.

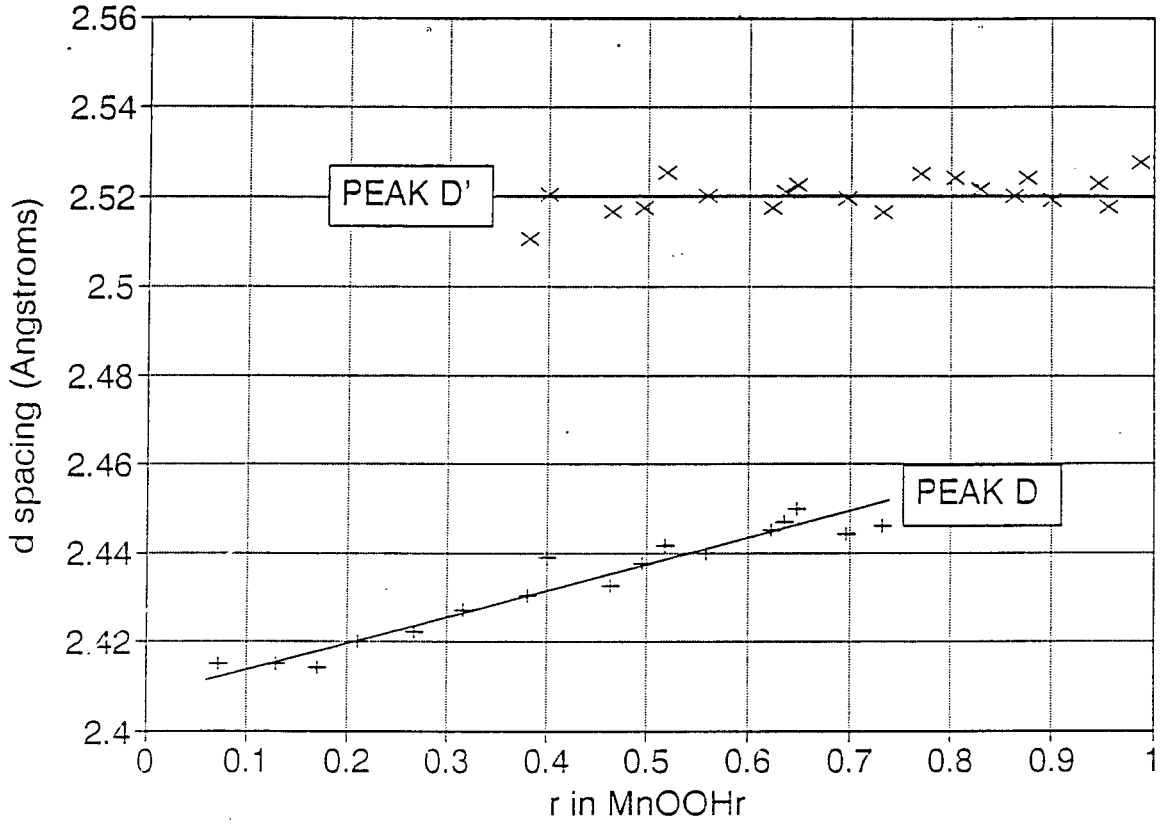

Figure 3.32.- Interplanar spacings of peak D vs H insertion. hydrazine hydrate reduction method.

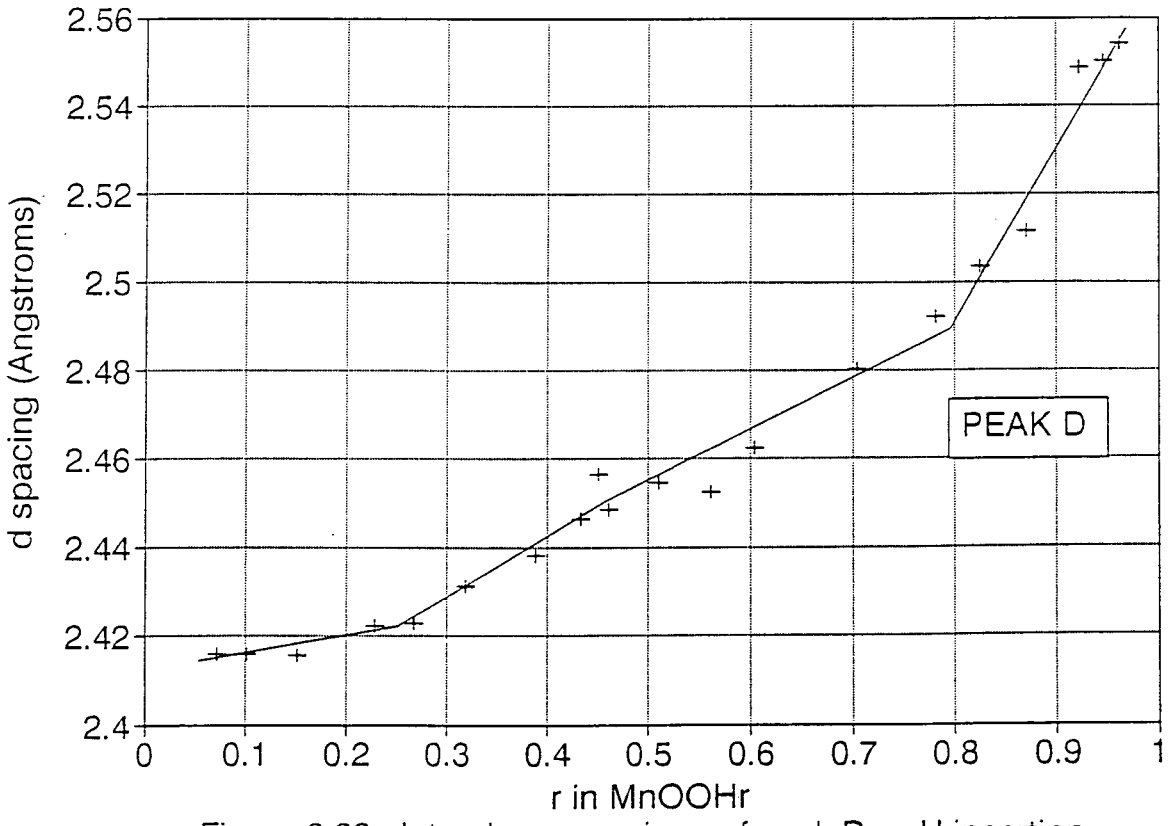

Figure 3.33.- Interplanar spacings of peak D vs H insertion. propan-2-ol reduction method.

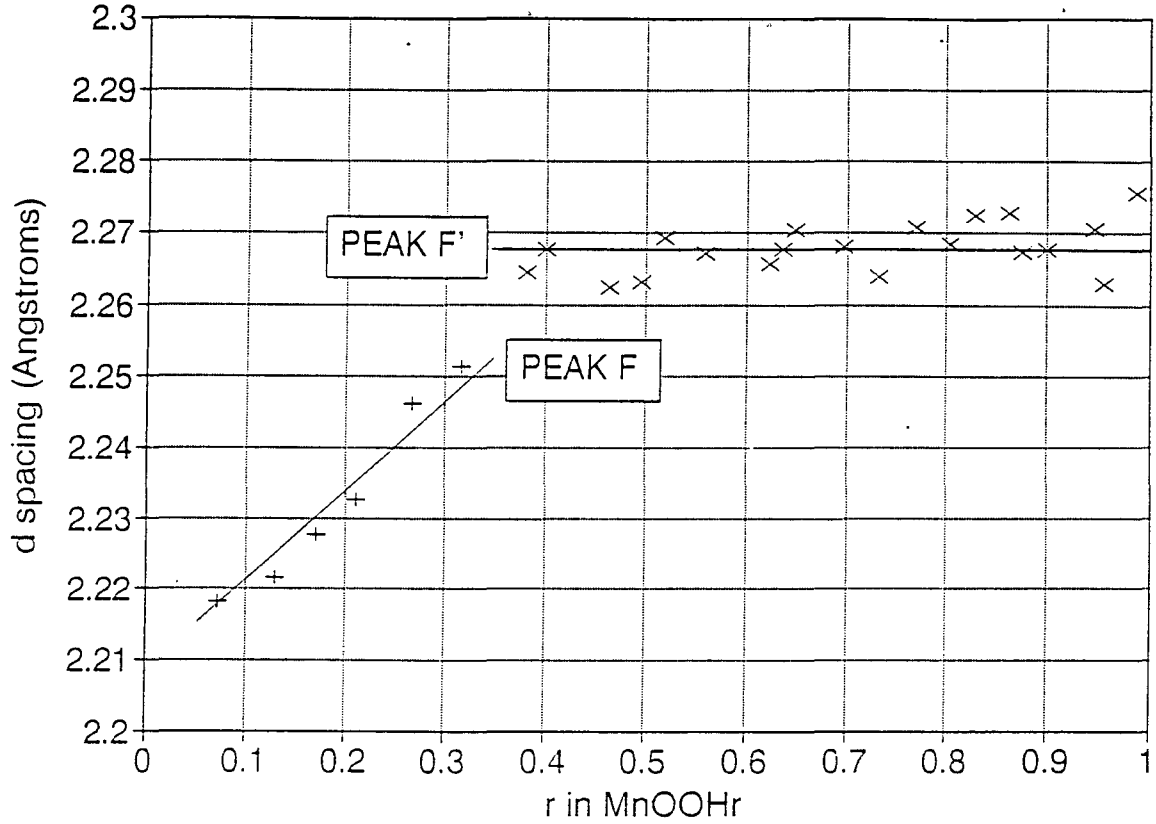

Figure 3.34.- Interplanar spacings of peak F vs H insertion. hydrazine hydrate reduction method.

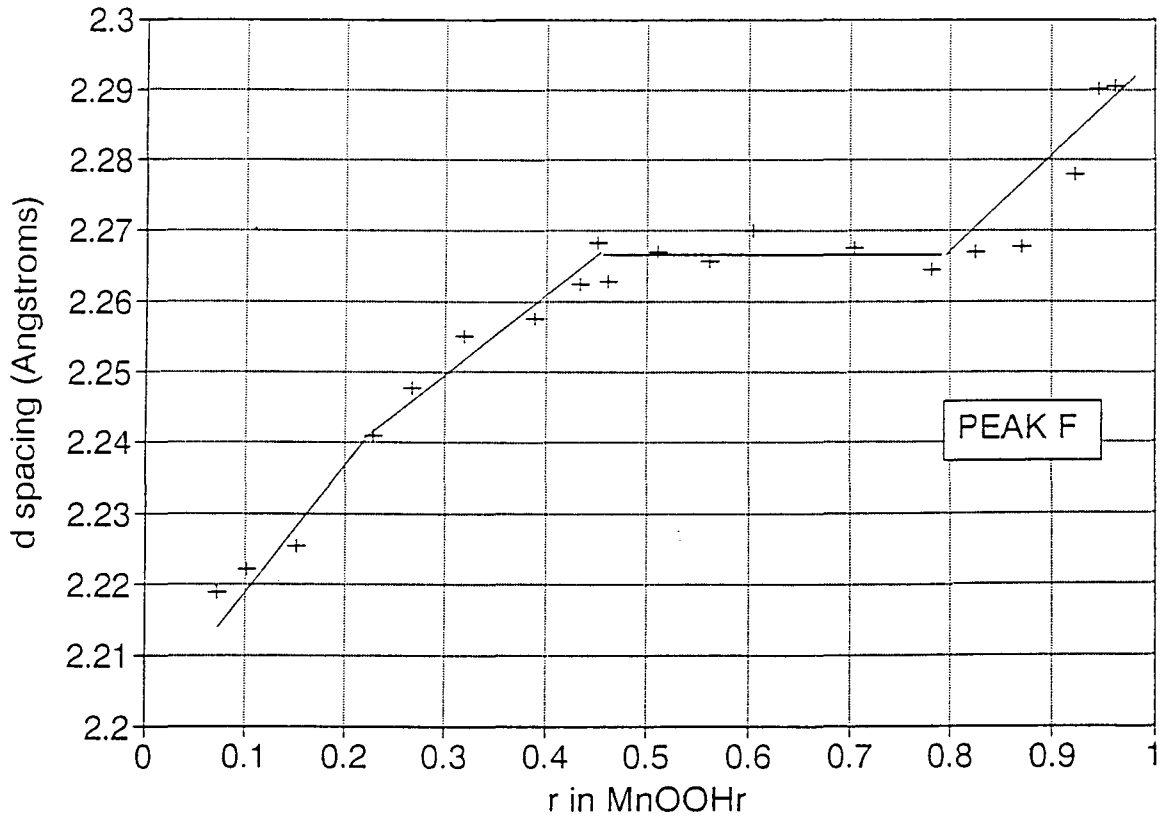

Figure 3.35.- Interplanar spacings of peak F vs H insertion. propan-2-ol reduction method.

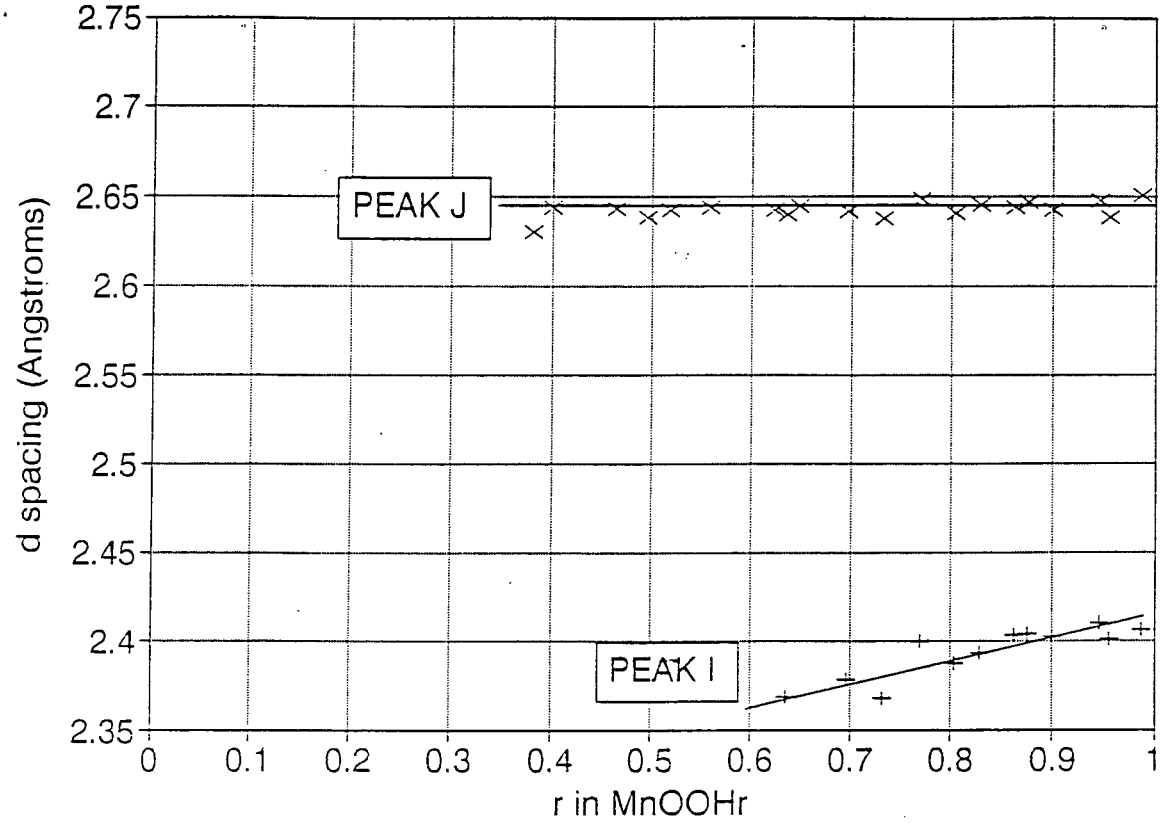

Figure 3.36.- Interplanar spacings of peaks I&J vs H insertion.
hydrazine hydrate reduction method.

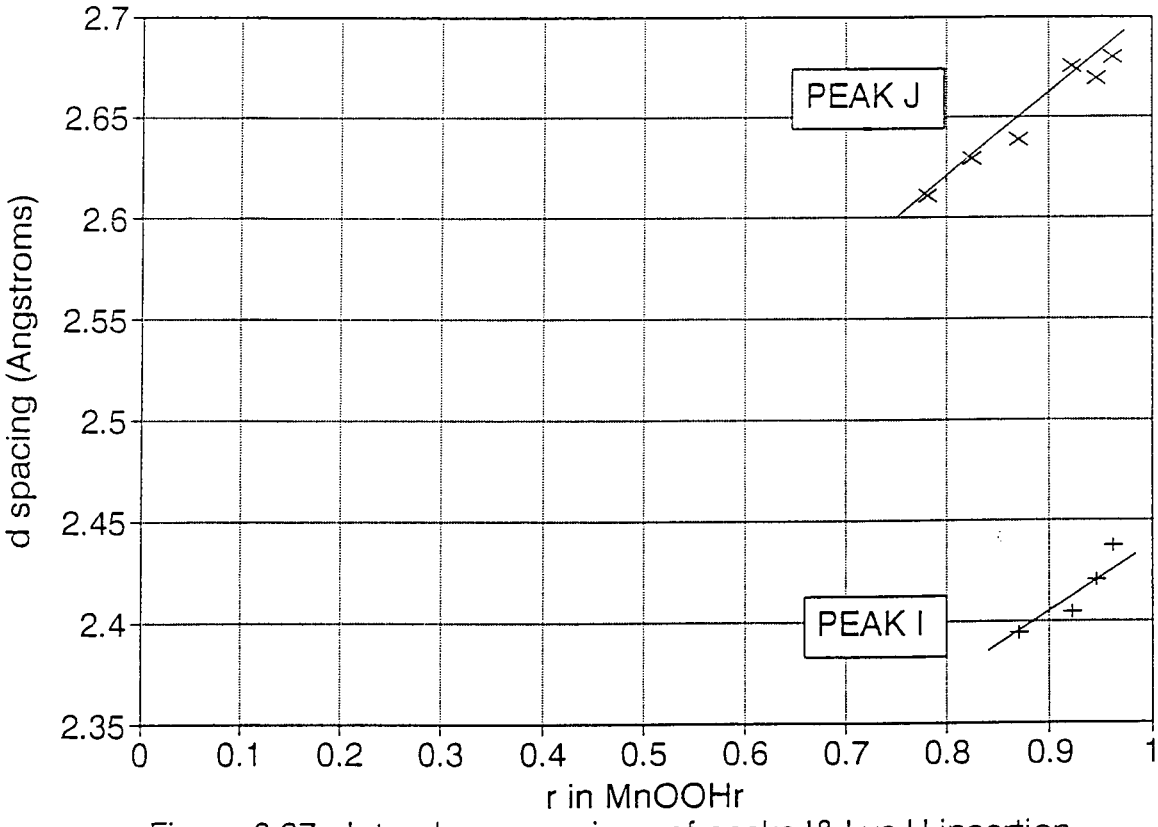

Figure 3.37.- Interplanar spacings of peaks I&J vs H insertion.
propan-2-ol reduction method.

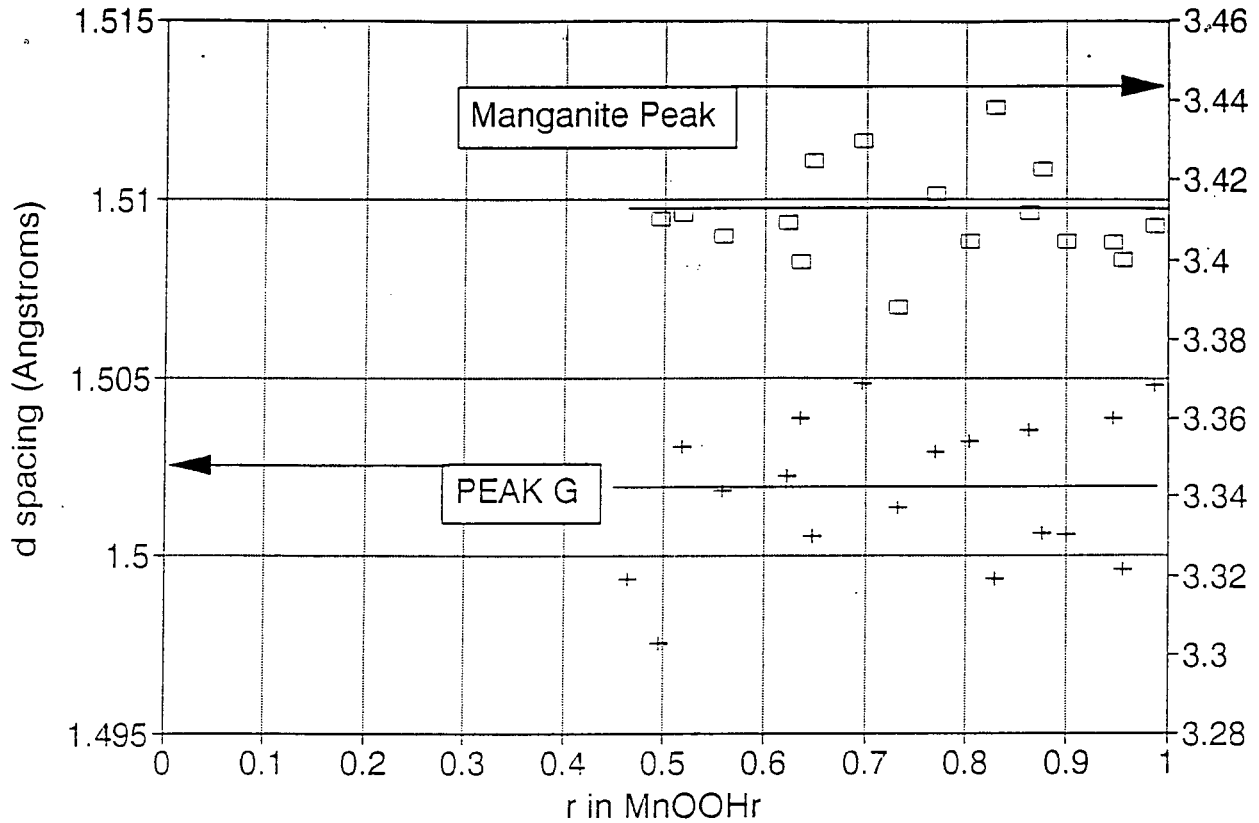

Figure 3.38.- Interplanar spacings of Manganite peaks vs H insertion. hydrazine hydrate reduction method.

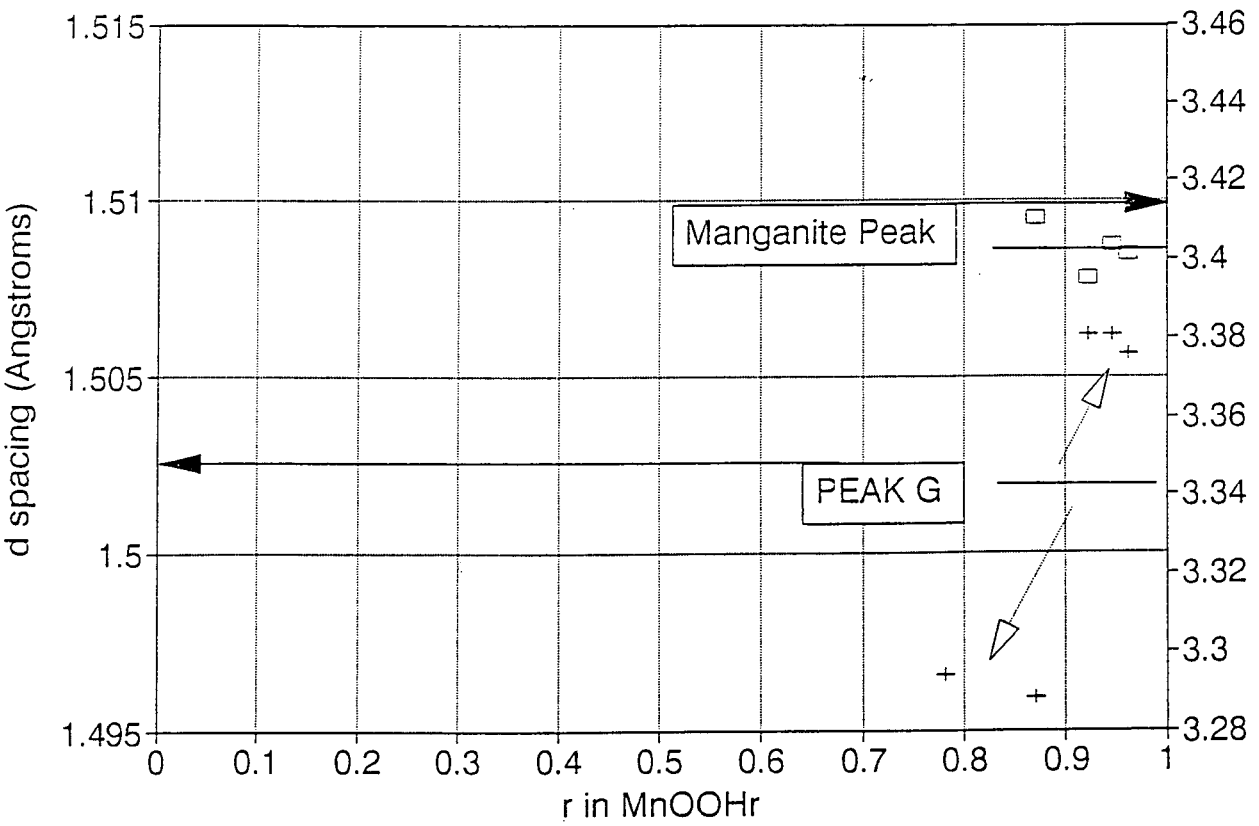

Figure 3.39.- Interplanar spacings of Manganite peaks vs H insertion. propan2-ol reduction method.

3.5.2.- Ratios of interplanar spacings vs H insertion level.

Ratios of peaks B, C, D and F with respect to peak A are presented as a function of r in Figures 3.40 to 3.47 for both hydrazine hydrate and propan-2-ol reduction methods. Peak E was not used as its width causes an inaccurate estimation of the associated interplanar spacings. These figures are useful because, if the dilation caused by H insertion were isotropic, then the calculated ratio of any two interplanar spacings would be independent of the level of H insertion [18].

For the hydrazine hydrate samples, the ratios remain constant up to a sharp change due to the emergence of the new peaks which occur at an r value of 0.4 (x equal to 1.8). Between r equal to 0.4 and 0.6 the overlapping between both "new" and "old" peaks is clearly shown as the "new" ones grow slowly at expenses of the "old" ones. Beyond this change, the ratios of the new peaks remain constant as well, close to those of the original ones.

However, for the propan-2-ol samples, the behaviour is different and follows the pattern previously explained in section 3.5.1.. The most important changes are focused in the region $r > 0.8$-0.9, being the sharp change of interplanar spacings derived from peaks C and D most apparent than those derived from peaks A and B. Thus in the region $r > 0.9$ dilation was anisotropic. These results clearly agree with the findings of Fitzpatrick and Tye [18], who carried out the reduction with xylene, acetone, cinnamyl alcohol and combinations of them.

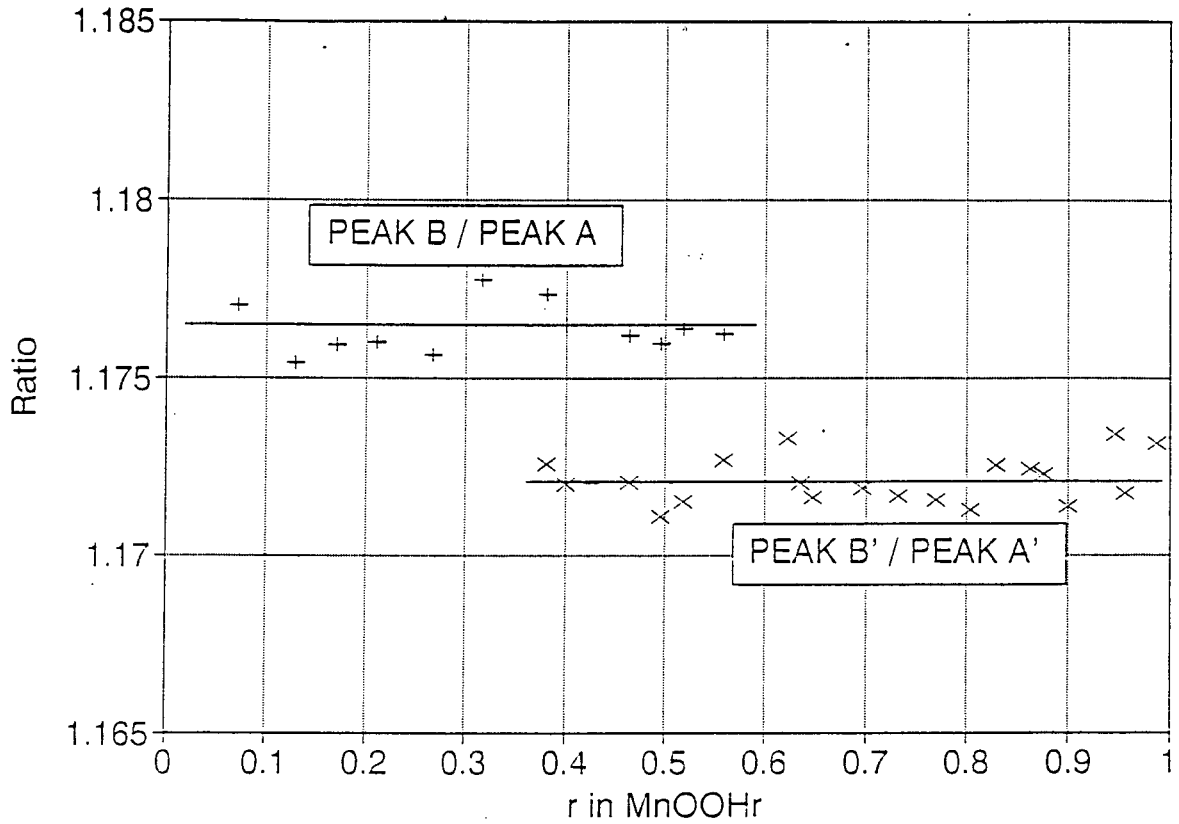

Figure 3.40.- Ratios of interplanar spacings of peaks B,B',A&A' vs H insertion level. Hydrazine hydrate reduction method.

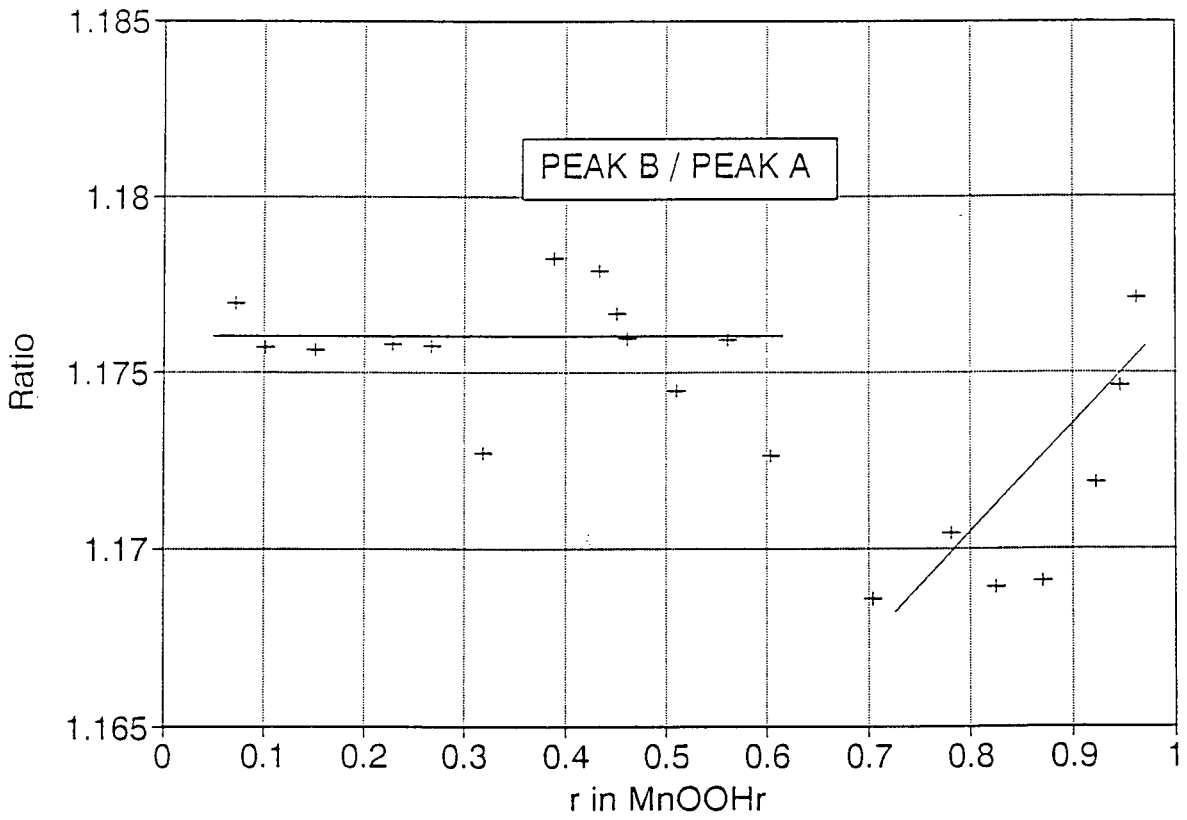

Figure 3.41.- Ratios of interplanar spacings of peaks B & A vs H insertion level. Propan-2-ol reduction method.

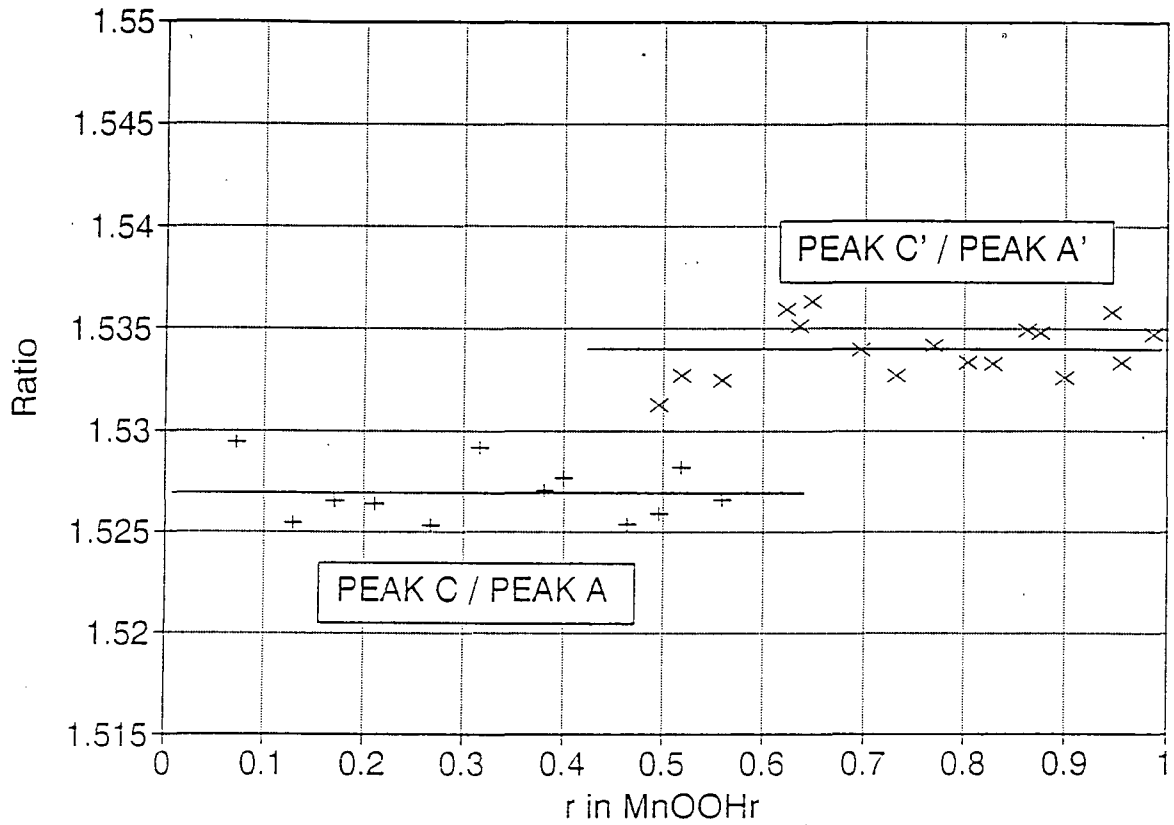

Figure 3.42.- Ratios of interplanar spacings of peaks C,C',A&A' vs H insertion level. Hydrazine hydrate reduction method.

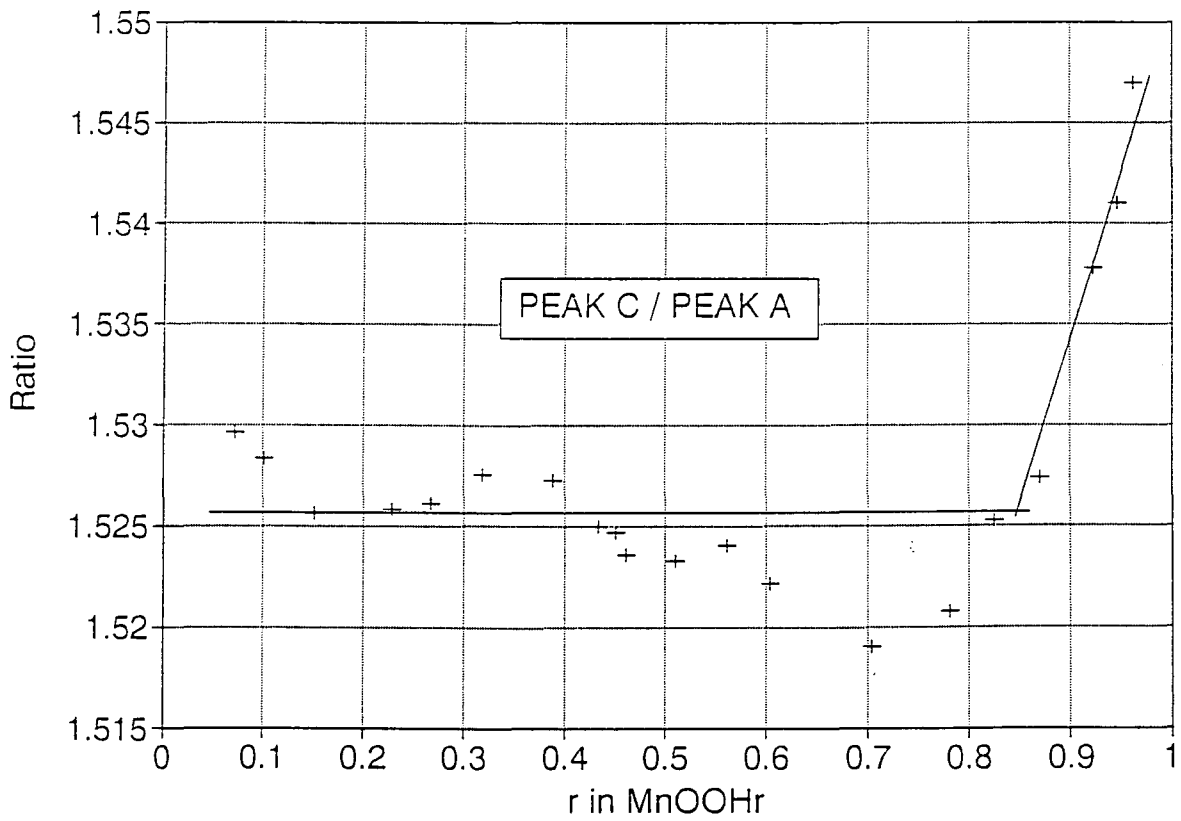

Figure 3.43.- Ratios of interplanar spacings of peaks C&A vs H insertion level. Propan-2-ol reduction method.

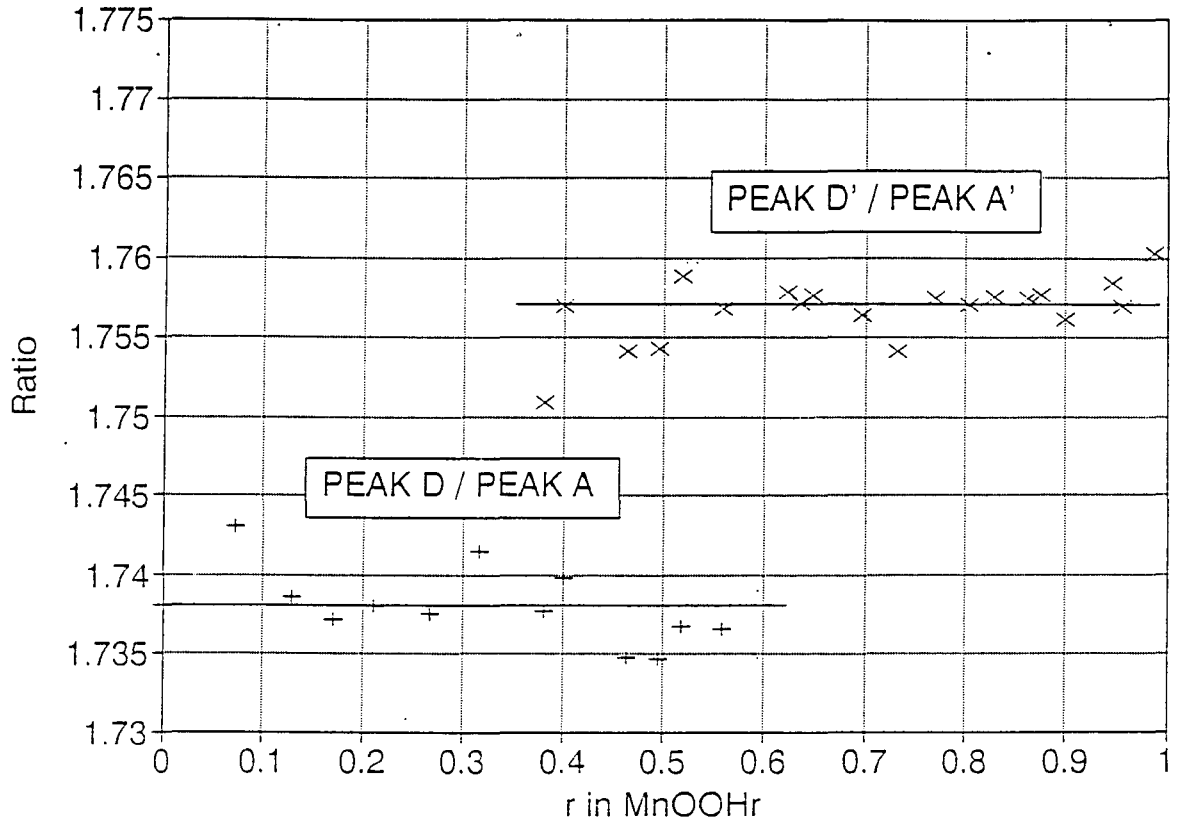

Figure 3.44.- Ratios of interplanar spacings of peaks D,D',A&A' vs H insertion level. Hydrazine hydrate reduction method.

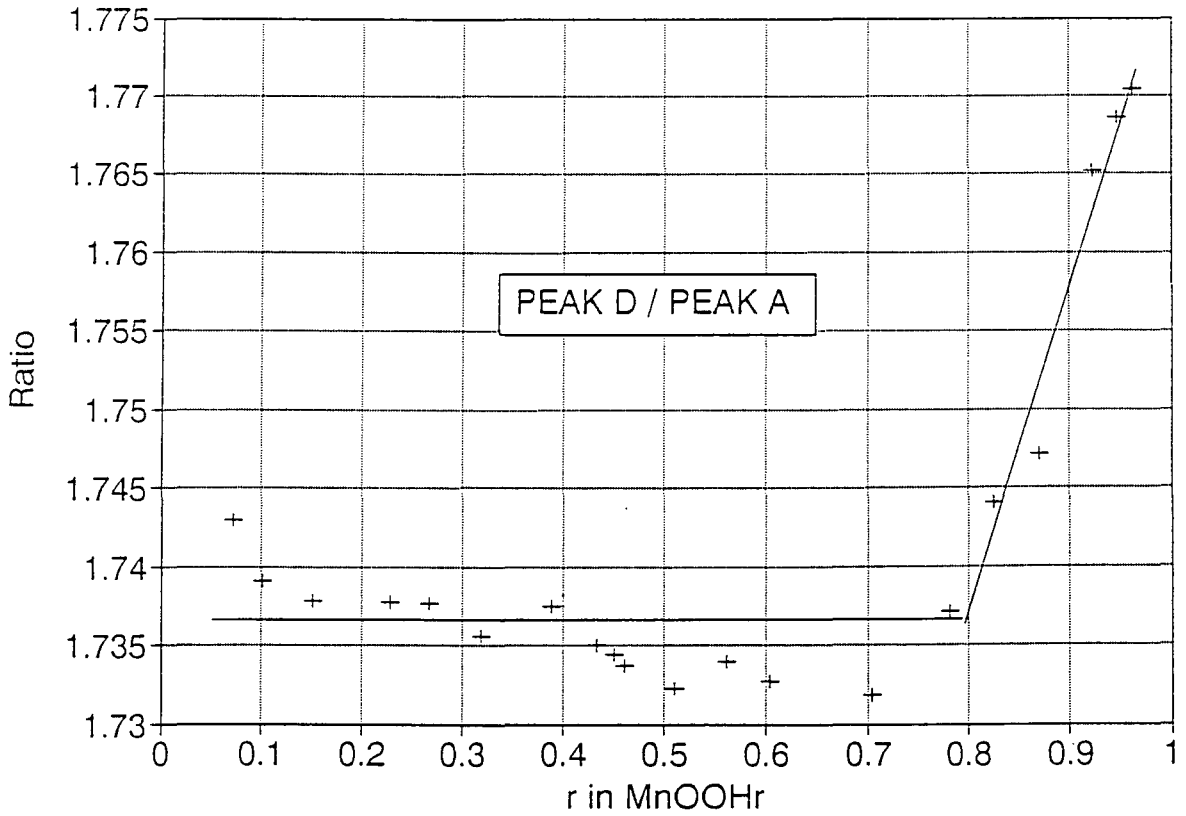

Figure 3.45.- Ratios of interplanar spacings of peaks D&A vs H insertion level. Propan-2-ol reduction method.

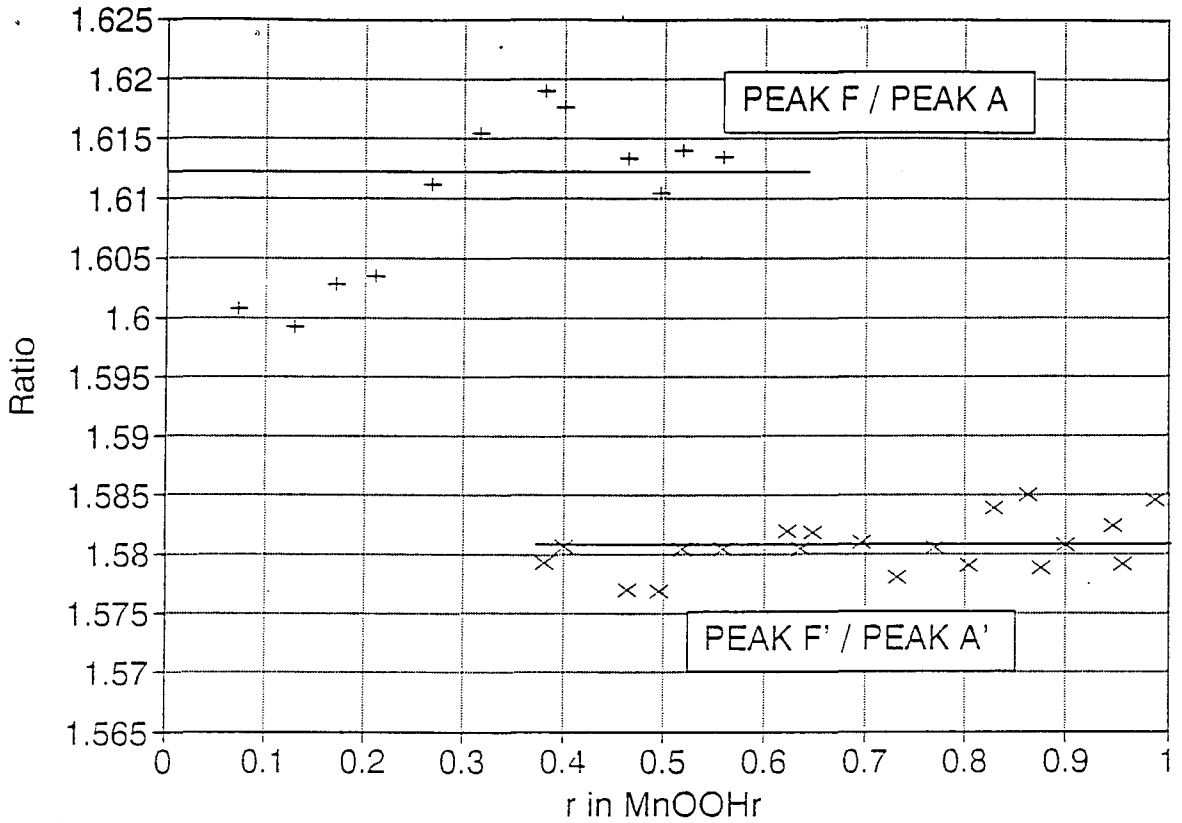

Figure 3.46.- Ratios of interplanar spacings of peaks F,F',A&A' vs H insertion level. Hydrazine hydrate reduction method.

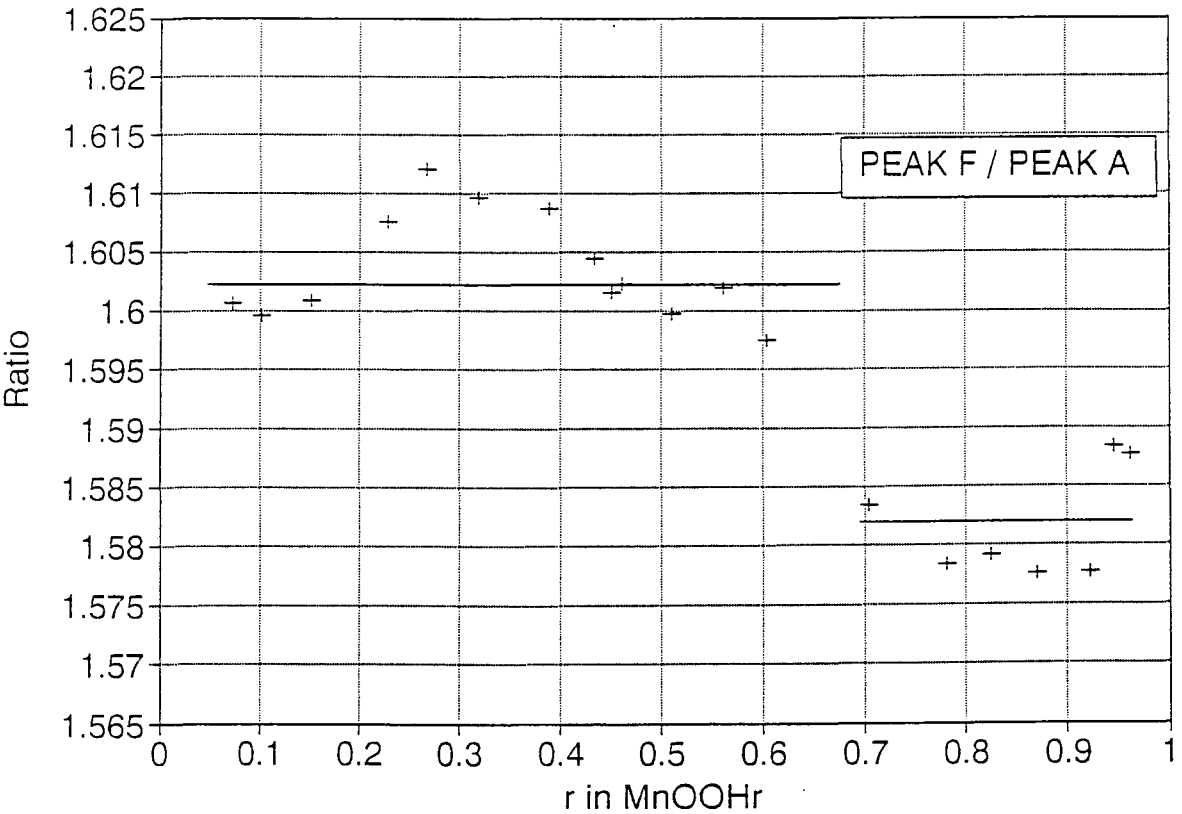

Figure 3.47.- Ratios of interplanar spacings of peaks F&A vs H insertion level. Propan-2-ol reduction method.

3.6.- XRD CONCLUSIONS.

From the results obtained with X-Ray Diffraction, the following can be concluded:

3.6.1.- Hydrazine hydrate reduction method.

The presence of heterogeneity using this reduction method at a very low degree of reduction, r values close to 0.3-0.4, has been demonstrated by :

- The appearance of new peaks which grow at the expense of the original ones (section 3.4, Figures 3.5 to 3.9).
- This appearance together with changes on both "original" and "new" peaks along the reduction has been more exhaustively shown by studying very carefully the evolution versus H insertion level of:
  - Interplanar spacings (section 3.5.1, Figures 3.26, 3.28, 3.30, 3.32, 3.34, 3.36 and 3.38) : it has been clearly confirmed the initial dilation of the structure up to the onset of heterogeneity. Afterwards, the interplanar spacings of the new peaks remained constant.
  - Ratios of interplanar spacings (section 3.5.2, Figures 3.42, 3.44 and 3.46) : sharp change on ratio values beyond an early level of H insertion.

- Prediction of X-ray diffraction patterns from the patterns of the two phases participating in the heterogeneous reduction (section 3.4.1, Figures 3.10 to 3.20) : an almost exact prediction has been achieved.
- Evolution behaviour of XRD patterns of dry mixtures of reduced compounds (section 3.4.1, Figures 3.21 and 3.22) : no change with time for mixtures of compounds in the range of heterogeneity.

The importance of the speed of reduction on the r value at which heterogeneous reduction commences has also been demonstrated (section 3.4.2, Figures 3.23 to 3.25) : this means not only the reduction method employed that is important but also the different ways of carrying out one specific method.

3.6.2.- Propan-2-ol reduction method.

In contrast to the Hydrazine Hydrate reduction method, this method has corroborated previous results indicating a homogeneous reduction. This has been corroborated by :

- Movement of peak positions due to lattice dilation over the complete reduction range, together with the not appearance of new peaks until a high degree of H insertion (r values close to 0.9), seen as :
  - An increase of interplanar spacings of all the peaks with H insertion (section 3.5.1, Figures 3.27, 3.29, 3.31, 3.33, 3.35, 3.37 and 3.39).

- Independence of the ratios of interplanar spacings up to close the end of reduction, indicative of isotropic H insertion (section 3.5.2, Figures 3.43, 3.45 and 3.47).

Moreover, changes in the behaviour which occurred with H insertion at different levels have been explained (sections 3.5.1 and 3.5.2) and attributed to :

- Generation of enlarged regions of disorder between crystallites at $r = 0.25$.
- Change on the type of site occupied by the inserted species at $r = 0.45$.
- Change on the cell shape at $r > 0.8$.

4.- FOURIER TRANSFORM INFRARED (FTIR)

Fourier Transform InfraRed (FTIR) spectroscopy has been suggested [44, 45, 79] as a useful technique for the characterisation of battery active EMD. FTIR spectrometers require a Fourier Transform to produce the conventional frequency spectrum and have advantages over the traditional dispersive instruments in the areas of energy, such as sensitivity and wavenumber accuracy [80, 81]. The absorption of infrared radiation is associated with the vibration of chemical bonds. Consequently, the FTIR spectrum contains information about both the atoms present in the sample and the way in which they are bonded.

Unlike X-Ray Diffraction, FTIR gives information on both amorphous and crystalline structures. Nevertheless, in contrast to XRD, even today the available literature on the characterisation of manganese dioxide polymorphs by infrared studies seems to be inconclusive. Infrared spectra of pyrolusite [82, 83, 84] and other manganese minerals [85, 86, 87] have been published by various workers. More recently, Yanchuk and Povarennyk [88] presented the infrared absorption spectra and characteristic absorption frequencies of a large number of manganese oxides such as pyrolusite, ramsdellite, nsutite, birnessite, cryptomelane, hollandite and romanechite. Brenet and Faber [89] believe that the infrared frequency data, especially the shifts in the Mn-O absorption frequency, are related to catalytic and electrochemical activity.

Recent high resolution infrared spectral measurements carried out by Potter and Rossman [44] provided information on the structure and H_2O content of various Mn(IV) oxide phases. However, there exists scarce information on infrared spectra of γ-manganese dioxides and of their insertion compounds [40, 90]. For EMD, in the 400-800 cm^{-1} region [91], absorptions are mainly thought to be due to vibrations associated with the $[MnO_6]$ octahedra, resulting in a distinctive peak (labelled a in this work) in the pattern. A typical EMD pattern is shown in Figure 4.1.

The intention with this technique was to complement the results and conclusions before obtained with the XRD technique and mentioned in chapter 3 and thereby substantiate the differences arising from the two reductions methods studied in the present work.

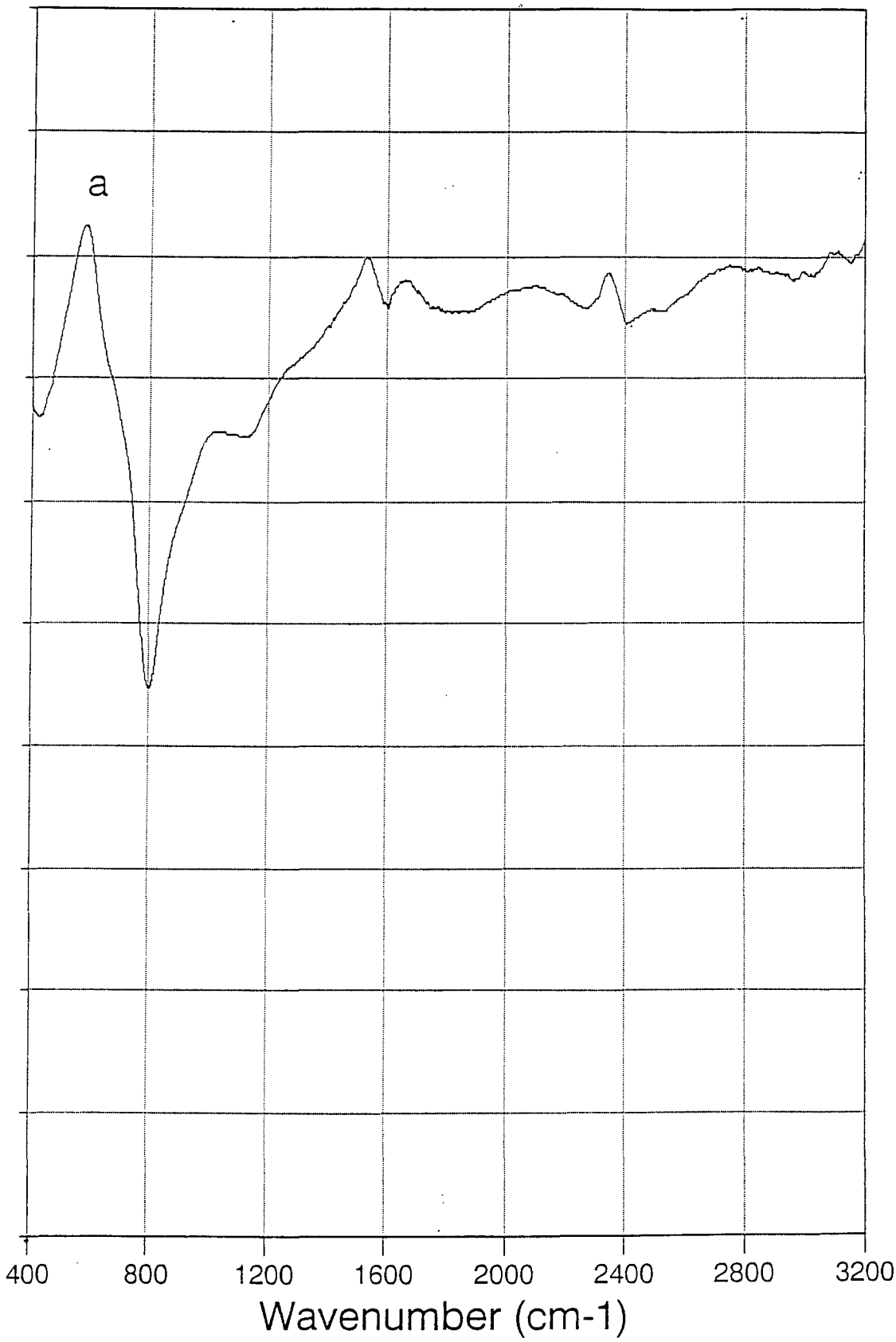

Figure 4.1.- Typical EMD FTIR pattern.

4.1.- EXPERIMENTAL METHOD

The conditions used to obtain all the FTIR spectra were as follow :

About 3 mg of each sample were mixed manually in an agate mortar with about 450 mg of CsI for 5 minutes. With this mixture, two parts of about 225 mg were separated and each part was pressed into a pellet. All actual weights were recorded. The pellets were subsequently stored in a desiccator for two days to remove the possible absorbed water.

The spectra of the pellets were taken in transmission using a Perkin Elmer PE 1710 FTIR spectrometer over the wavenumber range 400 - 4400 cm^{-1}. 50 scans were taken for each spectrum with a resolution of 2 cm^{-1} (scan time = 7.1 min). The interferometer area was sealed and desiccated, in order to reduce water interference during the process of measurement.

The data were adjusted by subtracting the CsI blank (with about the same amount of CsI as in the samples) measured during the same run and the spectra were adjusted to a standard 1 mg $MnOOH_x/cm^2$ loading using the weight data previously recorded. The data were converted to spreadsheet files for the purposes of data manipulation.

The characteristics of the equipment PE 1710 FTIR manufactured by Perkin Elmer employed in this research were :

- A 1700 series optical module.
- A 1700 series intelligent controller module.
- A 1700 series electronics module.
- A Perkin Elmer Model PP1 Plotter Printer.
- A Coated FR-DTGS detector with moisture resistant CsI window.
- Maximum output power of 5 mW.
- Visible radiation at a wavelength of 633 nm.
- Temperature stabilised ceramic source operating at 1400 K.
- Abscissa accuracy of 0.01 cm^{-1}.
- Ordinate precision better than 0.1% T.
- Signal to noise typically better than 0.1% T peak to peak.

4.2.- PROPAN-2-OL REDUCED SAMPLES

The spectra obtained over the frequency range 400-4400 cm^{-1} have been considered in two approximately distinct regions [91] : In the region 400-800 cm^{-1}, absorptions are mainly thought to be due to vibrations associated with the $[MnO_6]$ octahedra, whereas those in the region 800-4400 cm^{-1} are associated with various OH^- vibrations. The absorptions which emerge with H insertion in the 800-4400 cm^{-1} region due to OH bonds are thought to be associated with restricted mobility of H in the structure.

In spite of all the precautions taken to avoid the presence of water (manipulation of the pellets in desiccator, use of interferometer area sealed and desiccated, ...), unavoidable peaks appeared in the 3400 cm^{-1} region in some of the spectra attributable to water. Also some small peaks that appear at about 1400 cm^{-1} and 1550 cm^{-1} are probably due to overtone vibrations of the octahedra. Theoretically overtones result from anharmonicity of the vibration [99] , causing vibrations at wavenumbers close to but never exactly that of an integral number times the wavenumber of a fundamental vibration, as has been noted for H-inserted EMD by Fitzpatrick et al [91].

As explained by Russel [98], in order to obtain optimum quality infrared spectra of inorganic compounds, the particle size should be less than the shortest wavelength investigated. At a wavenumber of 4000 cm^{-1} this corresponds to a particle size of 2.5 μm,

whereas the mean particle sizes of the products used in this work are 15 to 20 times greater than this. Fitzpatrick et al [91] have pointed out that the broad rising band that appears above 800 cm^{-1} is probably a background effect caused by the scattering from the large particles which decreases when particle size is reduced by H insertion due to demicrotwinning.

The evolution of the spectra in the frequency range 400-3200 cm^{-1} for the Propan-2-ol samples with degree of reduction is shown in Figure 4.2., where the nomenclature for the new absorption peaks which appeared during the reduction is presented. Figure 4.2. shows that there is no significant change in the spectra up to r values close to 0.8. However, for insertion levels greater than $r > 0.8$, new peaks emerged, labelled b, c, d (appears at $r = 0.704$ although becomes completely developed at $r > 0.8$), e, f, and g.

The appearance of these new peaks is attributed to restricted mobility of H when H starts to "freeze" or locate within the structure. As explained before, with more insertion, the tendency is to increase the amount of the low mobility structure, and the new peaks become more clearly developed.

These findings are in total agreement with those previously established with the X-Ray Diffraction technique (Chapter 3.3).

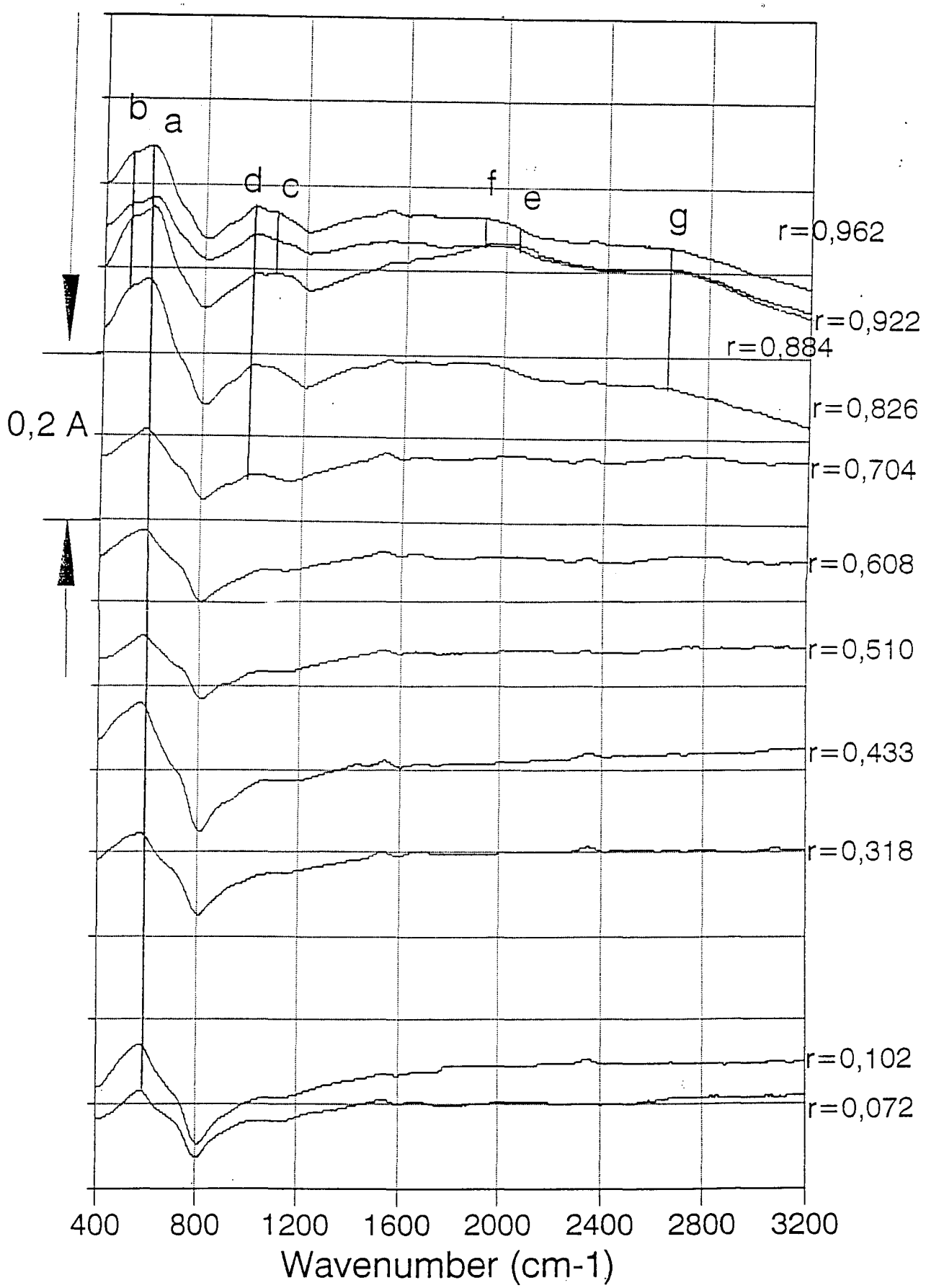

Figure 4.2.- FTIR pattern evolution for propan-2-ol reduction method

4.3.- HYDRAZINE HYDRATE REDUCED SAMPLES

As is done for the Propan-2-ol samples, the spectra evolution with the reduction degree is presented in Figure 4.3 for the Hydrazine Hydrate reduced samples. Such evolution is clearly different from that of the Propan-2-ol reduced samples, and is again in total concordance with the findings revealed by X-Ray Diffraction. The new peaks previously mentioned which are attributed to OH bonds and arise from restricted mobility of H in the structure, emerge earlier in the Hydrazine Hydrate samples; r = 0.380 in contrast to r = 0.80 for the Propan-2-ol samples.

It should be noticed that, unlike the X-Ray diffraction patterns, the spectra of the end products are slightly different depending on the reduction method employed, and further work is required to understand such behaviour.

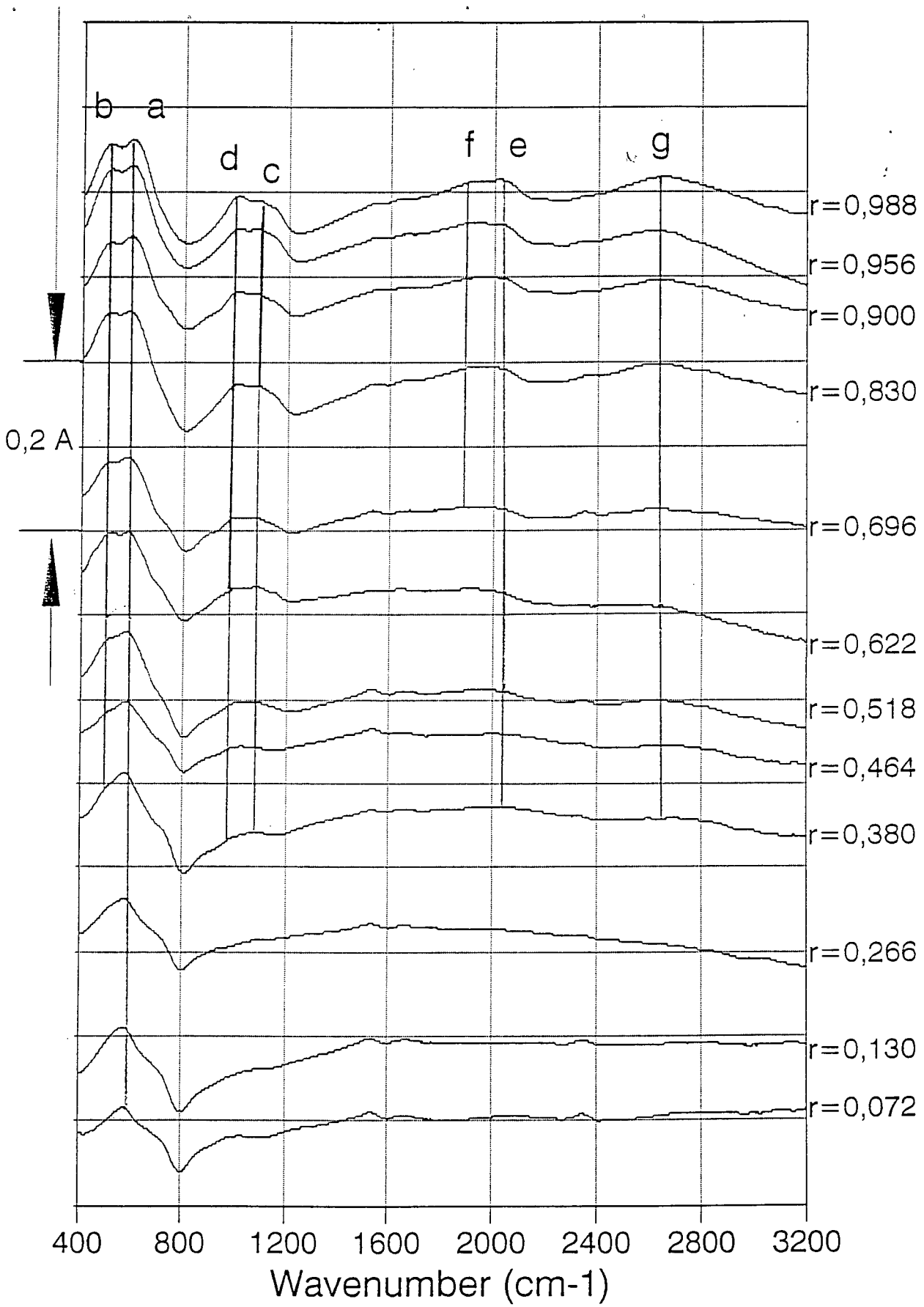

Figure 4.3.- FTIR pattern evolution for hydrazine reduction method

4.4.- DIFFERENCES BETWEEN PROPAN-2-OL AND HYDRAZINE HYDRATE REDUCED SAMPLES.

4.4.1.- Mathematical mixtures.

Following the same idea as was carried out with the X-ray patterns, the FTIR spectra of the samples were predicted by mixing mathematically the spectra at the products of the edges of the assumed heterogeneous reduction region in the appropriate proportions. The chosen end-members for the mixture were those available which were most similar to the ones used in the previous section 3.4.1.:

Hydrazine Hydrate : $MnOOH_{0.380}$ and $MnOOH_{0.830}$,

Propan-2-ol : $MnOOH_{0.318}$ and $MnOOH_{0.826}$

In the case of the hydrazine hydrate samples, an almost exact prediction was obtained as shown in Figures 4.4 to 4.7., where a nearly parallel trend is observed, even for wavenumbers of 1600-3200 cm^{-1}. However, when attempting to predict the spectra of the Propan-2-ol samples from arithmetic mixing, the result obtained was different from that for the hydrazine hydrate samples. This is shown in Figures 4.8 to 4.11. where it is possible to check :

a.- Peaks less developed in the experimental spectra in relationship to the theoretical.

b.- Different shapes for experimental and calculated spectra more clearly observed in the region 1600 - 3200 cm^{-1}, where they are clearly not parallel in contrast to the behaviour mentioned previously for the hydrazine hydrate samples.

This finding is a further indication of the different heterogeneous (hydrazine hydrate) / homogeneous (Propan-2-ol) reduction behaviour of the methods studied in this work.

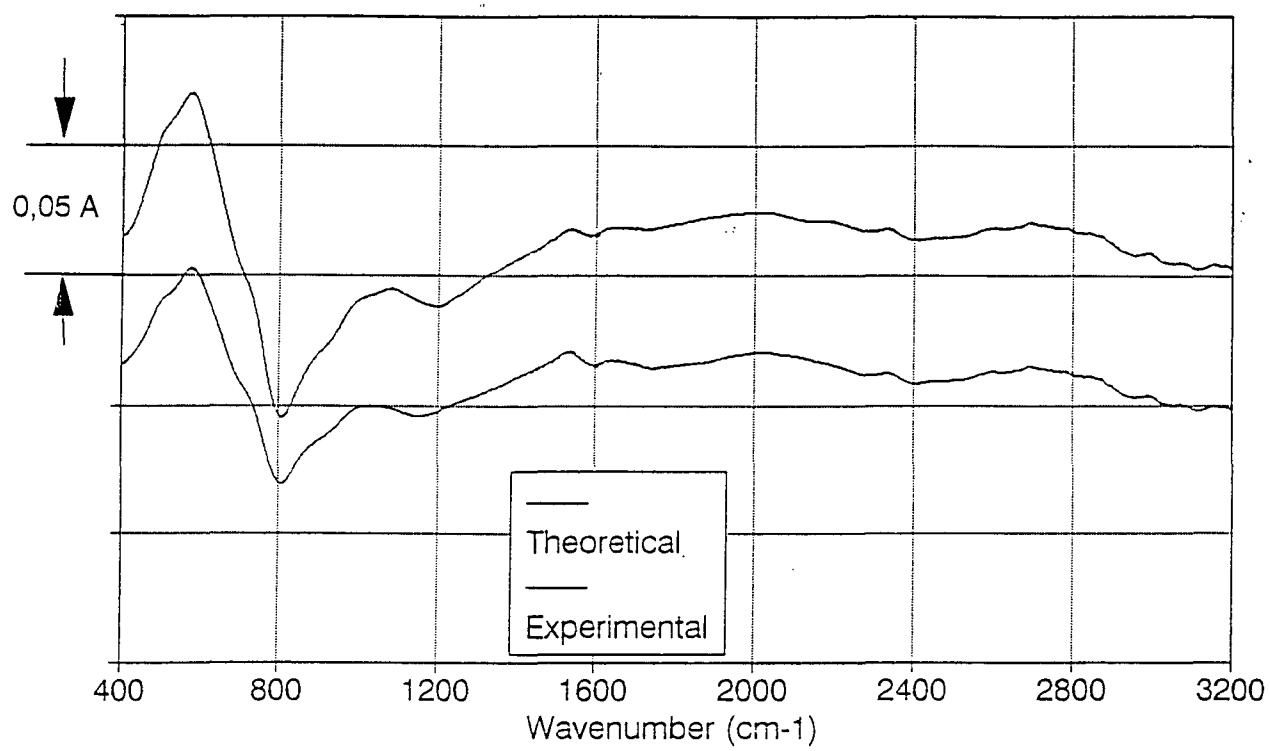

Figure 4.4.- Comparison of math. mixture (81,3% MnOOH0,380/18,7% MnOOH0,830= MnOOH0,464) and experimental (hydrazine hydrate MnOOH0,464) FTIR patterns

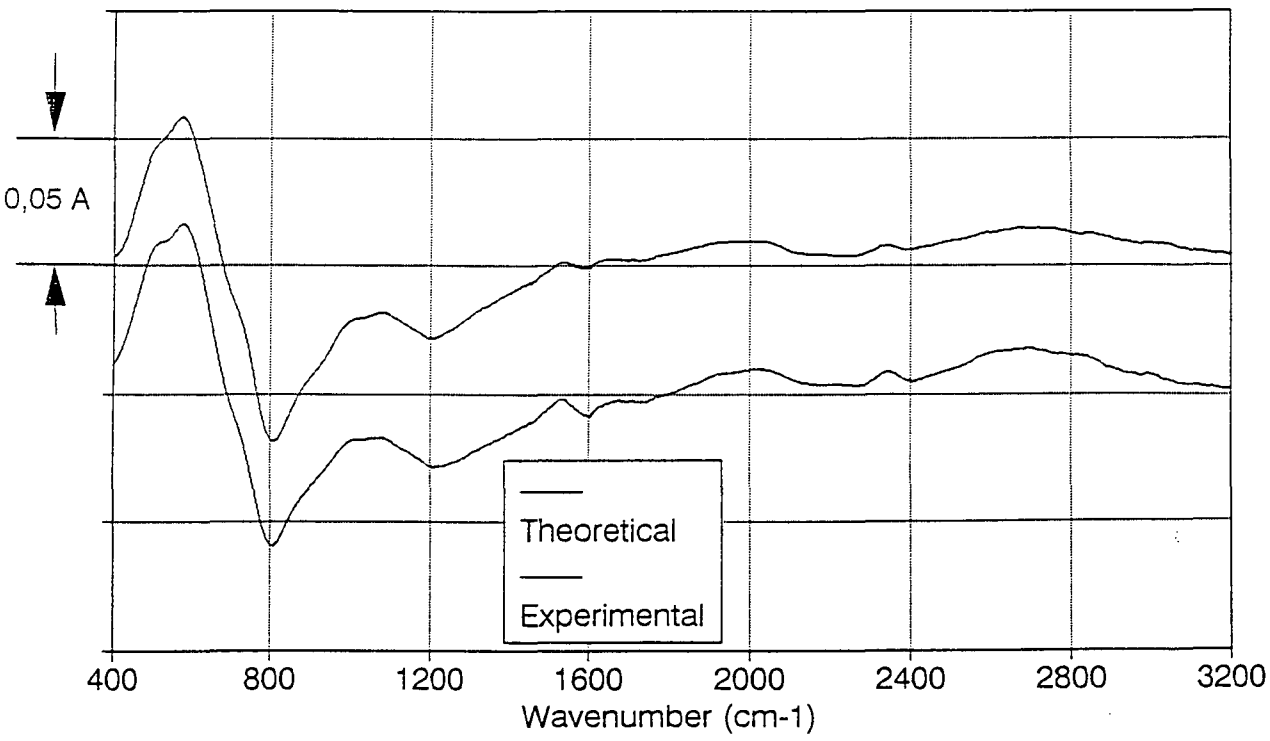

Figure 4.5.- Comparison of math. mixture (69,3% MnOOH0,380/30,7% MnOOH0,830= MnOOH0,518) and experimental (hydrazine hydrate MnOOH0,518) FTIR patterns

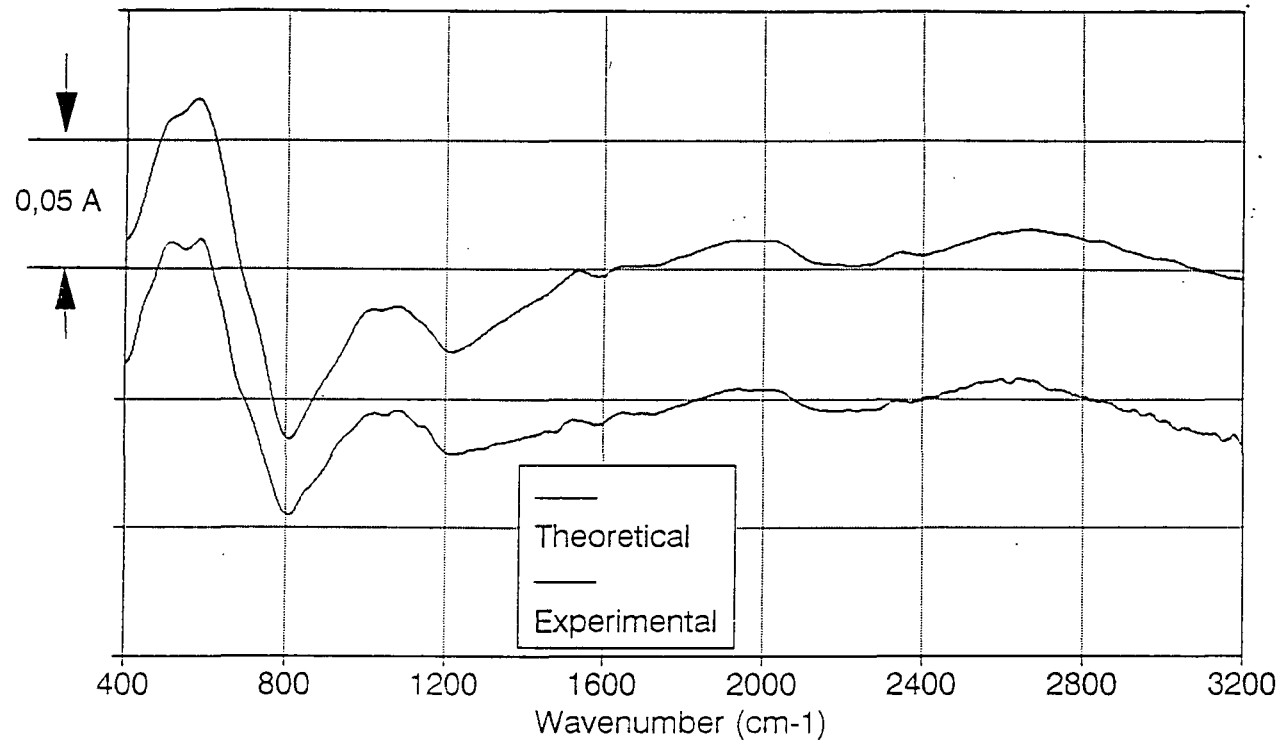

Figure 4.6.- Comparison of math. mixture (46,2% MnOOH0,380/53,8% MnOOH0,830= MnOOH0,622) and experimental (hydrazine hydrate MnOOH0,622) FTIR patterns

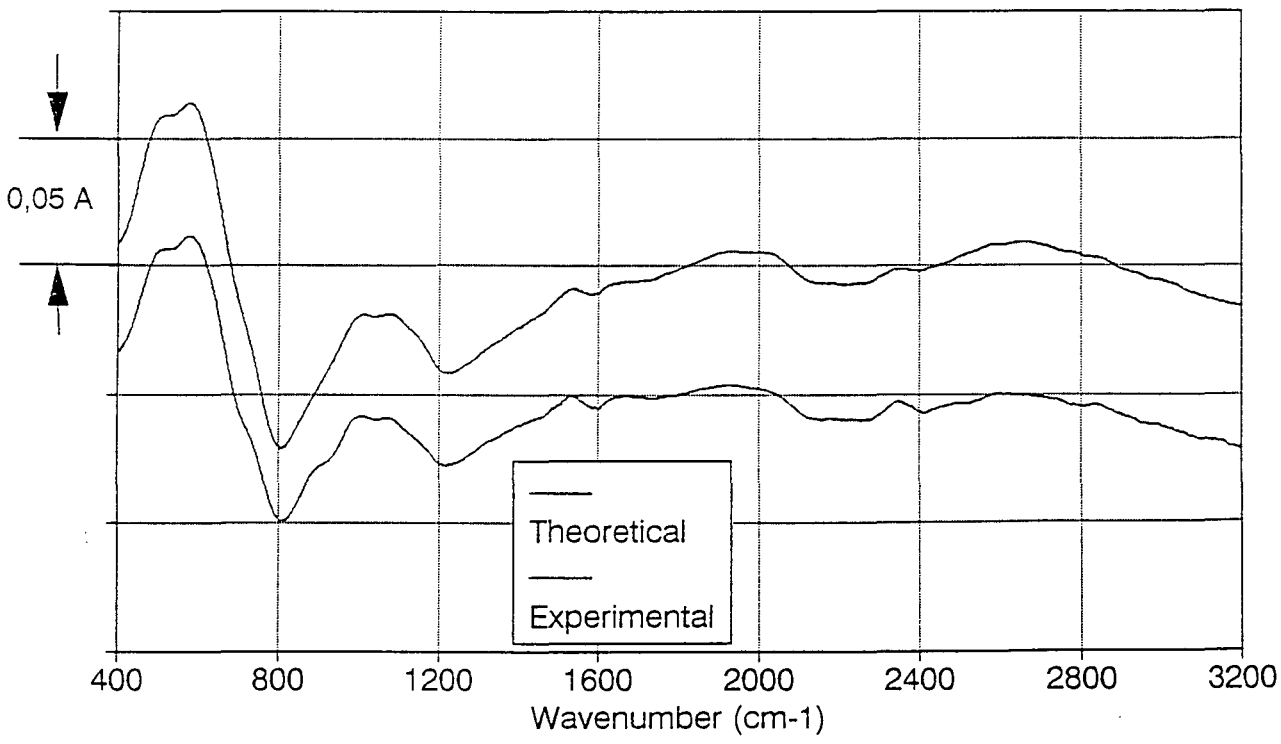

Figure 4.7.- Comparison of math. mixture (29,8% MnOOH0,380/70,2% MnOOH0,830= MnOOH0,696) and experimental (hydrazine hydrate MnOOH0,696) FTIR patterns

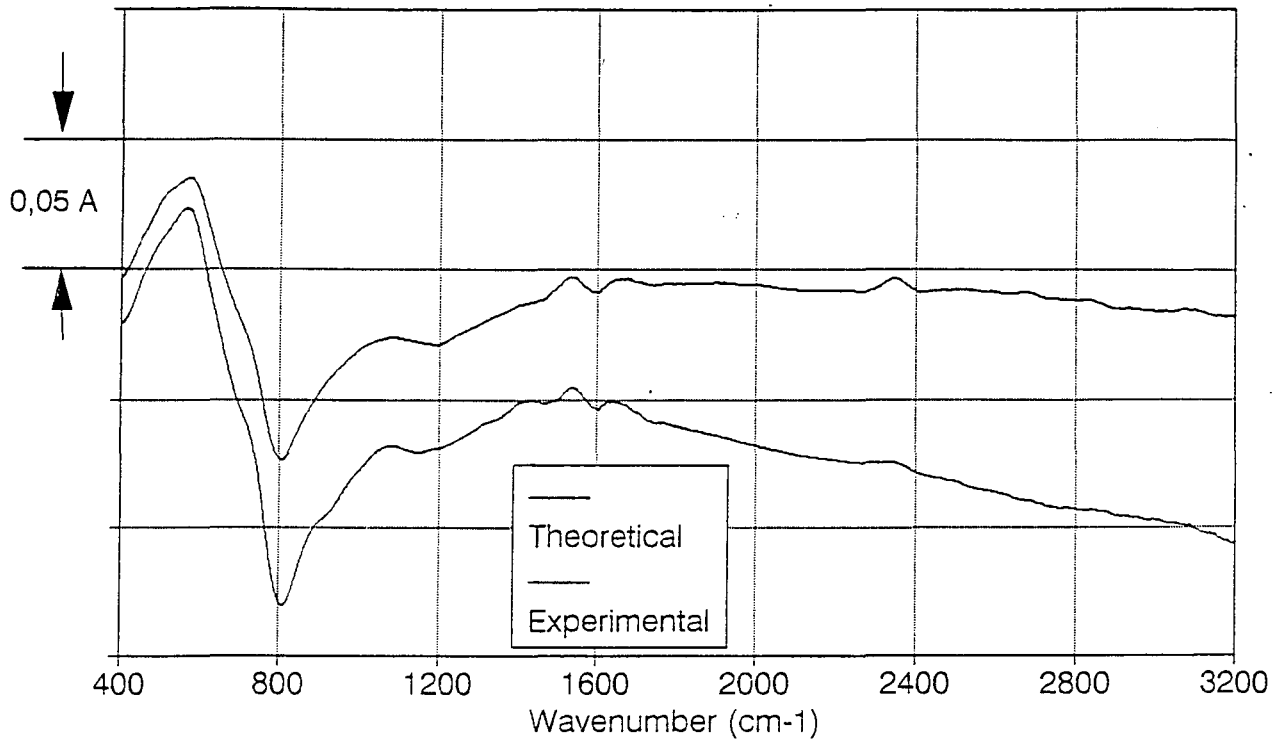

Figure 4.8.- Comparison of math. mixture (77,4% MnOOH0,318/22,6% MnOOH0,826= MnOOH0,433) and experimental (propan-2-ol MnOOH0,433) FTIR patterns

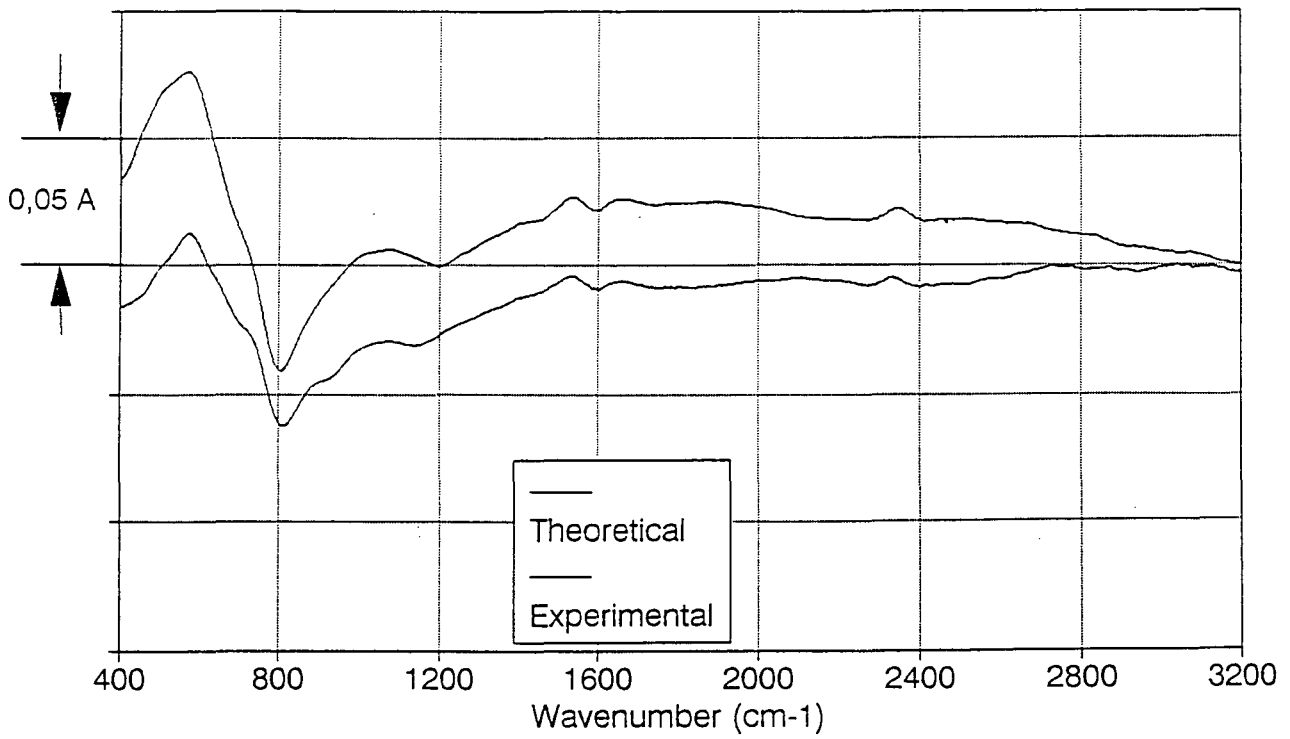

Figure 4.9.- Comparison of math. mixture (62,2% MnOOH0,318/37,8% MnOOH0,826= MnOOH0,510) and experimental (propan-2-ol MnOOH0,510) FTIR patterns

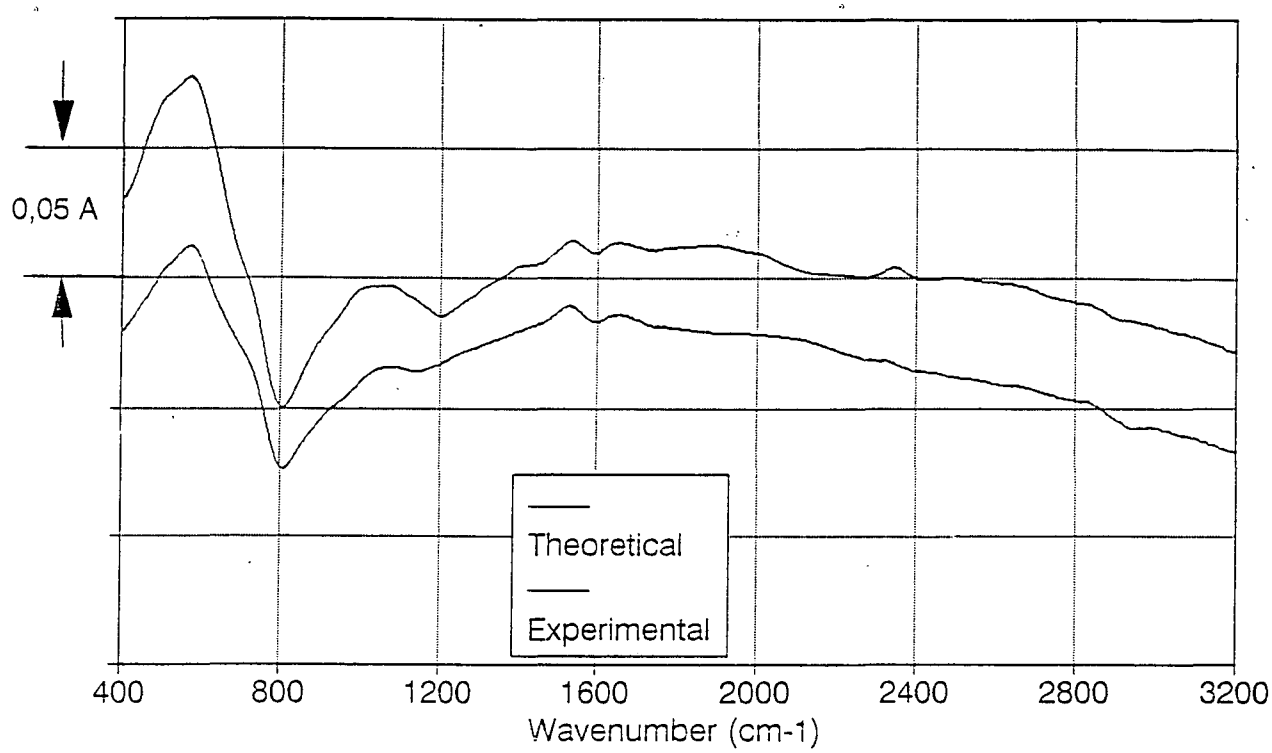

Figure 4.10.- Comparison of math. mixture (42,9% MnOOH0,318/57,1% MnOOH0,826= MnOOH0,608) and experimental (propan-2-ol MnOOH0,608) FTIR patterns

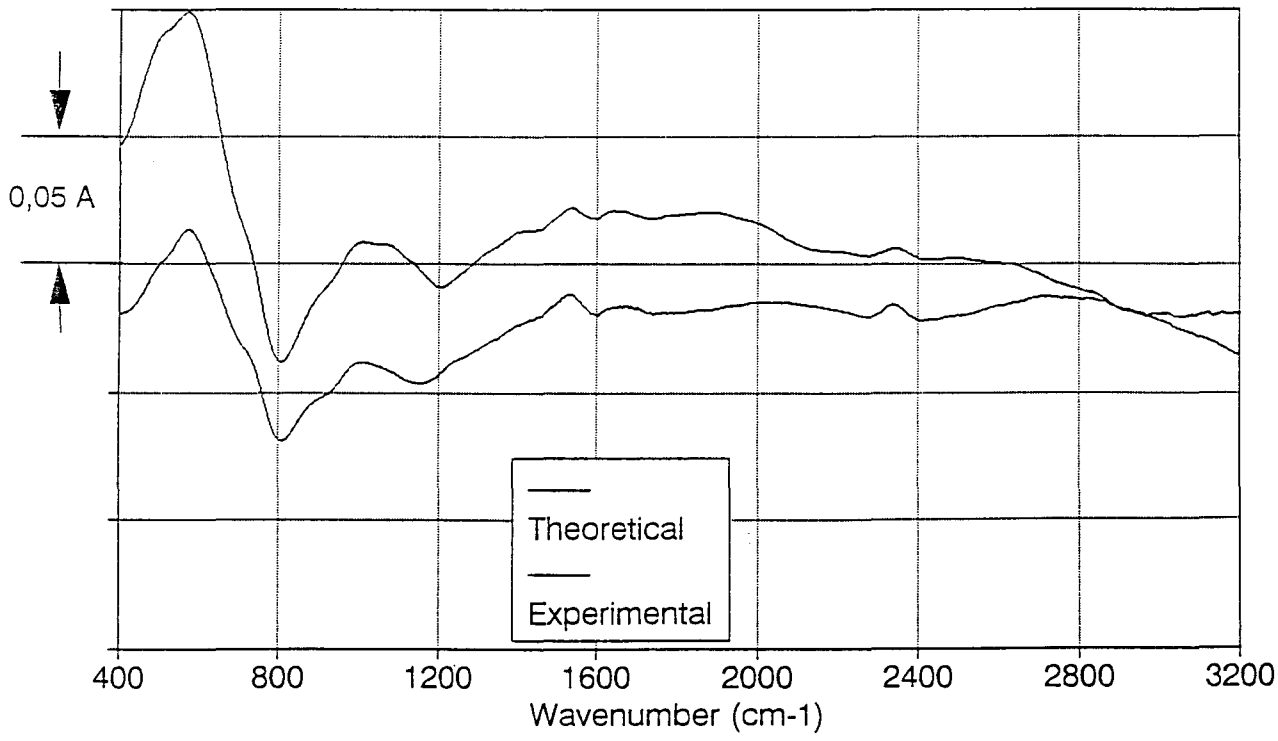

Figure 4.11.- Comparison of math. mixture (24,0% MnOOH0,318/76,0% MnOOH0,826= MnOOH0,704) and experimental (propan-2-ol MnOOH0,704) FTIR patterns

4.4.2.- Evolution of peak positions along H insertion.

In a similar way to the data presentation used for XRD, the evolution of the peak positions with H insertion level is shown comparatively for both hydrazine hydrate and propan-2-ol reduction methods in figures 4.12., 4.13. (peaks a and b), 4.14. and 4.15. (peaks c, d and f). It is worth noting that there were difficulties for the software to detect, in some cases, certain peaks such as e, f, and g, particularly for propan-2-ol reduced samples where these peaks are not so developed. No plots are presented for peaks where it has not been possible to detect a precise value of the peak position.

Looking at figures 4.12. and 4.13., it is observed that H insertion appear to have little effect on the position of the peaks a and b. As explained by Fitzpatrick et al [91], these peaks are associated with vibration in the a and c orthorrombic directions, which show less expansion than that in the b direction. However, towards the end of the reduction, a sharp change occurs in the position of peak (a) for samples made by both methods. Also the new peaks that appear with H insertion (figures 4.14 and 4.15) are not affected by H insertion. Concerning the absolute values, the position of peak a seems to be at a slightly higher value and the position of peak c at lower value for the hydrazine hydrate reduced samples, whereas those of peak b and d are in very similar values.

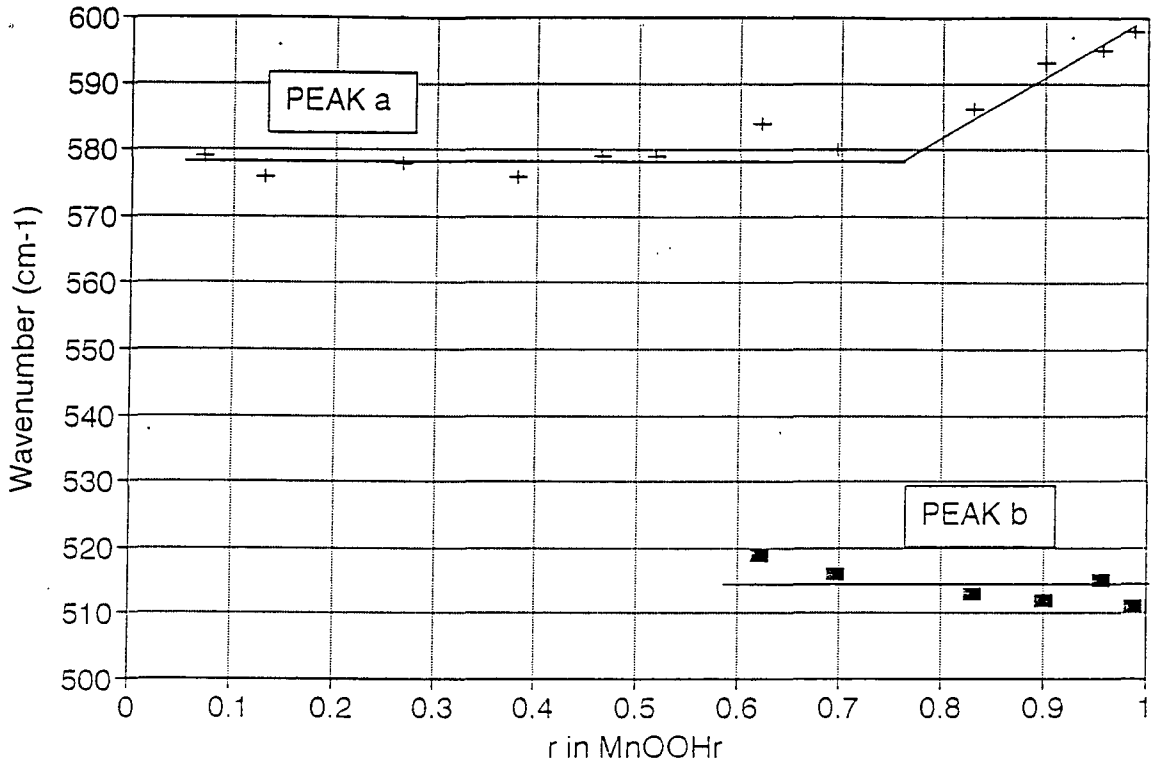

Figure 4.12.- Position of peaks a and bvs H insertion
Hydrazine hydrate reduction method

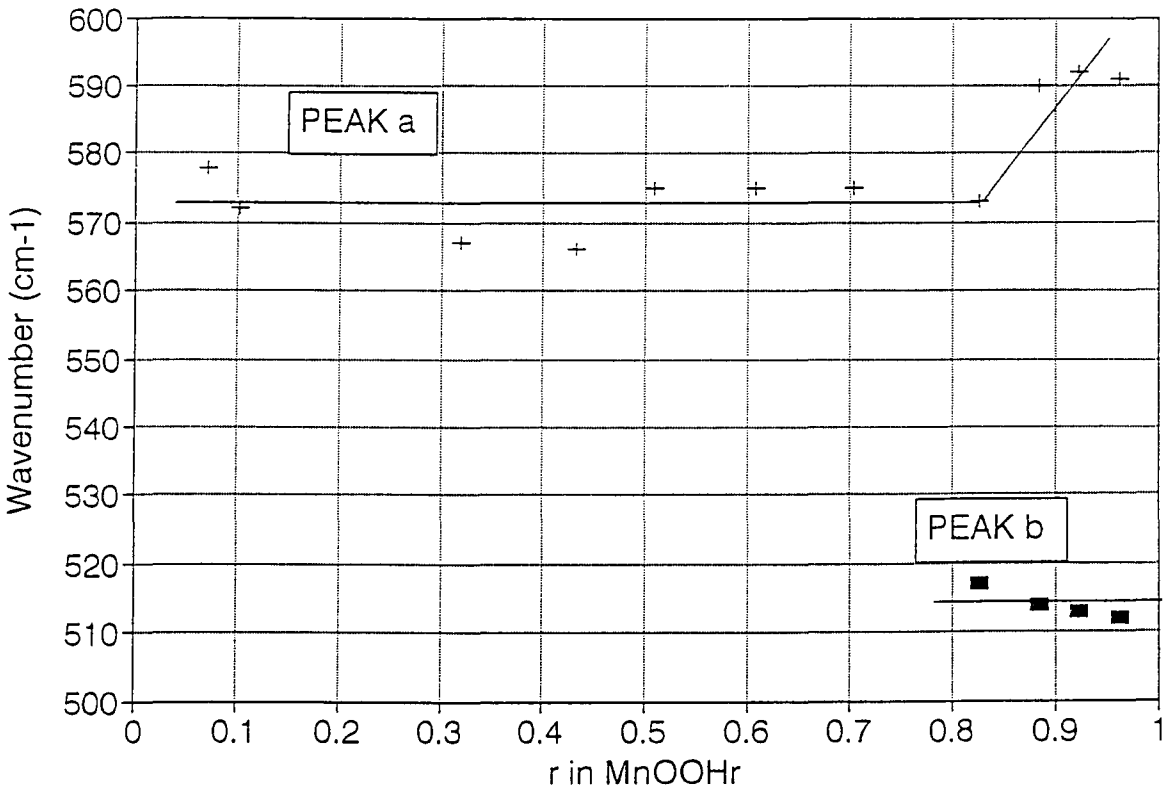

Figure 4.13.- Position of peaks a and bvs H insertion
propan-2-ol reduction method

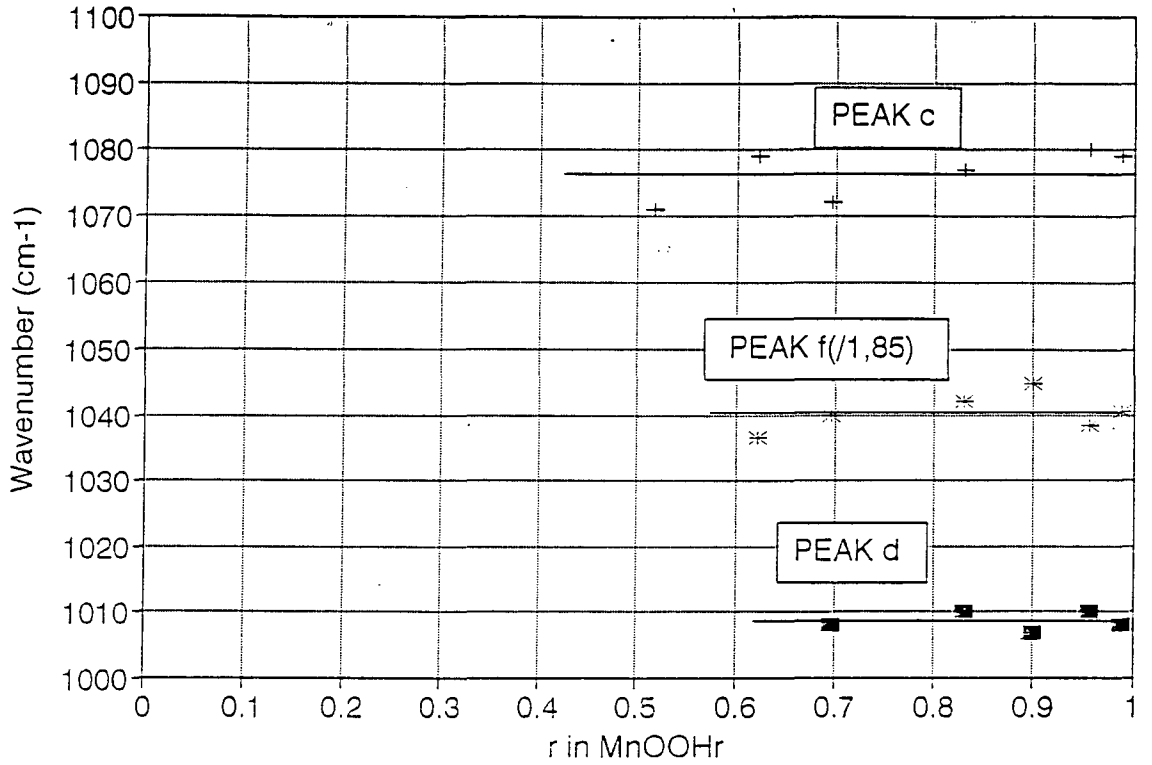

Figure 4.14.- Position of peaks c, d and f(/1,85) vs H insertion level hydrazine hydrate reduction method

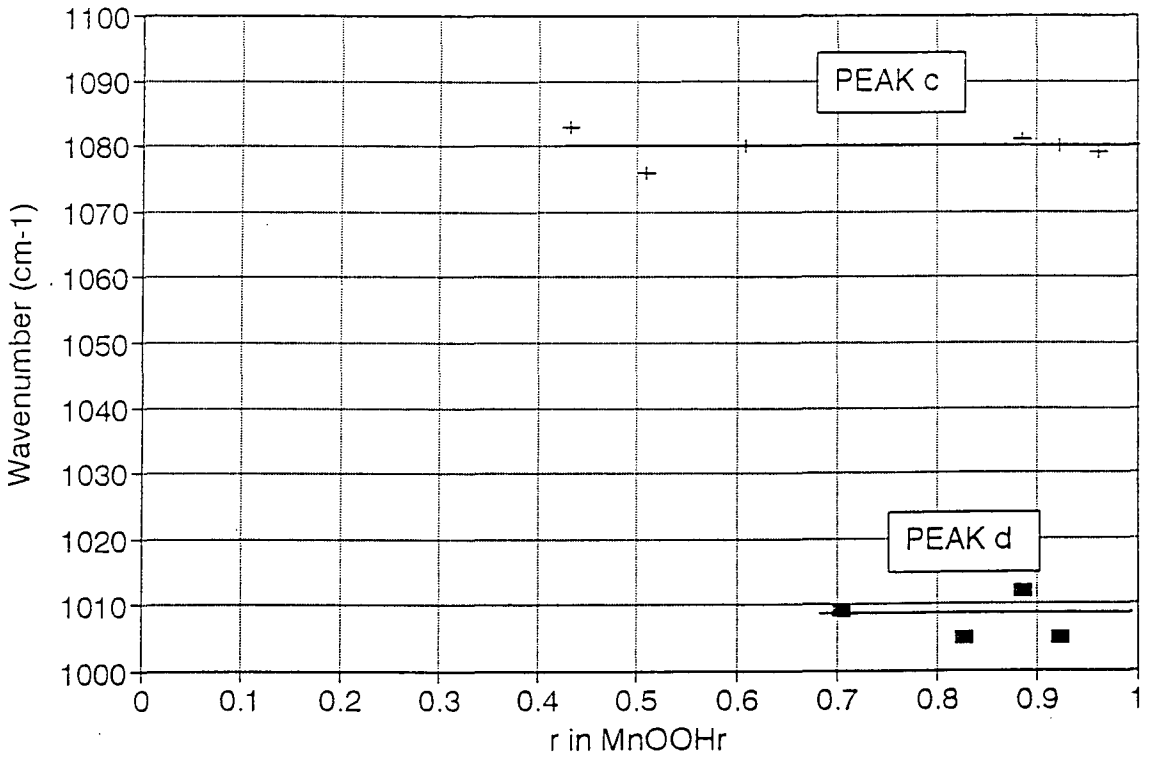

Figure 4.15.- Position of peaks c and d vs H insertion level propan-2-ol reduction method

4.4.3.- Normalised absorbances and areas.

The differences in the spectra evolution with the degree of reduction arising from the two reduction methods employed are more evident when considered in the following way: Swinkels [90] has shown that, for some wavenumbers (for example 488, 512, 624 and 628 cm^{-1}), the absorbance of the spectra is independent of the reduction level. Figures 4.16. to 4.19. contain the FTIR patterns obtained in this work show that the absorbance is essentially independent of r at the wavenumber of 624 cm^{-1}. Because of this, the absorbance at 624 cm^{-1} wavenumber was used to normalise all the data.

By using the normalised absorbance data, the net integrated areas defined as area(1), area(2) and area(4) used previously by Fitzpatrick et al [91] and by MacLean and Tye [75] were measured. The positions of the boundaries for the measurements were as follows :

area	Boundaries (cm^{-1})
(1)	2248-3200
(2)	1752-2152
(4)	856-1224

These three regions captured the expected emergence of peaks associated with O-H bond formation. For the measurements, subtraction of the background delineated by the straight line connecting the boundaries from the integrated area gave the net areas. This

was carried out for each H-insertion level and the results are displayed in figures 4.20 (propan-2-ol reduction method) and 4.21(hydrazine hydrate reduction method).

In the case of propan-2-ol reduction method, area(1), area(2) and area(4) are almost independent of insertion level until a common sharp breakpoint is reached at about r=0.7. Above this insertion level there is a linear increase in peak area. These results fully agree with those found by Fitzpatrick et al [91] in their work. For hydrazine hydrate reduction method, the breakpoint is at about r=0.4. For area(1) a slight continuous increase of net area rather than a horizontal line is observed below the break point.

Independence from insertion level of the net area value indicates the mobility of H in the solid solution, whereas the increases in net areas is evidence of H location as a result of O-H bond formation due to the formation of microdomains of the end product as previously proposed by Tye and Tye [74].

When comparing both insertion methods, it is clear that the formation of such microdomains with located H occurred at a lower reduction level for the hydrazine hydrate samples, confirming the results previously found by XRD. It is also worth noting that the net areas arising from O-H bond formation are much lower (about the half) with the propan-2-ol reduction method than for the hydrazine hydrate reduction method.

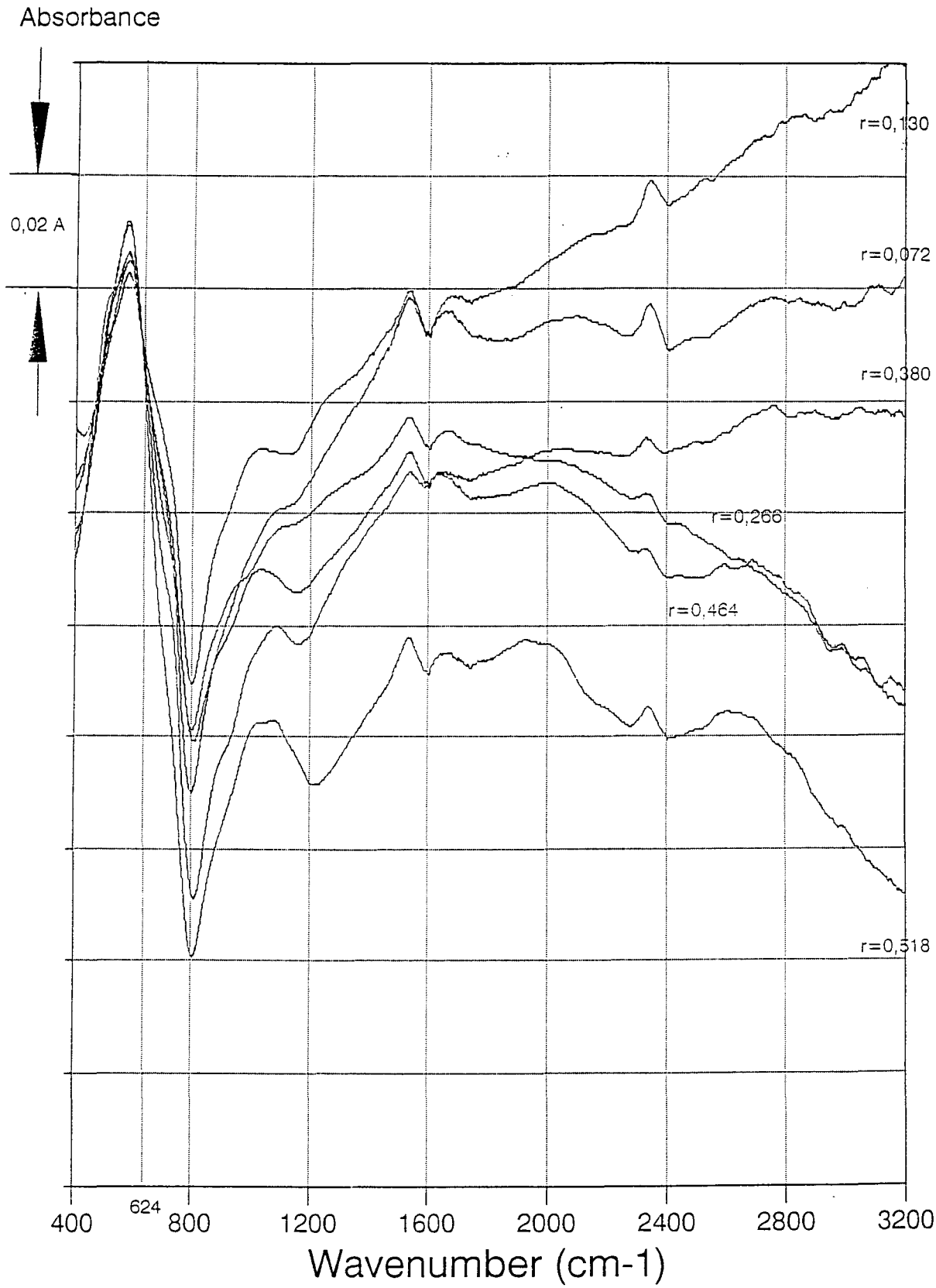

Figure 4.16.- FTIR patterns without stepping. Hydrazine hydrate reduction method (1)

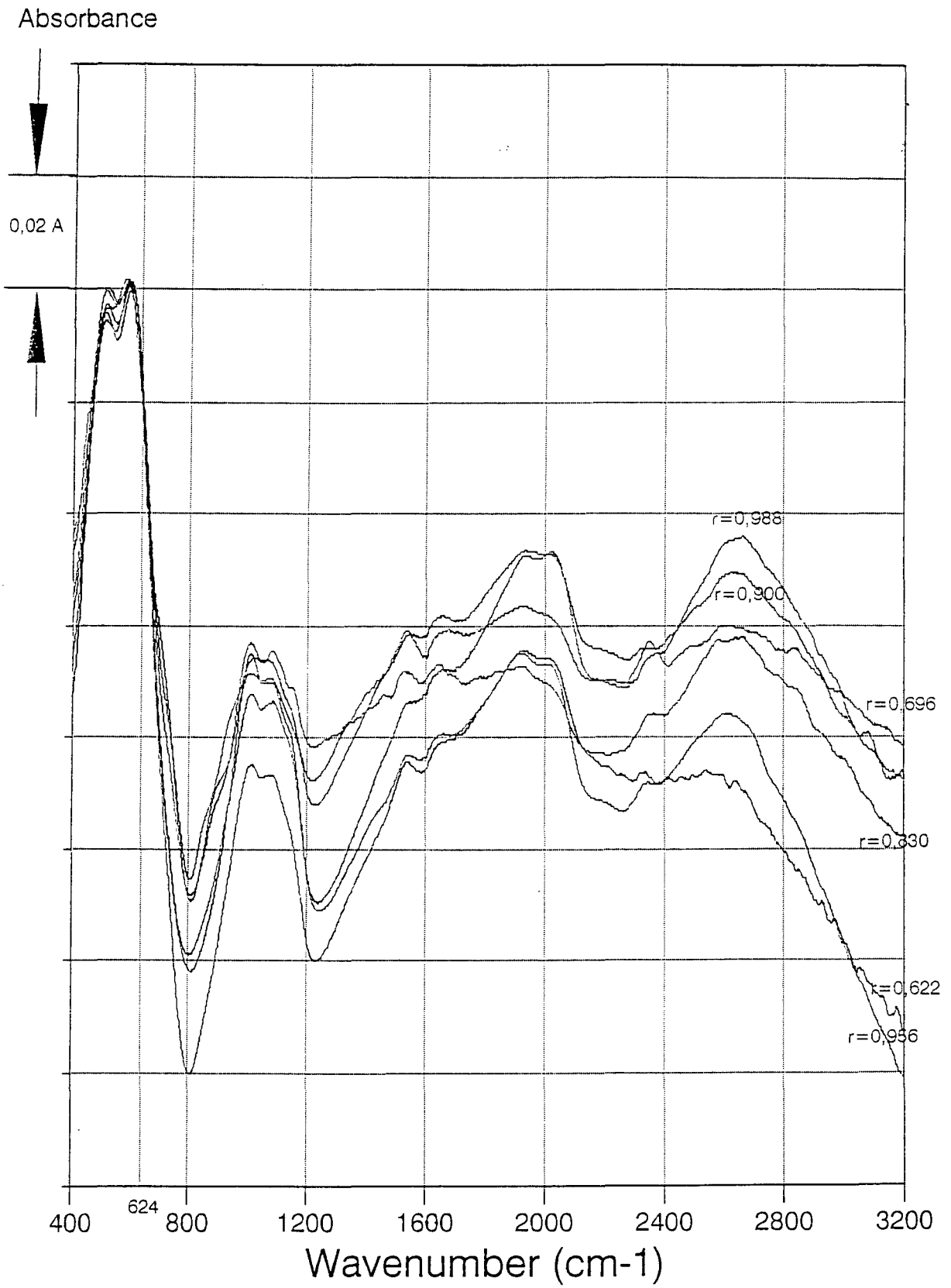

Figure 4.17- FTIR patterns without stepping. Hydrazine hydrate reduction method (2)

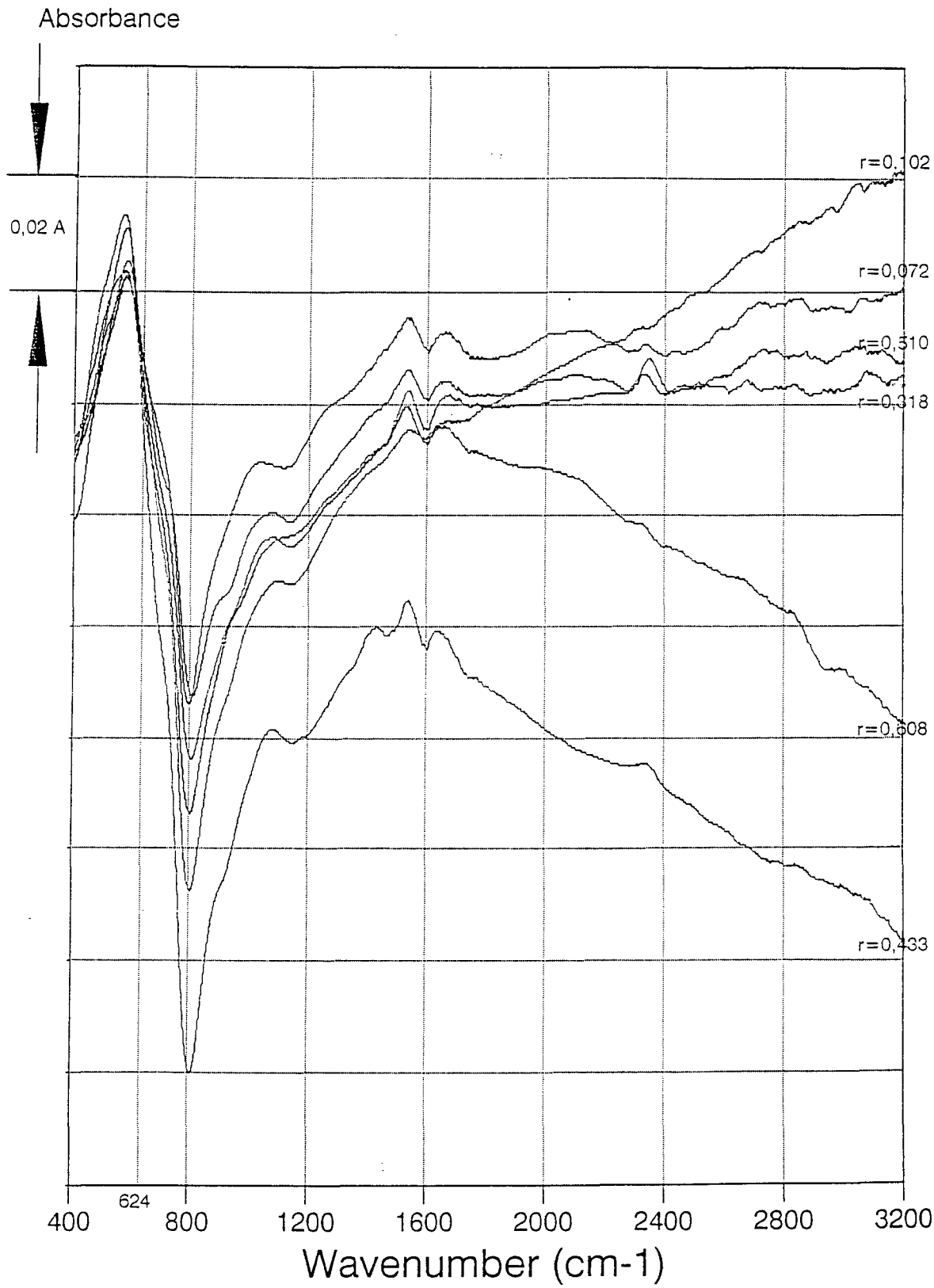

Figure 4.18.- FTIR patterns without stepping. Propan-2-ol reduction method (1)

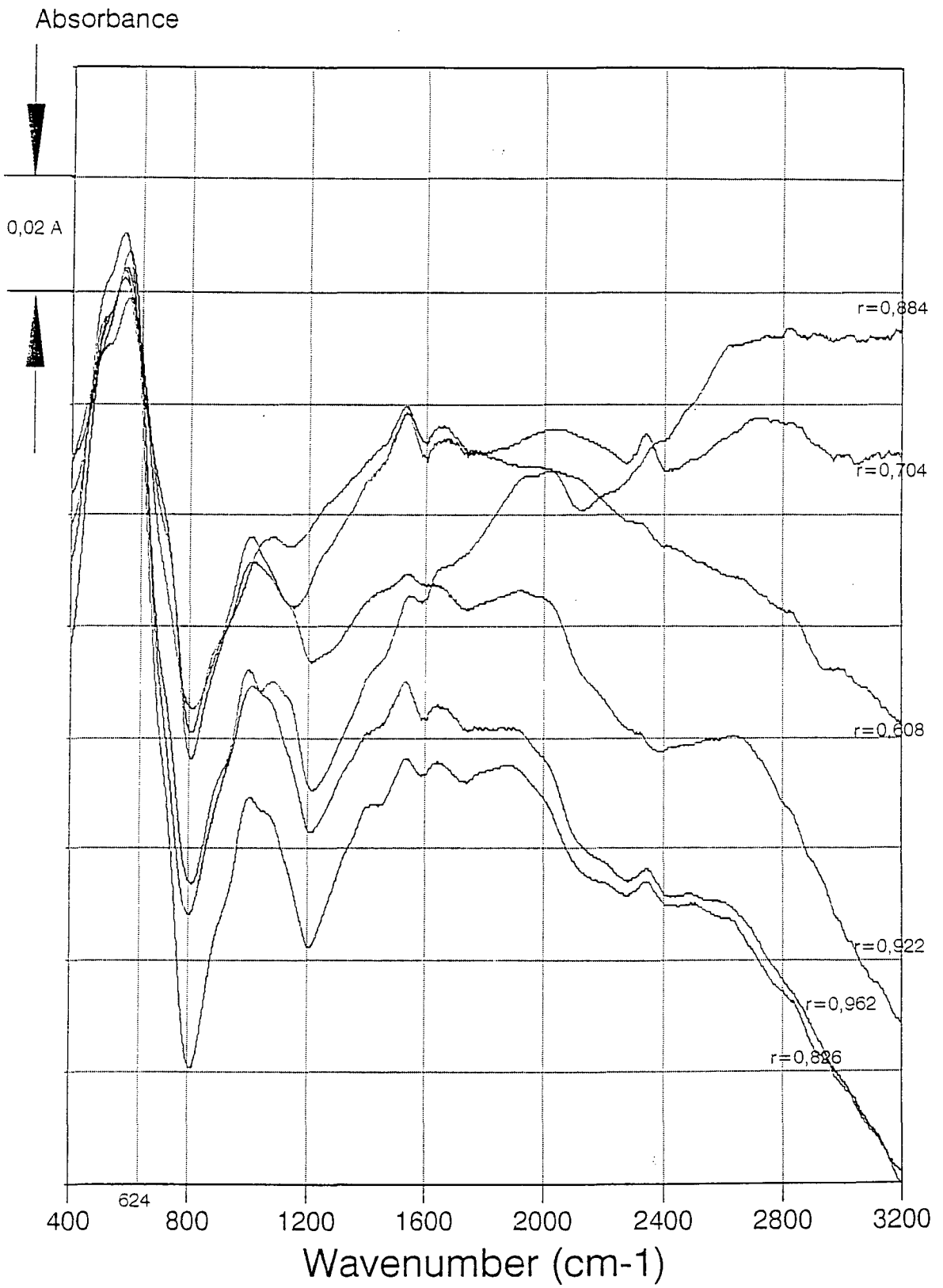

Figure 4.19.- FTIR patterns without stepping. Propan-2-ol reduction method (2)

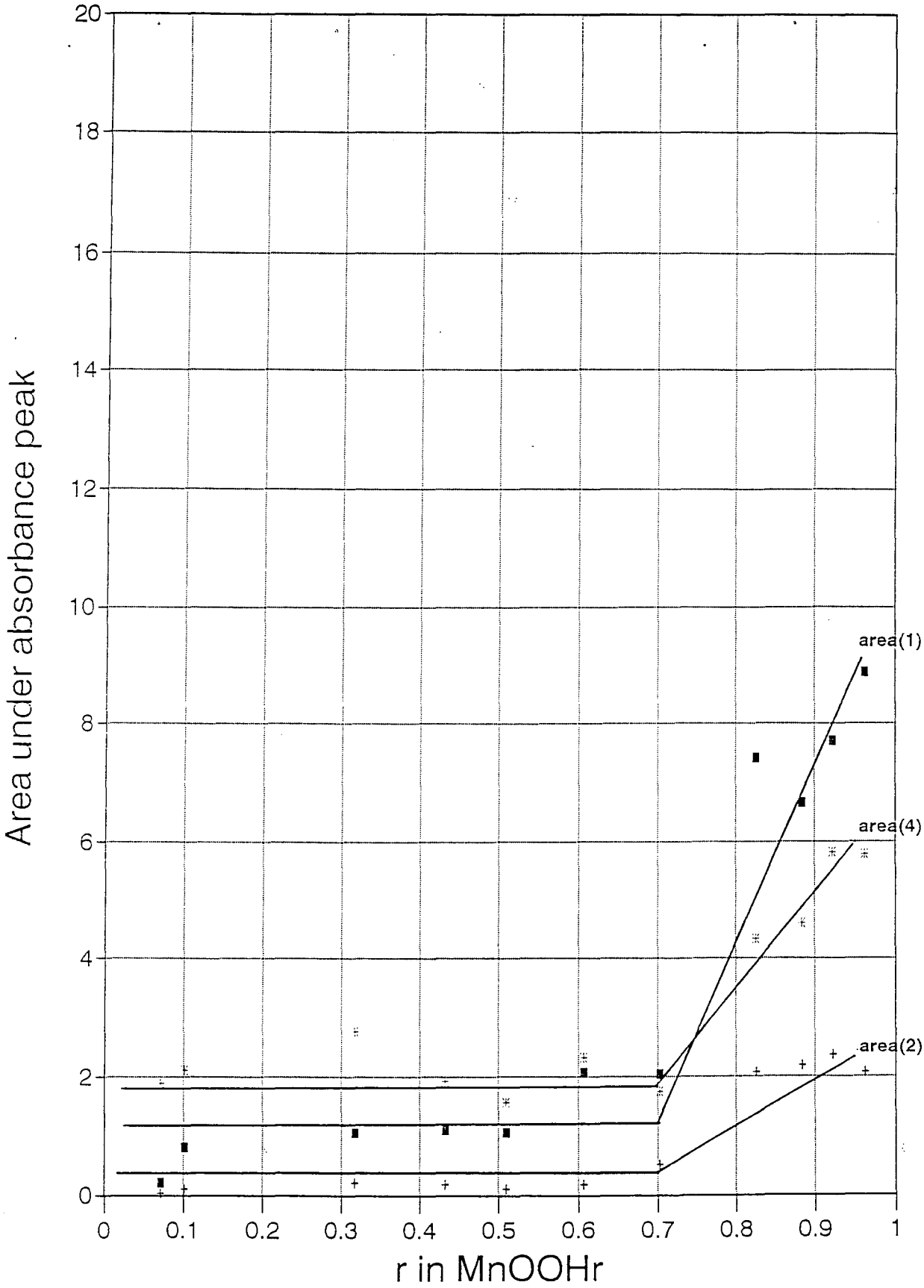

Figure 4.20.- Integrated net peak areas vs H-insertion level. Propan-2-ol reduction method

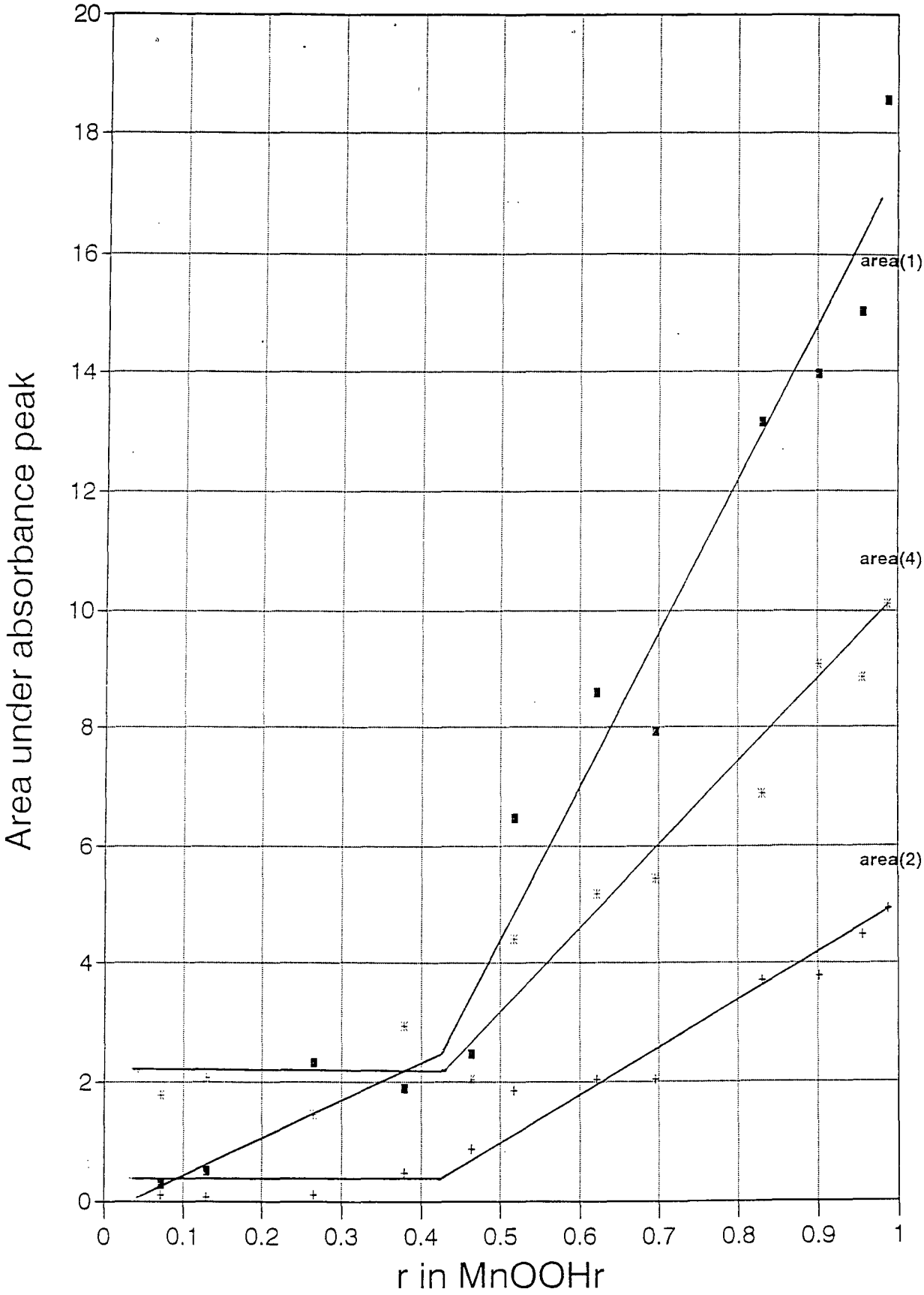

Figure 4.21.- Integrated net peak areas vs H-insertion level. Hydrazine Hydrate reduction method

5.- ELECTRODE POTENTIAL MEASUREMENTS

5.1.- INTRODUCTION

Electrode potentials are useful to examine the electrochemical behaviour of reduced samples and to reveal electrochemical differences between "homogeneous" and "heterogeneous" reductions. The potential E of an electrochemical cell is given by the equation :

$$E = \frac{\Sigma N_r (\mu^o_r + RT \ln a_r) - \Sigma N_p (\mu^o_p + RT \ln a_p)}{n F} \qquad (10)$$

being

μ^o .- Gibbs free energy of formation per mole in the standard state

N .- Number of moles of each participant in the cell reaction

a .- Activity

$_r$.- Reactants

$_p$.- Products

R .- Gas constant

T .- Absolute Temperature

F .- Faraday

n .- Number of equivalents of charge transferred from one electrode to the other in the cell reaction

For a reaction such as

$$Zn + HgO \longrightarrow ZnO + Hg \qquad (11)$$

during discharge as the reactants change to products, all participants remain as distinct phases, so

$$E = \frac{(\mu^0_{Zn} + \mu^0_{HgO} - \mu^0_{ZnO} - \mu^0_{Hg}) + RT \ln [(a_{Zn} . a_{HgO}) / (a_{ZnO} . a_{Hg})]}{2F} = \text{constant} \qquad (12)$$

As the participants are present as distinct phases in their standard states, the activity terms are unity and make no contribution, so the cell potential remains unaltered throughout the discharge. Then, the cell reaction is termed heterogeneous.

If, at least, one of the reactants changes to a product in solid solution so that the composition of the solid phase changes continuously as reaction proceeds, the Gibbs free energy per mole of this participant is not independent of the presence and concentration of the other component of the solid solution. This is the case for manganese dioxide and its reduction product MnOOH, which form a solid solution. For example, for the following reaction in alkaline electrolyte:

$$2 (MnO_2)_{ss} + H_2O + Zn \longrightarrow 2 (MnOOH)_{ss} + ZnO \qquad (13)$$

where $(\ )_{ss}$.- denotes a solid solution, the cell potential is

$$E = E_{MnO2,MnOOH} - E_{ZnO,Zn} = \textbf{constant} - RT\ln (a_{MnOOH}/a_{MnO2}) \qquad (14)$$

The activity term $RT\ln(a_{MnOOH}/a_{MnO2})$ can change from a large negative value to a large positive value as the reaction proceeds, so the cell potential decreases continuously throughout the discharge. This is the cause of the characteristic sloping circuit voltage curve of batteries containing manganese dioxide cathodes. Such a reaction is termed homogeneous. Thus, electrode potentials of reduced samples provide a means of distinguishing whether the reduction has occurred in a homogeneous or heterogeneous way.

In the past, potential measurements have confirmed that the reduction of EMD takes place in homogeneous phase in the range MnO_2 - $MnO_{1.5}$ [14, 20, 21, 23]. It has been also shown that not all the polymorphs of manganese dioxide undergo homogeneous phase reduction throughout the range. For example, it has been reported [66, 92] that the range of compositions for the homogeneous reduction of ß-MnO_2 is very narrow (MnO_2 - $MnO_{1.96}$). On the contrary, using ß-MnO_2 obtained by heat treatment of EMD, it has been found [93] that a homogeneous reduction occurs over the entire range MnO_2 - $MnO_{1.5}$. For α-MnO_2, it appears [66] that the single-phase reduction occurs down to $MnO_{1.82}$ only.

It is the purpose of this chapter to clarify, using electrode potential measurements whether the reductions carried out in this investigation have occurred in a homogeneous or heterogeneous way, or in both, establishing in the latter case the ranges for which each type of reaction has occurred.

5.2.- POTENTIAL MEASUREMENTS IN $ZnCl_2$

Experimentally, reproducible potentials in alkaline solutions have been notably more difficult to achieve than the same measurements in neutral solution [12]. An electrolyte 2 to 3 molal in $ZnCl_2$ is normally used in zinc chloride Leclanché batteries. These batteries are becoming more important at the present time than the "normal" Leclanché batteries, where the electrolyte is saturated ammonium chloride and 1 to 2.5 molar in $ZnCl_2$. Furthermore, according to Chabre and Pannetier [7], in aqueous zinc chloride electrolyte specific reduction of surface Mn^{4+} has not been evidenced experimentally, and reduction is claimed to proceed smoothly up to 1 e^-/Mn.

For these reasons, for a first set of measurements, it was decided to use an electrolyte consisting of 2 molal zinc chloride, buffered to a constant pH in the presence of MnO_x with ZnO to compensate for ion-exchange. The use of this electrolyte, theoretically, should avoid instability and would therefore explore differences in the potential versus r relationship for heterogeneous and homogeneous reductions.

Before starting the measurements, preliminary work aimed at establishing the experimental procedure was carried out. Admixing of graphite and acetylene black with the MnO_x and different ratios MnO_x / electrolyte, etc.. were investigated. It was concluded that the most reproducible results were obtained with the method normally employed at CEGASA which is now described.

2.25 grams of the starting EMD material and of the reduced samples (all of them having been previously ground) were mixed with 0.25 grams of acetylene black and then placed in contact with 25 ml of a $ZnCl_2$ solution, 2 molal buffered with ZnO to a pH close to 5. The whole mix was then mixed thoroughly for 2 hours in an agitator and the bottle subsequently stored with no air and no possible access of it at 20°C. The mixtures were centrifuged prior to potential measurement for 5 minutes. Potentials were measured at 20 °C with a platinum wire electrode introduced into the MnO_x sample versus a calomel reference electrode placed in the supernatant solution. Potential was recorded when its variation was very small (less than 1 mV in 5 minutes). Potentials were obtained for the samples obtained by both reduction methods (hydrazine hydrate and propan-2-ol) on the same day of mixing (called initial in the graphs), and after 1 month of storage at 20 °C with no possible air access. For further calculations, the final pH of the solution was also recorded.

The results obtained are shown in the attached Figures 5.1 and 5.2 (comparison between initial and 1 month values for propanol and hydrazine samples respectively), and

5.3 (comparison propanol. / hydrazine samples 1 month potential), after having been corrected to E (vs SHE) + 0.0592 pH (by using the value of pH before recorded and taking into account that $E_{SHE} = E_{Hg/HgCl2} + 0.2458$ V).

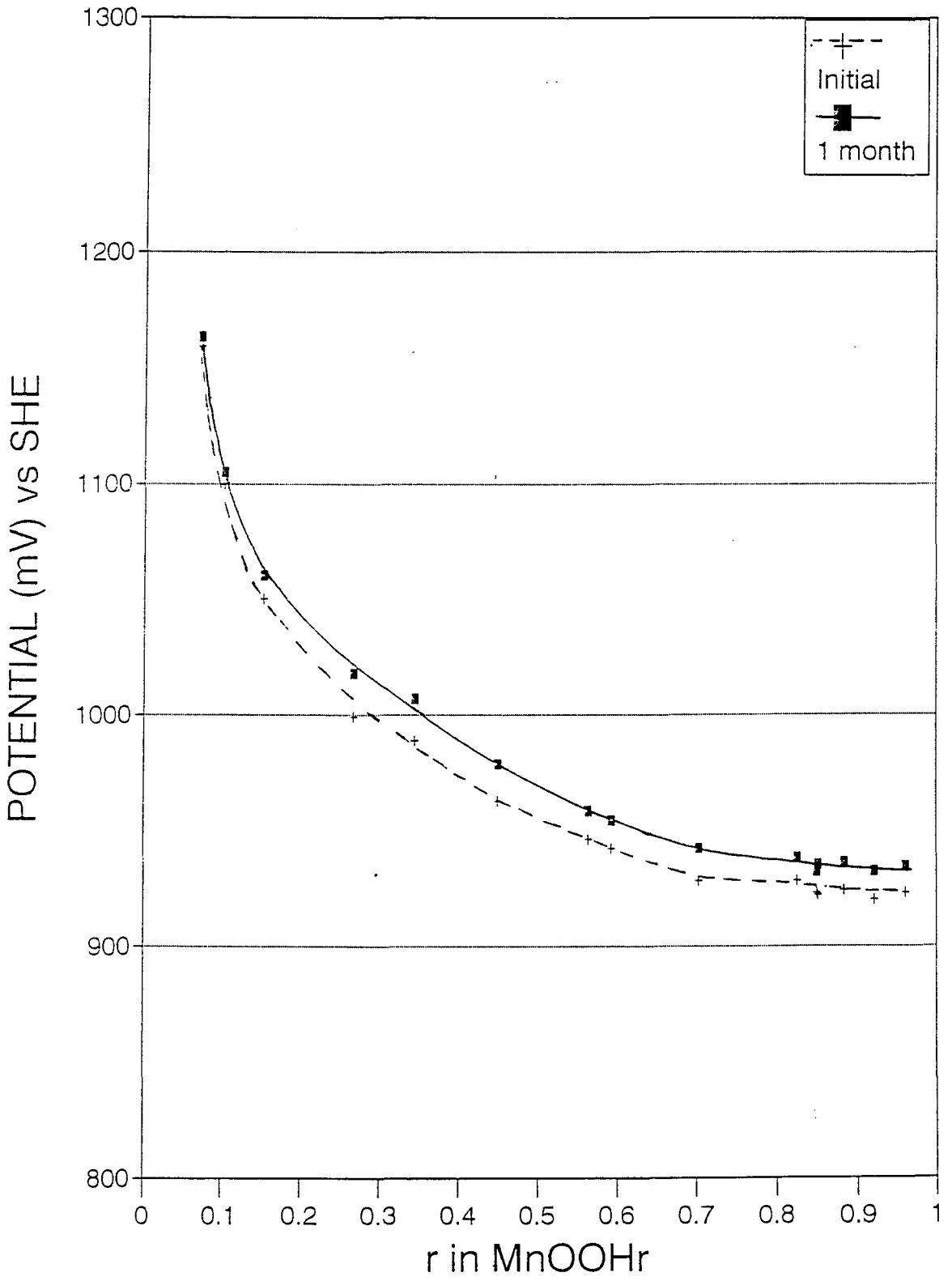

Figure 5.1.- Potentials of Propan-2-ol samples after storage in ZnCl2

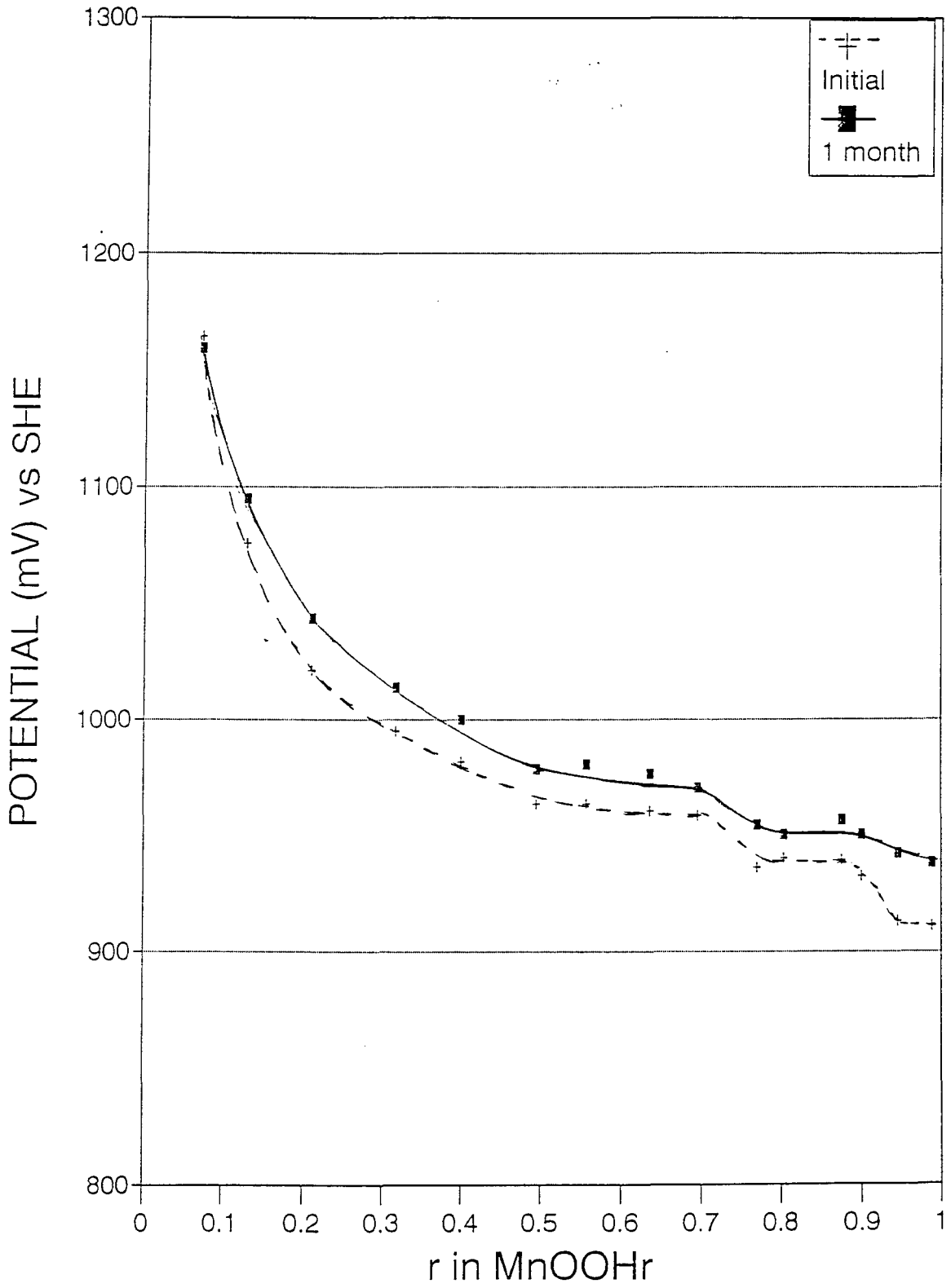

Figure 5.2.- Potentials of Hydrazine hydrate samples after storage in ZnCl2

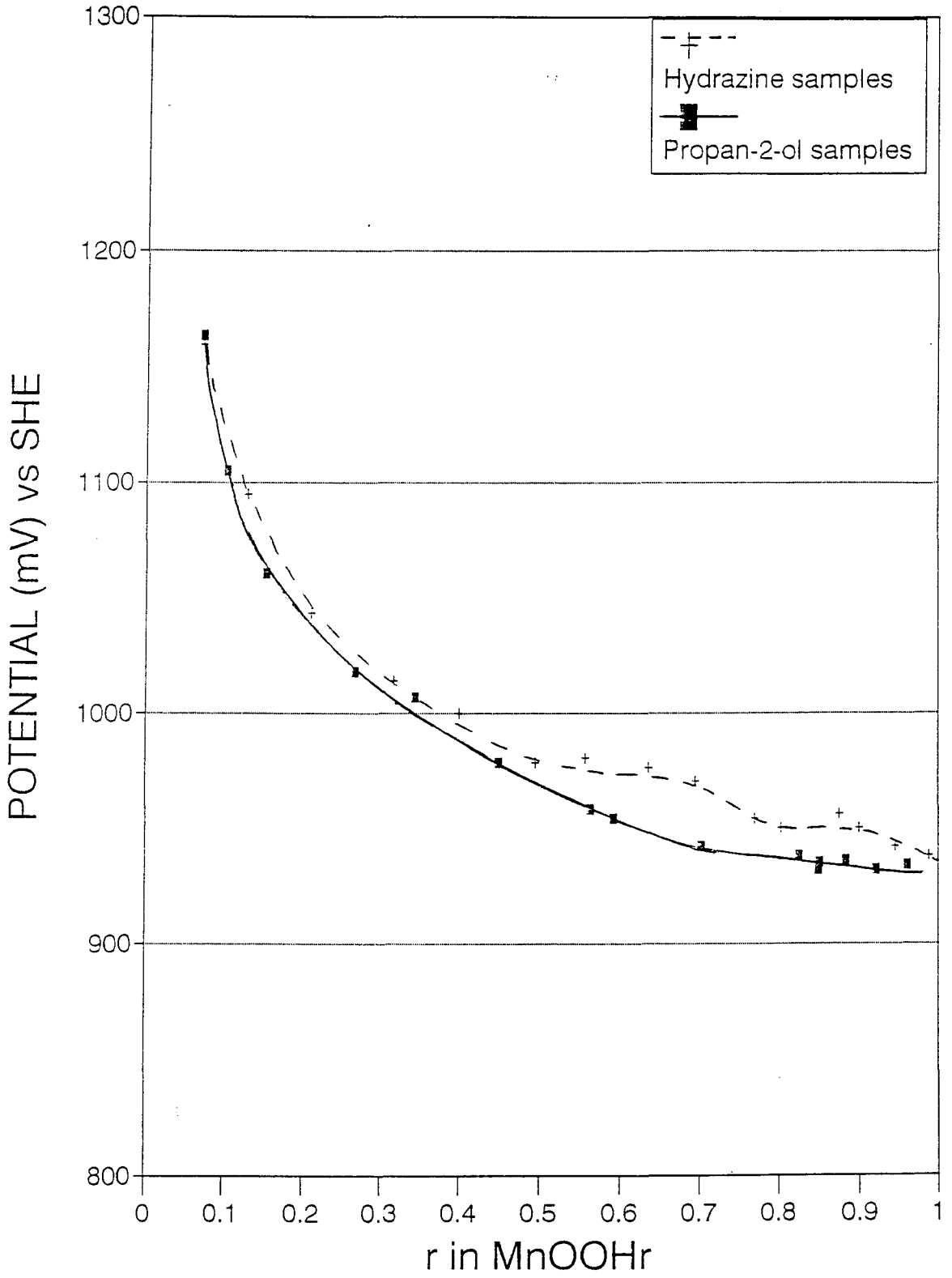

Figure 5.3.- Comparisons of potentials after 1 month storage in ZnCl2

Figures 5.1 and 5.2 show that in both reduction methods the effect of storage is a slight increase in the potential. It is also possible to see that the initial and 1 month curves follow a nearly parallel trend.

Comparison of the potentials for the two reduction methods is shown in Figure 5.3. For the propanol samples there is a continuous decrease in potential up to an r value of 0.80 followed by a nearly constant potential after this value. However, for the hydrazine samples, the behaviour appears different : between r values from 0.50 to 0.70 there exists a region of nearly constant potential followed by a small drop in potential to another plateau for r values from 0.70 to 0.90. At the end, a final drop leads to similar values for the two methods of reduction. The differences of potential caused by the two methods of reduction are however quite small.

It has not been possible to find data in the literature for potential measurements in the electrolyte here employed (zinc chloride) for manganese dioxide reduced samples. However, there are data available [14] of potential measurements on samples obtained by reduction in a special Leclanché cell, 90% NH_4Cl / 10% $ZnCl_2$ electrolyte and incorporating in the mixes excess solid NH_4Cl to minimise changes in the electrolyte. The comparison of this data with the potentials found in this investigation is shown in Figure 5.4. The figure shows a similar trend with Maskell's data up to an r value equal to 0.5. After this value, the potentials do not decrease similarly and show completely different behaviour.

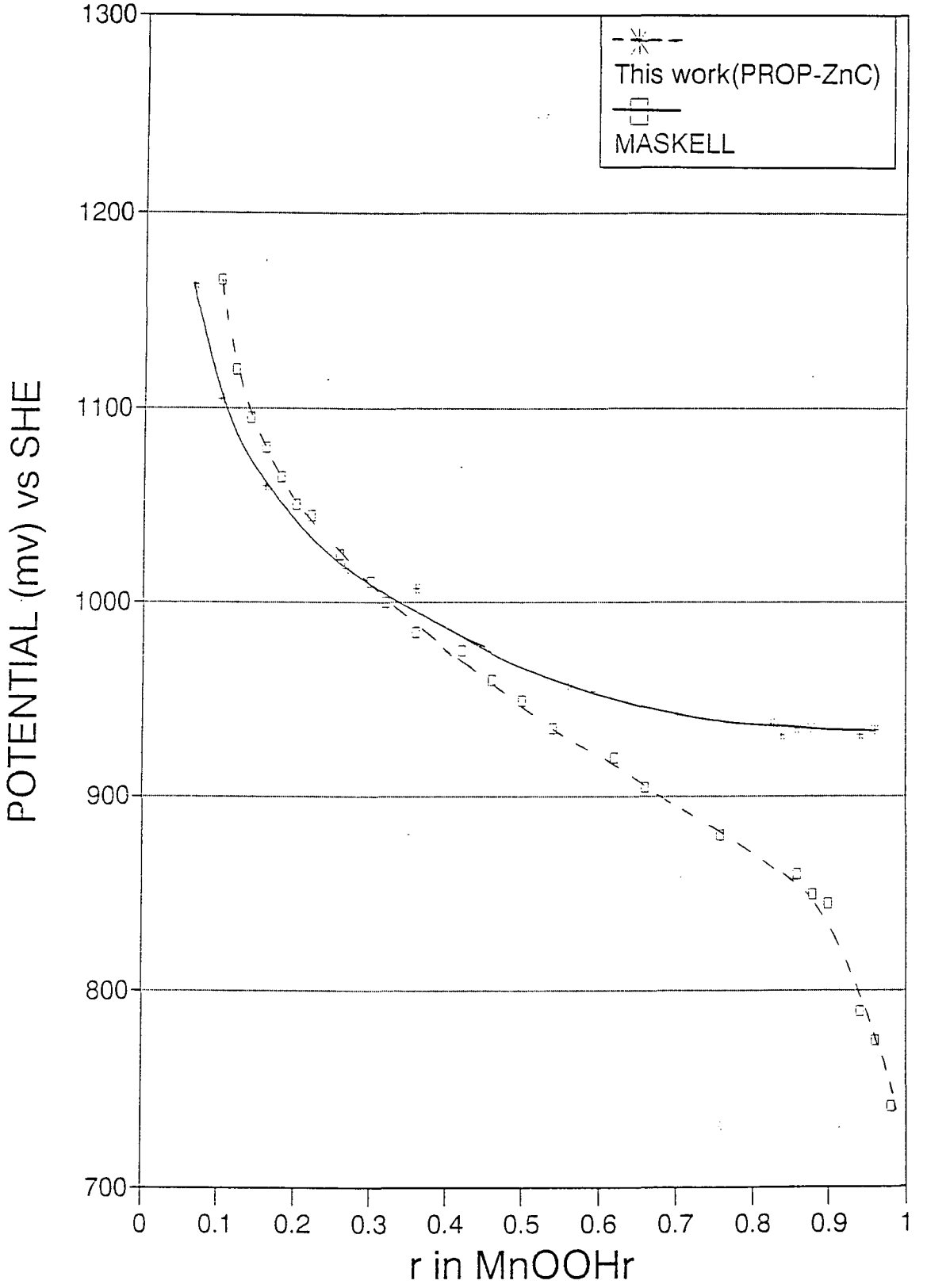

Figure 5.4.- Comparison of Potentials after storage.

In trying to explain these differences, it is worth bearing in mind that, during the actual electrode potential measurements, it was not possible to exclude completely the presence of air in the same way as was done during sample preparation and storage. In Maskell et al's potential measurements, oxygen was absent (scavenged by zinc). This fact could cause variations of potential due to a slight oxidation of the $MnOOH_r$ samples with air during the measurement. However, as the measurement time was very small, it is not believed this was the main reason for the disagreement.

Another difference is that in Maskell et al's work the ratio of electrolyte volume to weight of manganese dioxide was much lower, so possible effects due to dissolution of manganese could be much lower. Vosburgh et al [94] has showed that the concentration of $MnCl_2$ in the electrolyte in this type of measurements was negligible up to the half-reduction point and appeared to increase almost exponentially during the second half of the reduction. So, the composition of the solid phase would be seriously affected by the increase of Mn^{2+} solubility (and the dissolution of the oxyhydroxide phase) :

$$\mathbf{2\ MnOOH \longrightarrow MnO_2 + Mn^{2+} + 2\ OH^-} \qquad (15)$$

To check this hypothesis, XRD of the samples after 1 month storage in the zinc chloride electrolyte was carried out.

Firstly, it is significant to mention that, in the XRD patterns of all the samples the appearance of new phases was not observed. From the patterns and from the set of XRD peak positions of the reduced samples obtained in Chapter 3, it is possible to deduce the state of reduction of the recovered samples. These were as follows :

Table 5.1.- **r values (in $MnOOH_r$) of the samples before and after 1 month storage in $ZnCl_2$. Propan-2-ol reduced samples.**

Sample no. (from Chapter 2)	Initial value of r (in $MnOOH_r$)	r after 1 month of storage in $ZnCl_2$
2	0.388	0.376
10	0.466	0.466
13	0.534	0.520
14	0.560	0.508
17	0.608	0.578
18	0.704	0.590
19	0.826	0.746
22	0.878	0.804

Table 5.2.-- r values (in $MnOOH_r$) of the samples before and after 1 month storage in $ZnCl_2$. Hydrazine hydrate reduced samples.

Sample no. (from Chapter 2)	Initial value of r (in $MnOOH_r$)	r after 1 month of storage in $ZnCl_2$
40	0.130	0.114
43	0.266	0.364
47	0.464	0.530
52	0.636	0.638
55	0.732	0.670
56	0.770	0.694
58	0.830	0.698
62	0.946	0.712
64	0.988	0.794

For the propan-2-ol samples, Table 5.1 shows a slight oxidation after the storage in $ZnCl_2$, which is more pronounced for r values higher that 0.534. For the hydrazine hydrate samples, two different regions appear in Table 5.2. In the first one, up to r = 0.6, there exists a slight reduction of the samples, whereas in the second one, for r values higher than 0.7, there is a remarkable oxidation of the samples, even greater than the second half in the propanol samples. Surely, the two hours of initial mixing of the reduced samples with the electrolyte may have been a mistake and have caused a false set of measurements. Surely it would also have been better to carry out the initial mixing with much less electrolyte. Equilibrium between solid and solution according the reaction (15) would have had a very much smaller effect on the composition of the solid phase. It is worth to notice that also there is the effect of O_2 on increasing the potential values, due to slight oxidation of the $MnOOH_r$ samples.

5.3.- POTENTIAL MEASUREMENTS IN KOH

Because of the unsatisfactory results noted in section 5.2, it was decided to try potential measurements in KOH electrolyte using a lower volume of electrolyte to $MnOOH_r$ weight thereby reducing solubility complications.

For this electrolyte, the method employed for the electrode potential measurements was as follow : About 8 g of the previously ground starting EMD and of the reduced samples were put in contact with 20 ml of a 7M KOH solution. The bottles containing the samples were subsequently stored at 20 °C.

Potentials were measured at 20 °C with the sample in contact with a platinum electrode and a Hg/HgO reference electrode, with both electrodes immersed in the 7M KOH solution and pressed against the powder of MnO_x at constant pressure to ensure good contact between the electrodes and the samples. The potential values were recorded when the potential variation was very small (less than 1 mV in 5 minutes). The final pH of the solution was also recorded.

It was observed that the potentials for the first few days indicated a lack of stabilisation of the samples. The potentials were then evaluated after 14 days of storage and corrected to E (vs SHE) + 0.0592 pH (by using the value of pH before recorded and taking into account that $E_{SHE} = E_{Hg/HgO} + 0.926$). The results obtained in this way for both

Propan-2-ol and Hydrazine hydrate methods are shown in Figure 5.5.

In a similar way as was previously done for the electrode measurements in $ZnCl_2$, a comparison of the results obtained here with data in the literature (Holton et al [12] (30% w/w KOH electrolyte)) is shown in fig 5.6. Holton used for the reductions hydrazine hydrate (adding the hydrazine very slowly) but unlike this work in a way designed to produce a homogeneous reduction.

In Figure 5.7 a further comparison is carried out on the Propan-2-ol reduced samples with Maskell et al [14] (homogeneous reduction in a special Leclanché cell, NH_4Cl-$ZnCl_2$ electrolyte) and Donne et al [95] (9M KOH electrolyte) data.

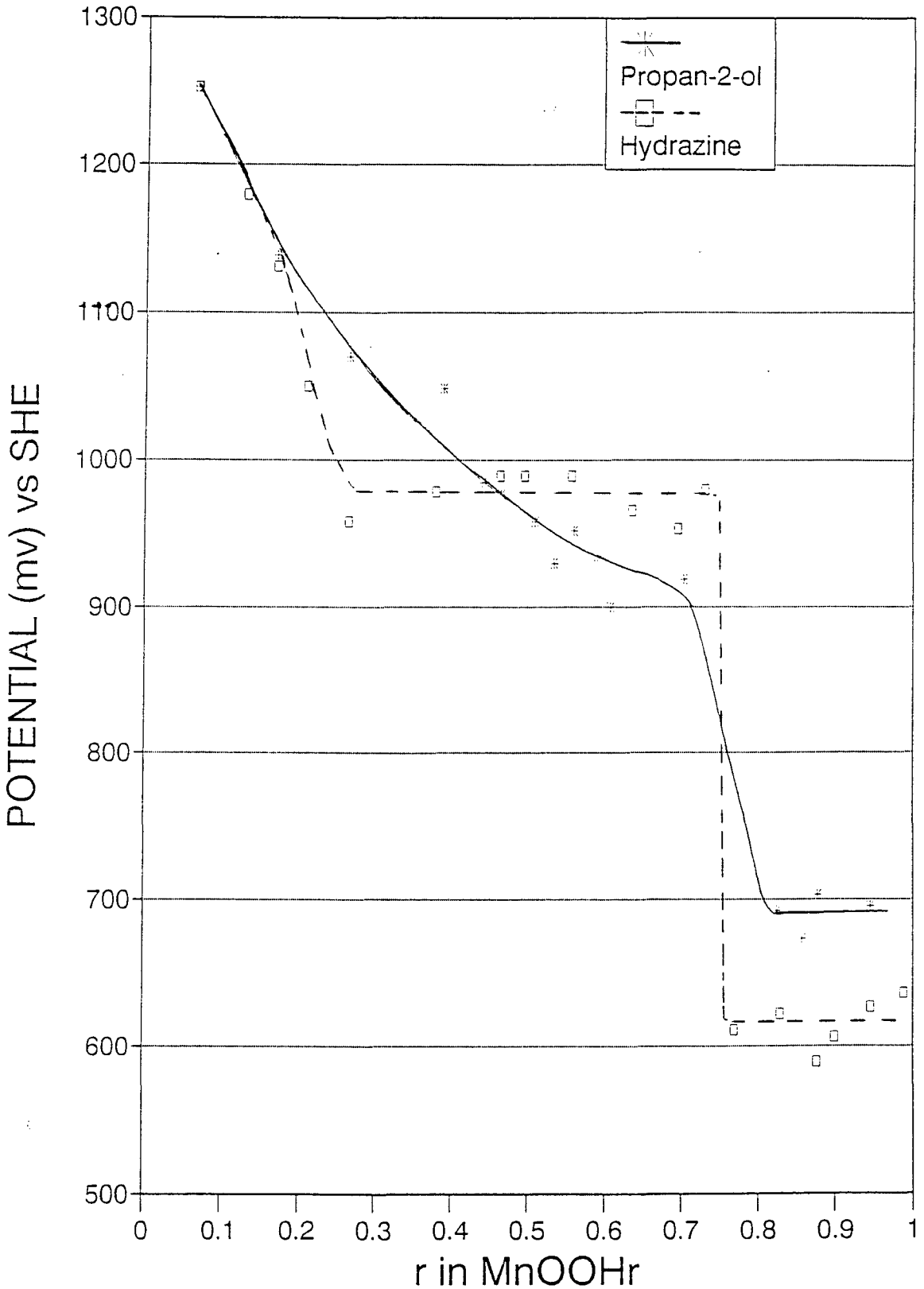

Figure 5.5.- Comparison of Potentials after 14 days storage in KOH.

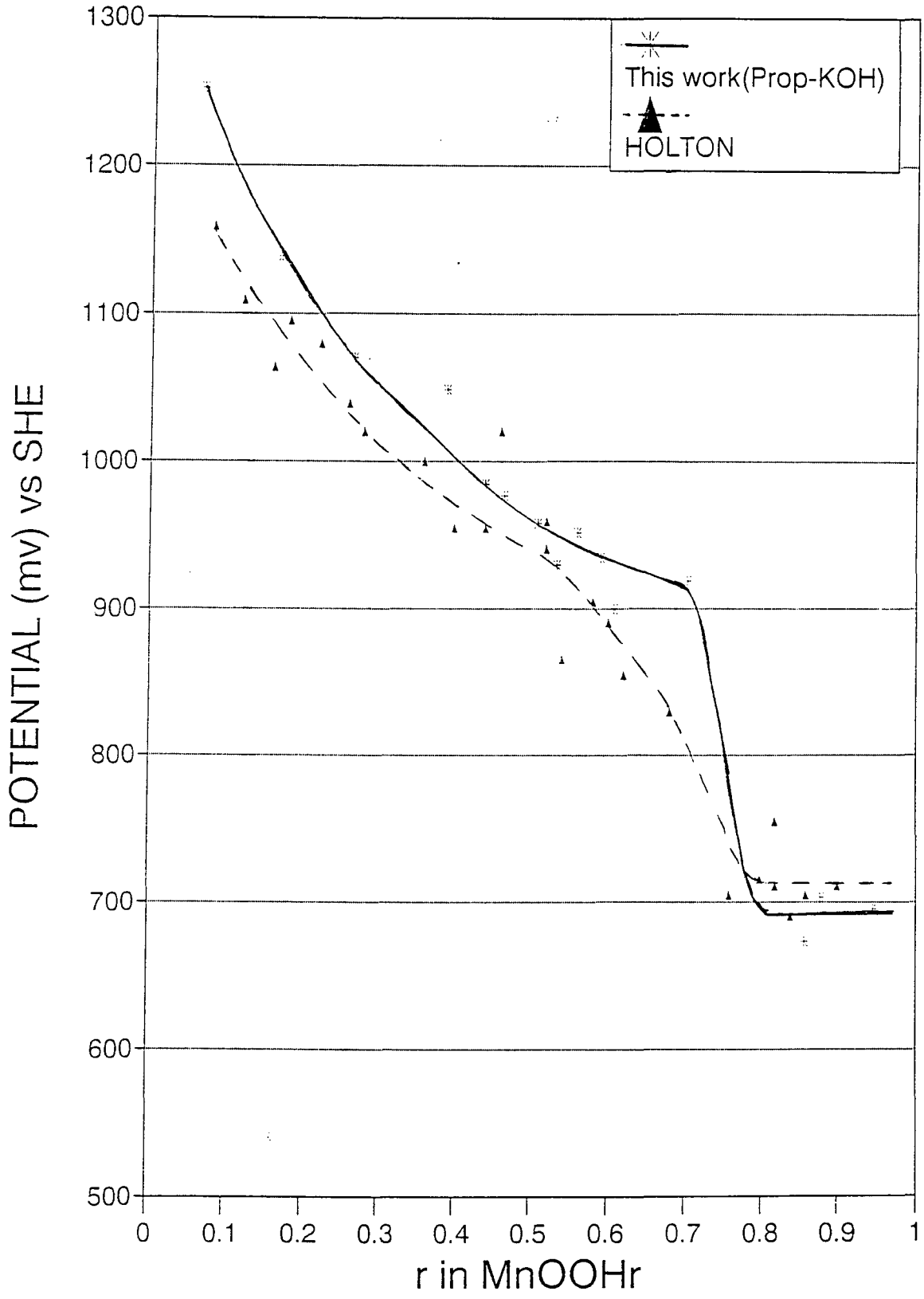

Figure 5.6.- Comparison of Potentials after storage.

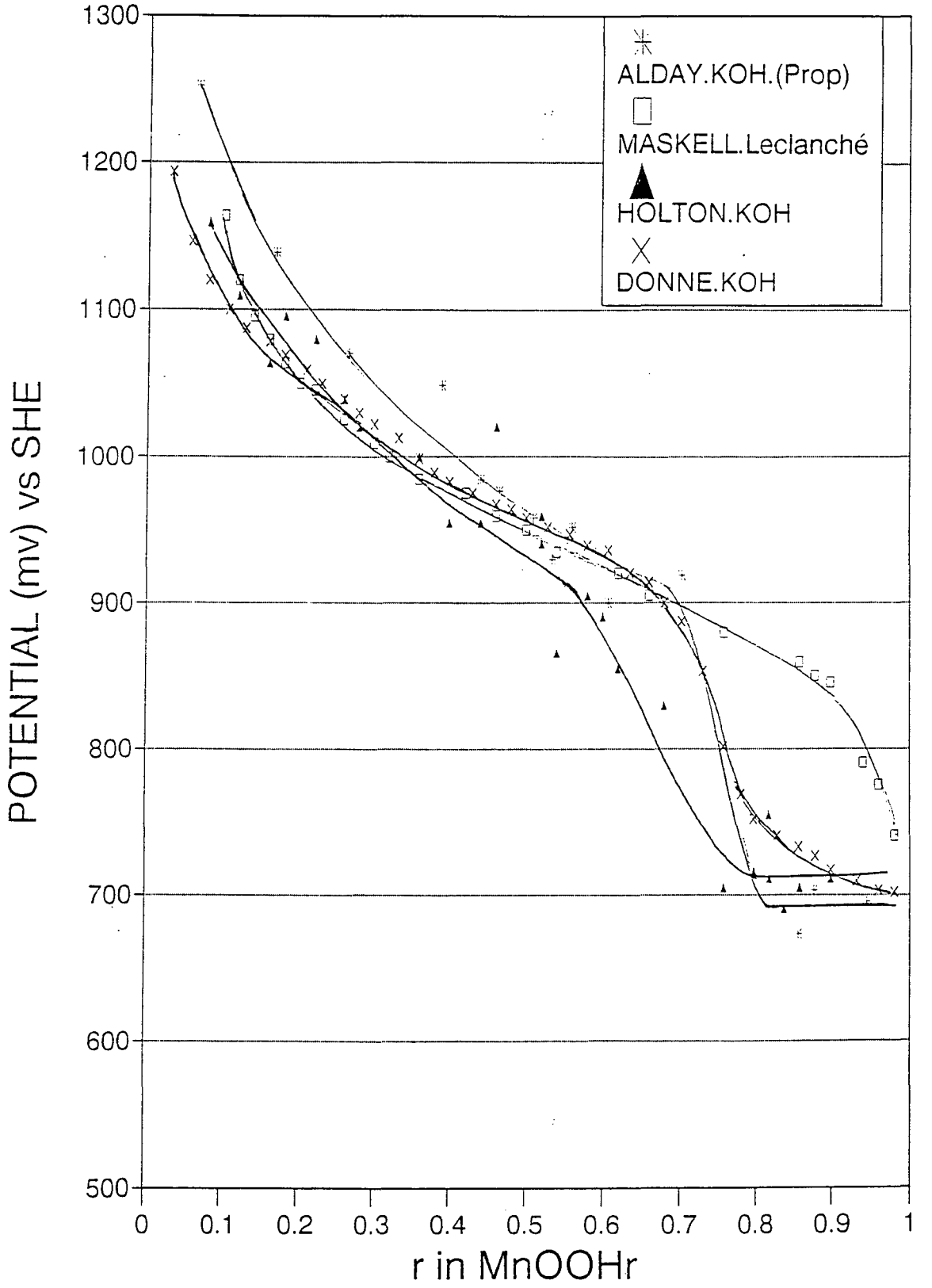

Figure 5.7.- Comparison of Potentials after storage.

5.3.1.- Propan-2-ol reduced samples

When comparing the four sets of data, it is possible to check that the behaviour of the potential of these samples exhibit very similar trends along all the reduction to the Donne (see fig 5.7) and Holton values (see figs 5.6 and 5.7). Up to about r = 0.5, the potential values decrease continuously running parallel for the four sets of data. The differences in potential values could be possible due to the different electrolyte concentrations used for the measurements or even different EMD's used for the studies. Holton values deviated and became lower than Maskell's data for r > 0.5, whereas Donne's data and the values found in this work start to deviate around r = 0.7. According to the explanation of Holton, the reason for the deviation of the values from Maskell's data was due to the oxidation state of the solid solution being lower than indicated by the analysis, due to the presence of birnessite ("δ-MnO_2") of oxidation state $MnO_{1.75}$ in the samples. The presence of δ-MnO_2 was clear from XRD evidence.

In this work, XRD evidence (Section 5.4.) of the presence of δ-MnO_2 on the reduced samples does not occur until r values higher than 0.7. This is the point at which there is a sharp drop in potential and the data start to deviate from Maskell's curve, confirming the explanation above described of Holton for the deviation. Unfortunately, there is no XRD data available in Donne's work.

It can be concluded that at oxidation states lower than $MnOOH_{0.7}$, the solid solution obtained with this propan-2-ol reduction method are unstable and disproportionate producing δ-MnO_2 and a $MnOOH_r$ compound with higher r value. Then, the storage electrode potential is determined by heterogeneous reactions remaining at a constant value. The r value of 0.7 coincides with the r value at which the new XRD lines emerge (Chapter 3), the H locates as revealed by FTIR (Chapter 4), and stable microdomains of a demicrotwinned product, the one which is not stable in KOH electrolyte, first form.

5.3.2.- Hydrazine hydrate reduced samples

In this case, the behaviour was quite different from that of the Propan-2-ol samples (see fig 5.5). The continuously decreasing potential from the starting EMD material parallel to that of Propan-2-ol is only maintained to an r value of 0.17 (x equal to 1.915). After this, there is a region of constant potential between r ≅ 0.25 and r = 0.75 (x equal to 1.625), which is completely different from the behaviour of the Propan-2-ol samples. As previously explained, this constant potential is a further evidence of heterogeneous behaviour.

This is very similar to the conclusions drawn from the X-ray diffraction patterns (Section 3) and FTIR spectra (Section 4) about the onset of a heterogeneous reduction with this hydrazine hydrate method below an r value of 0.4 (x equal to 1.8). The

difference in the onset of heterogeneity is probably due to the fact that XRD and FTIR techniques do not detect new phases until minority phases reach a sufficient proportion of the whole mass, whereas the potential data are more sensitive.

In this region of r (0.25-0.75), the samples as prepared must consist of two phases, $MnOOH_{0.25}$ and $MnOOH_{0.75}$, with varying proportions of each, the constant potential being determined by the reaction :

$$\mathbf{MnOOH_{0.25} + 0.5\ e^- + 0.5H^+ \Longrightarrow MnOOH_{0.75}} \qquad (16)$$

At oxidation states lower than about $MnOOH_{0.76}$, a large decrease of the potential is noticed, falling down to similar values (although slightly lower) than the values for the Propan-2-ol samples. It can be concluded that at this low oxidation values, the samples obtained under both reduction methods are quite similar and behave in an unstable way on storage in KOH as previously mentioned for the Propan-2-ol samples.

These potential measurements in KOH electrolyte are a further indication of the different effects of the two methods of chemically inserting hydrogen into a electrodeposited manganese dioxide on the structure and properties of the resulting compounds, obtaining heterogeneous products which determine potential values at higher oxidation states for the Hydrazine Hydrate reduction method than for the Propan-2-ol method.

5.4.- X-RAY DIFFRACTION OF SAMPLES STORED IN KOH

The purpose of this section was to investigate the stability in concentrated potassium hydroxide of the samples obtained by the two methods noted in section 2 (Hydrazine hydrate and Propan-2-ol). Reduced samples of both methods, which had been stored in concentrated KOH (6 months, no O_2 access), were recovered from the solution by washing them on a filter open to the atmosphere with distilled water until filtrates were neutral. The residues were then dried under vacuum at room temperature in the way explained by Holton et al [12]. While recovering the stored samples, special care was taken in order to observe and know the insertion level at which cementation arose. Cementation is considered to arise from an instability process involving soluble species and precipitation.

The insertion levels at which cementation occurred were as follow for the two sets of samples here studied (Propan-2-ol and Hydrazine Hydrate) :

	x	r
Propan-2-ol	**1.587**	**0.826**
Hydrazine hydrate	**1.652**	**0.696**

From the results described in Chapter 3, the change on X-ray diffraction patterns (appearance of new peaks) was detected at $MnOOH_{0.50}$ ($MnO_{1.75}$) for the Hydrazine hydrate reduced samples and at $MnOOH_{0.80}$ ($MnO_{1.60}$) for the Propan-2-ol ones. This value

for the Propan-2-ol samples is similar to the value at which cementation was observed, so it is confirmed that the species formed due to instability and corresponding to the new XRD peaks are the responsible of the observed cementation.

However, for the hydrazine samples, the cementation appears at more reduced levels than the growing of the new peaks in the XRD patterns, probably as a greater proportion of "precipitated" phase is needed in order to see the "cementation" than to see the new peaks on the XRD patterns.

XRD of such samples was carried out, and the pattern evolution for both reduction methods are presented in the Figures 5.8 and 5.9.

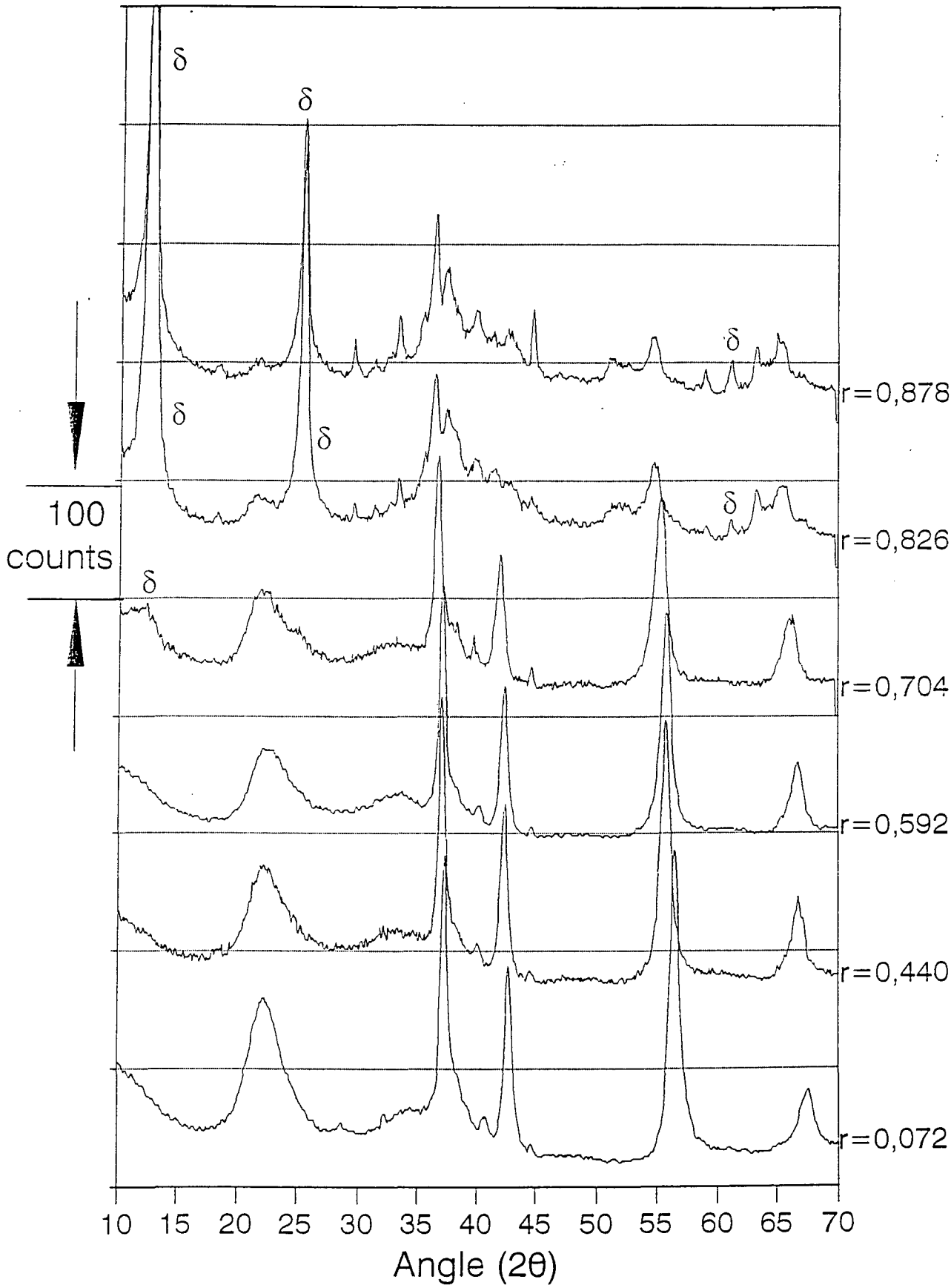

Figure 5.8.- Pattern evolution for Propan-2-ol reduced samples

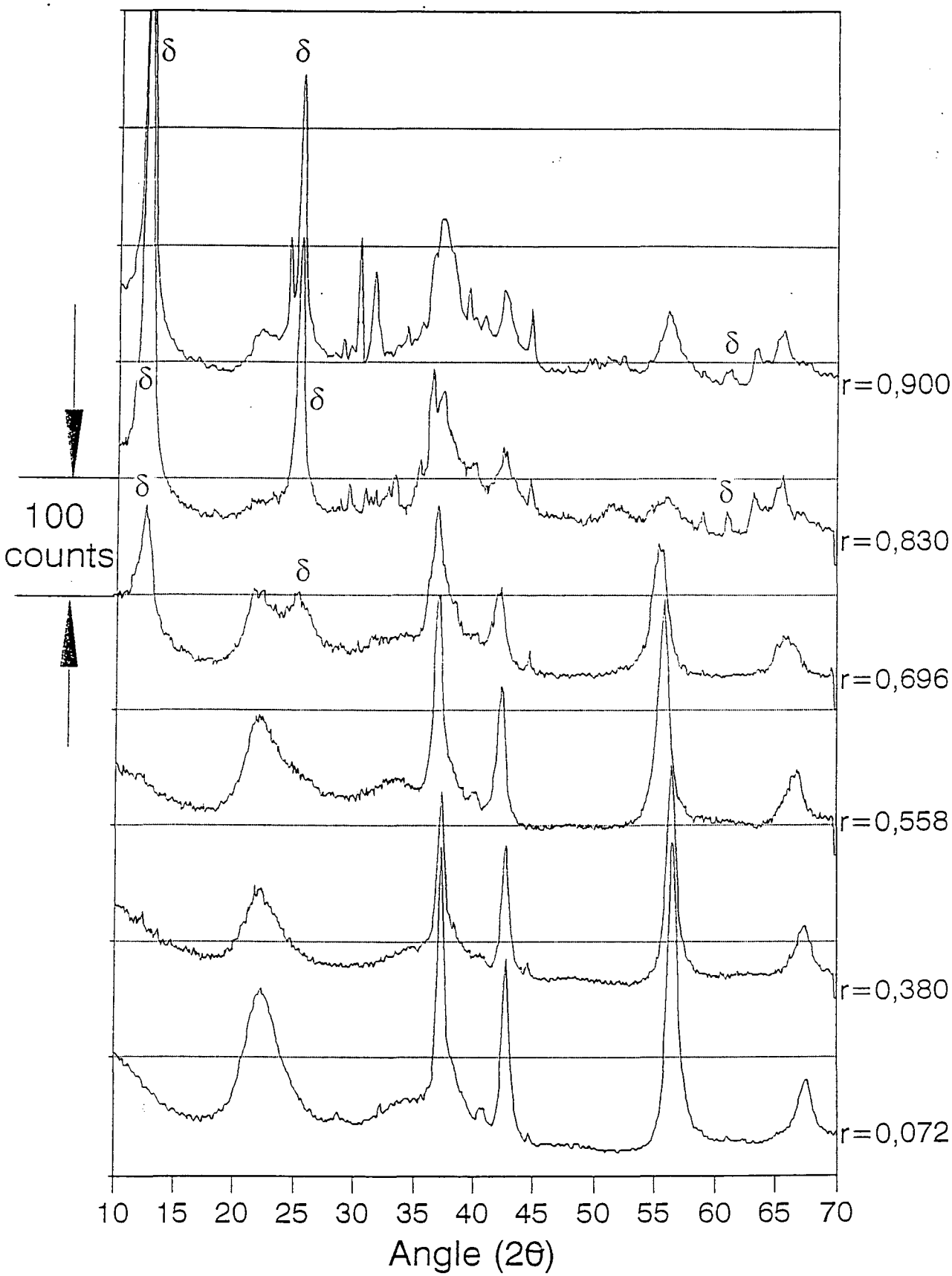

Figure 5.9.- Pattern evolution for Hydrazine hydrate reduced samples

5.4.1.- Propan-2-ol reduction method

1) From $MnOOH_{0.072}$ up to $MnOOH_{0.704}$, there is no significant change in the patterns of the original reduced samples prior to storage in KOH (see fig 5.8). When comparing the patterns before and after the storage, it is observed that the samples have become very slightly oxidised during the storage in KOH (higher 2θ values). A small proportion of δ-MnO_2 is present in the $MnOOH_{0.704}$ sample.

2) From $MnOOH_{0.704}$ up to end reduction, as previously observed by Holton et al [12], the manganese oxyhydroxide solid solution becomes increasingly metastable as the oxidation state decreases and the structure dilates, until the original structure collapses, giving as a result two phases : (i) a compound with a lower x value than initially, with clear changes on the main peaks (see for the $MnOOH_{0.826}$ sample the comparison with the XRD pattern before storage in figure 3.2.), and (ii) a new phase, δ-MnO_2 / K-Birnessite (three new clear peaks at 12.4; 25.1; and 63.2 2θ). This phase is the cause of the observed cementation. Sugimori [96] observed a similar behaviour and concluded that the formation of δ-MnO_2 was through the reaction of Mn^{3+} in solution, developed during the storage in KOH of the reduced samples, with the remaining oxide. Chabre and Pannetier [7] have proposed a mechanism which involves a surface reaction of the partly reduced MnO_x yielding K-Birnessite.

3) Near full reduction members, other peaks appear, which according to Chabre and Pannetier [7] could be due to the partial transformation of K-Birnessite to manganite.

The above behaviour explains the observation of lower capacity of alkaline manganese batteries in prolonged intermittent discharges. On such regimes, the end of the discharge appears to be at a oxidation state of the positive electrode of about $MnOOH_{0.8}$ rather than MnOOH which can be achieved in Leclanché batteries [1,38,97].

5.4.2.- Hydrazine hydrate reduction method.

The three ranges 1), 2), and 3) as explained for the Propan-2-ol samples, also appear with the samples from the Hydrazine hydrate reduction method. The main difference between this reduction method (heterogeneous) and the Propan-2-ol (homogeneous) comes from the different point in which the new lines corresponding to δ-MnO_2 appear, earlier for this method, at $MnOOH_{0.696}$ ($MnOOH_{0.826}$ in the Propan-2-ol method). This confirms again that the samples formed through a heterogeneous process are clearly instable in storage in KOH electrolyte.

Applying this fact to the alkaline manganese batteries, it could be easily deduced that those manganese oxyhydroxide solid solutions which were produced heterogeneously, collapse at an earlier reduction level, so the previously mentioned deficiency of alkaline batteries would be more pronounced.

6.- CONCLUSIONS AND FURTHER WORK

It has been clearly proved that the method of H insertion into an electrolytic manganese dioxide (EMD) or rather the rate at which the insertion is attempted can result in the insertion occurring homogeneously or heterogeneously.

As in previous studies, it has also been shown that H insertion into EMD produces dilation of the crystal structure in which H^+ and e^- are mobile and thermodynamically independent components until a certain value of r in $MnOOH_r$ is reached. It has been demonstrated in this work that this r value depends on the rate at which H was inserted within the crystal structure, what depends on the chosen method of insertion.

In this investigation evidence for the differences between propan-2-ol and hydrazine hydrate reduction methods have been presented. In chapter 3 by using X-Ray Diffraction, the presence of heterogeneity process during the hydrazine hydrate reduction method at a low degree of reduction (r = 0.3-0.4) has been shown, whereas in the propan-2-ol reduction method previous results indicating a homogeneous reduction have been corroborated. Several techniques have been employed to reach these conclusions. The observation of the evolution of peaks with H insertion have shown the movement of peaks with no appearance of new peaks for the propan-2-ol reduction method until a value of $r \cong 0.9$. However, for the hydrazine hydrate method, new peaks which grow at the expense of the original ones have been found at r values close to 0.3-0.4. A different r value for the onset of heterogeneity has been established for different rates of reduction when using the

hydrazine hydrate reduction method. These findings have been further confirmed looking at the evolution of interplanar spacings and at their ratios, as well as by mathematical mixing techniques of the diffraction patterns and by physical mixtures of $MnOOH_r$ compounds.

In chapter 4, Fourier Transform Infrared (FTIR) has been employed for confirmation of the onset of microdomains of the end product due to location of H^+ and formation of O-H bonds coinciding with the appearance of new lines in XRD patterns and the onset of heterogeneity. Techniques such as mathematical pattern mixing, evolution of peak positions and measurement of peak areas have been also employed.

In addition, careful studies of electrode potentials in zinc chloride and potassium hydroxide electrolytes of H inserted products have been carried out. The onset of early heterogeneity with the hydrazine hydrate samples implies a region of constant potential between r = 0.25 and r = 0.75. Such behaviour not observed with propan-2-ol samples where the insertion was homogeneous. When studying the stability of the reduced samples in KOH electrolyte, it has been found that when microdomains of the end product form and formation of O-H bonds start, the reduced samples become metastable and the structure collapses to form a δ-MnO_2 (K-birnessite).

Further work to obtain more understanding of the influence of reduction rate on the formation of the $MnOOH_r$ insertion compounds could be carried out by studying different rates of reduction for the hydrazine hydrate method. Also it would be interesting

to try to achieve heterogeneous conditions by an electrochemical method. Even better, a direct application of these finding to the batteries would be a demonstration that homogeneous / heterogeneous processes occur in batteries under different discharge regimes.

Another interesting work would be to manufacture batteries with samples known to behave on both homogeneous and heterogeneous ways. For this purpose, it would be necessary previously to obtain enough amount of different samples. Then, it would be possible to study the performance of such batteries under different discharge regimes (heavy, intermittent, ...), and under different storage times and electrolytes. It is believed that the discharge behaviour of the batteries could be completely different to those of the actual batteries with electrolytic manganese dioxide containing cathodes, for example, with the appearance of regions of constant potential. This regions could improve service time for low discharge regimes, although this improvement would not be achieved in KOH electrolyte due to the collapse of the structure on storage of heterogeneously produced samples in this electrolyte.

REFERENCES

1.- F.L. Tye, Electrochemical Power Sources, Chapter 3. "Primary batteries for civilian use", (Ed. M. Barak, London, (1980)), p.50.

2.- A. Kozawa, "Chapter 3 - Electrochemistry of Manganese Dioxide and Production and Properties of Electrolytic Manganese Dioxide (EMD)", Volume 1, Manganese Dioxide, (edited by K.V. Kordesch, Marcell Dekker, Inco (1974)), p.385.

3.- Handbook of Manganese Dioxides Battery Grade, (edited by D. Glover, B. Schuum Jr. and A. Kozawa), The Int'l Battery Material Ass'n (IBA,Inc.) (1989), p.3.

4.- G.D. Van Arsdale and C.B. Maier, Transaction Electrochemical Society, 33, (1918), p.109.

5.- P. Ruetschi, J. Electrochem. Soc., 131, (1984), p.2737.

6.- P.M. de Wolff, Acta. Cryst., 12, (1959), p.341.

7.- Y. Chabre and J. Pannetier. Prog. Solid. St. Chem., 23, (1995), p.1.

8.- F.L. Tye, Proc. 7th Australian Electrochem. Conf., (edited by T. Tran and M.Skyllas-Kazaoos), The Royal Australian Chemical Institute (1988), p.37.

9.- J.P. Gabano, B. Moirgnat, E. Fialdes, B. Emery and J.F. Laurent. Zeit. Physikal. Chem., 46, (1965), p.359.

10.-. R. Giovanoli, K. Bernhard and W. Feitknecht. Helv. Chim. Acta, 51, (1968), p.355.

11.- W.C. Maskell, J.E.A. Shaw and F.L. Tye. Electrochim. Acta, 26, 10, (1981), p.1403.

12.- D.M. Holton, W.C. Maskell and F.L. Tye. J. Power Sources, ed L. Pearce, The Paul Press Ltd, 10, (1985), p.247.

13.- J.J. Coleman, Trans. Electrochem. Soc., 90, (1946), p.545.

14.- W.C. Maskell, J.E.A. Shaw and F.L. Tye. J. Power Sources, 8, (1982), p.113.

15.- W.C. Maskell, J.E.A. Shaw and F.L. Tye. Electrochim Acta, 28, (1983), p.225.

16.- F.L. Tye, Electrochim Acta, 30, (1985), p.17.

17.- W. Feitknecht, H.R. Oswald and U. Feitknecht-Steinmanm, Helv. Chim Acta, 43, (1960), p.1947.

18.- J. Fitzpatrick and F.L. Tye, J. Appl. Electrochem., 21, (1991), p.130.

19.- J. Brenet, "8e Reunion du CITCE, Madrid 1956", Butterworks, London (1957), p.394.

20.- H. Bode and A. Schmier, 3rd Int. Symp. on Batteries, Bournemouth (1962).

21.- K.J. Vetter and N. Jaeger, Electrochim. Acta, 11, (1966), p.401.

22.- F.L. Tye, Electrochim. Acta, 21, (1976), p.415.

23.- K.J. Vetter, Z. Elektrochem., 66, (1962), p.577.

24.- A. Kozawa and R.A. Powers. J. Electrochem. Soc., 113, (1966), p.870.

25.- J. Brenet, P. Mallessan and A. Grund, C. R. Acad. Sci., 243, (1956), p.111.

26.- K. Neumann and W. Fink, Z. Elektrochem., 62, (1958), p.114.

27.- A. Kozawa and J.F. Yeager, J. Electrochem. Soc., 112, (1965), p.959.

28.- J. Desilvestro and O. Haas, J. Electrochem. Soc., 137, (1990), p.5c.

29.- K.J. Euler, Materials Chemistry, 7, (1982), p.291.

30.- G. Coeffier and J. Brenet, Bull. Soc. Chim., 11, (1964), p.2835

31.- J.P. Gabano, B. Morignat and J.F. Laurent. Electrochem. Technol., 5, (1967), p.531.

32.- A. Kozawa and R. Powers, J. Electrochem. Soc. Japan, 37, (1969), p.31.

33.- D. Boden, C.J. Venuto., D. Wisler and R.B. Wylle. J. Electrochem. Soc. 114, (1967), p.415.

34.- J. Ambrose and G.W.D. Briggs, Electrochem. Acta, 16, (1971), p.111.

35.- R. Giovanoli, W. Feitknecht and F. Fischer, Helv. Chim. Acta, 54, (1971), p.1112.

36.- M. Sugimori. Proceedings of the Manganese Dioxide Symposium, Vol. 1, Cleveland. A. Kozawa and R.J.Brodd, eds. I.C. Sample Office (1975), p.256.

37.- N.C. Cahoon and M.P. Korver, J. Eletrochem. Soc., 106, (1959), p.745.

38.- G.S. Bell and R. Huber, J. Electrochem. Soc, 111, (1964).

39.- T. Ohzuku and T. Hirai. "Symposium on Manganese Dioxide Electrode Theory and practice for Electrochemical Applications" (eds B. Schumm, R.L. Middaugh, M.P. Grotheers and J.C. Hunter), Electrochem. Soc., 85-4, (1985), p.141.

40.- L.A.H. Maclean, PhD Thesis, (1993), Middlesex University, CNAA.

41.- L.A.H. Maclean, private communication.

42.- V.M. Burns and R.G. Burns, MnO_2 Symp. Proc. Cleveland, Oh, 1, (1975), p.288.

43.- R.G. Burns, and V.M. Burns, Manganese Dioxide Symposium, Vol. 2, Tokyo. B. Schumm, H.M. Joseph and A. Kozawa, eds. I.C. Sample Office (1980), p. 97.

44.- R.M. Potter and G.R. Rossman, American Mineralogist, 64, (1979), p.1199.

45.- B.D. Desai, J.B. Fernandes and V.N. Kamat Dalal, J.Power Sources, 16, (1985), p.1.

46.- D.A.J. Swinkels. Handbook of Manganese Dioxide Battery Grade, (edited by D. Glover, B. Schumm Jr. and A. Kozawa), The Int'l Battery Material Ass'n (IBA, Inc.) (1989), Chapter 7, p.249.

47.- J. Larcin, PhD Thesis, (1991), Middlesex University, CNAA.

48.- W.C. Maskell, PhD Thesis, (1976).

49.- R. Giovanoli, MnO_2 Symp. Proc., Tokyo, 2, (1980), p.113.

50.- V.M. Burns and R.G. Burns, MnO_2 Symp. Proc. Cleveland, Oh, 1, (1975), p.306.

51.- A.D. Wadsley and A. Walkley, Rev. Pure Appl. Chem. 1, (1951), p.203.

52.- J. Brenet, Bull. Soc. Fr. Minéral. Crystallogr. 77, (1954), p.797.

53.- W. Buser and P. Graf, Helv. Chim. Acta, 38, (1955), p.810.

54.- W.C. Vosburgh, J. Electrochem. Soc., 106, (1955), p.839.

55.- M.A. Malati, Chem. Ind. (London), (1971) p.446.

56.- S.B. Kamungo and B.R. Sant, J. Sci. Ind. Res., 31, (1972), p.264.

57.- M. Fleischer and W.E. Richmond, Econ. Geol., 38, (1943), p.269.

58.- J. Brenet and A Héraud, C.R. Acad. Sci., 228, (1948), p.1487.

59.- W.F. Cole, P.D. Wadsley and A. Walkley, Trans. Electrochem. Soc., 92, (1947), p.133.

60.- J.A. Tauber, X-Ray Diffraction Key to Manganese Dioxide Minerals, E.J.Lavino, Philadelphia, (1964).

61.- W.F. Nye, S.B. Levin and H.H. Kedesdy, Proc. 13th Annual Power Sources Conf. Atlantic City, NJ, (1959), p.125.

62.- D.G. Malpas and F.L. Tye, in "Handbook of Manganese Dioxides Battery Grade", eds D. Glover, B. Schumm Jr and A. Kozawa, IBA Inc., Chapter 5, (1989).

63.- B.S. Acharya and L.D. Pradhan, J. Appl. Cryst., 19, (1986), p.214.

64.- J. Pannetier, "Progress in Batteries & Battery Materials", ITE-JEC Press Inc., 11, (1992), p.51.

65.- J.H.A. Laudy and P.M. de Wolff, Appl. Sci. Res., 10, Sect 3, (1963), p.157.

66.- J.B. Fernandes, B.D. Desai and V.N. Kamat Dalal. Electrochim. Acta, 29 (1984), p.181.

67.- J. Pannetier, Progress in Batteries and Battery Materials, 13, (1994), p.132.

68.- R. Giovanoli, K. Bernhard and W. Feitknecht, Helv. Chim. Acta., 52, (1969), p.2333.

69.- J. Pannetier, Y. Chabre, C. Poinsignon, ISSI lett., 1, No. 2, (1990), p.5.

70.- M. Ripert, C. Poinsignon, Y. Chabre and J. Pannetier, Phase Transitions, 32, (1991), p.205.

71.- M. Ripert, J. Pannetier, Y. Chabre and C. Poinsignon, Mat. Res. Soc. Symp. Proc., 10, (1991), p.359.

72.- A.R. West, "Solid State Chemistry and its Applications", Wiley, (1984), p.369.

73.- J.A. Lee, C.F. Newnham, F.L. Tye and F.S. Stone, J.Chem. Soc. Faraday Trans. I, 74, (1978), p.237.

74.- F.L. Tye and S.W. Tye, J. Appl. Electrochem., 25, (1995), p.425.

75.- L.A.H. Maclean and F.L.Tye, J. Mater Chem, 7, (1997), p.1029.

76.- Y. Miyake, Electrochemistry of Manganese Dioxide and Manganese Batteries in Japan, Chapter 3, "Studies on the crystal phases of manganese dioxide", (Ed. S. Yoshizawa, K. Takahashi and A. Kozawa, Cleveland, OH, (1971)), p.115.

77.- W.C. Maskell, J.E.A. Shaw and F.L. Tye, J. Applied Electrochem., 12, (1982), p.101.

78.- "Perry's Chemical Engineers' Handbook", ed R.H.Perry, 6th edn, Mc Graw-Hill Book Company, (1984).

79.- D.A.J. Swinkels, P.M. Fredericks and K.E. Anthony, "Symphosium on Manganese Dioxide Electrode Theory and practice for Electrochemical Applications" (edited by B. Schumm, R.L. Middaugh, M.P. Grotheers and J.C. Hunter), Electrochem. Soc., 85-4, (1985), p.158.

80.- J.L. Loenig, Appl. Spectrosc., 29, (1975), p.293.

81.- D.H. Chenery and N. Sheppard, Appl. Spectrosc., 32, (1978), p.78.

82.- G. Gattow and O. Glemser, Z. Anorg. Allg. Chem., 309, (1961), p.20.

83.- R.M. Veletta and W.A. Pliskin, J. Electrochem. Soc., 114, (1967), 9, p.944.

84.- J. V. Valarelli, M. Perrier and G. Vincente, An. Acad. Bras. Cienc., 40, (1968), p.289.

85.- J.M. Grey and A.P. Millmann, Econ. Geol., 57, (1962), p.325.

86.- R.E. Folino, Econ. Geol., 44, (1949), p.425.

87.- E.M. Shazly and G.S. Saleeb, Econ. Geol., 54, (1959), p.873.

88.- E.A. Yanchuk and A.S. Povarennyk, Mineral. Sb. (Lvov), 30(2), (1976), p.9.

89.- J.P. Brenet and P. Faber, Symp. ISE Batteries, Marcoussis, France, May 1975.

90.- D.A.J. Swinkels, private communication.

91.- J. Fitzpatrick, L.A.H. Maclean, D.A.J. Swinkels and F.L. Tye, J. Appl. Electr., 27, (1997), p.243.

92.- H. Bode, A. Schmier and D. Berndt, Z. Electrochem., 66 (1962), p.586.

93.- A. Kozawa and R.A. Powers. Electrochem. Technol., 5, (1967), p.535.

94.- W.C. Vosburgh, M.J. Pribble, A. Kozawa and A. Sam, J. Electrochem. Soc., 105, (1956), p.1.

95.- S.W. Donne, G.A. Lawrance and D. Swinkels, 10th IBA Battery Materials Symposium, Arizona (USA), 1996.

96.- M. Sugimori. Manganese Dioxide Symposium. Tokyo. Vol 2. (edited by B. Schumm. H.M. Joseph and A. Kozawa), The Electrochem. Soc., Cleveland, (1980), p. 443.

97.- J.P. Gabano. B. Morignat and J.F. Laurent. "Power Sources. 1965" (edited by D.H. Collins). Bergamon Press. Oxford. 49, (1967).

98.- J.D. Russel. 'Laboratory Methods in Vibrational Spectroscopy'. edited by H.A.Willis. J.H. Van Der Maas. R.G.J. Miller ; Ellis Horwood. Chichester. 3rd edn (1989), p. 428.

99.- K. Nakamoto. 'Infrared and Raman Spectra of Inorganic and Coordination Compounds'. Wiley. New York. 3rd edn. (1978). p. 9.